The Computational Modelling of Collecting Lymphatic Vessels

Submitted by Alison Jane Macdonald, to the University of Exeter as a thesis for the degree of Doctor of Philosophy in Engineering, April 2008.

This thesis is available for Library use on the understanding that it is copyright material and that no quotation from the thesis may be published without proper acknowledgement.

I certify that all material in this thesis which is not my own work has been identified and that no material has previously been submitted and approved for the award of a degree by this or any other University.

Alison Macdonald

Acknowledgements

I am most grateful to the EPSRC (Engineering and Physics Research Council) for funding this project.

Thank you to my examiners Professor Wen Wang and Dr Chris Smith. I enjoyed our discussions and their positive feedback made this project worth the hard work.

To Professor Noel McHale and Dr Kenton Arkill, thanks for their valuable experimental work in partnership with this thesis and for all I learnt from them. Thanks to my supervisors Dr Gavin Tabor and Professor Peter Winlove, for the benefit of their prodigious knowledge and experience.

A heartfelt thanks to my Grandfather Kenneth Soutar (deceased) for such a strong belief in my abilities ("That girls going to go far!") and to whom I dedicate this thesis. Thank you also to my new husband Bruce O' Connor for believing in me every bit as much as my Grandfather did. Thank you to Dr Richard and Dr Emma Forsey and all of my friends and family for their advice, support and for making me feel like I could do this.

The editorial input from my sister Frances, my father Peter and Bruce deserves much appreciation.

Lastly thanks to everyone who helped me more than survive my trauma-induced migraines over the last five years: especially my mother Janet and the people who taught me how to be well - Lucy, Trisha, Mo, Alison, Helen, Anne and Austin. I think we may have finally got the better of them.

Abstract

This thesis details a 1-d model of a lymphatic vessel, developed from a model by Reddy. Some additions to the modelling techniques were found to be necessary to prevent numerical phenomena not found in experiment. Furthermore the details of the wall and valve were important to the mechanics of the system. This developed model presents flow characteristics which are not represented in the existing lumped parameter or 1-d models of the lymphatic system. Additional terms allow more realistic representation of some modes of flow such as those occurring during collapse. The model was validated using Poiseuille flow calculations and experimental work. Features found in experiment were reproduced in the model. Such as the shark tooth shape of the radius time graph.

A study of the sensitivity of the model to experimental parameters was performed. Features that increased flow included: increased compliance of the vessel, a larger diameter, amplitude of contraction or frequency, or a faster contraction wave.

A lumped parameter model, relating the radius directly to the pressure, was investigated but this did not reproduce flow features such as the shark tooth shaped radius with time relationship or the radius peak at the beginning of a contraction or passive relaxation of the vessel. In the 1-d model the time constant of this passive relaxation increased with the magnitude of contraction. This value may have physiological relevance.

Contents

List of Figures

Chapter 1

Introduction

This chapter begins with an introduction to the lymphatic system and the problems and medical conditions which modeling may be able to help. Followed by relevant fluid dynamics and the historical development of theory and current understanding and finally an overview of this Thesis.

The lymphatic system is a converging drainage network of tubes, with intermittent nodes which act as filters and introduce elements of the immune system into the circulation. The larger vessels are able to contract as a pumping mechanism and will even continue to do so once excised from the body, given the correct conditions.

The principal role of the lymphatic system is to maintain the environment of the interstitium; the spaces between the structures of the body. Fluid continually leaks out of the arteries and veins into the interstitium, providing hydration and nutrition. This fluid must then be returned to the circulation at the thoracic duct by the lymphatic system. The lymphatic system allows 2-3 litres of interstitial fluid to return to the circulation from the interstitial spaces daily. The fluid contains long-chain fatty acids, vitamin K and immune cells [5].

The importance of the lymphatic system can be shown by the effects of its failure. This might be due to cancer surgery or conditions such as lymphatic filariasis where parasites block the vessels. Lymphatic filariasis is the major cause of the most extreme lymphatic malfunction - elephantiasis - and is common in the underdeveloped

world. In the developed world however surgery, such as cancer surgery, is more likely to be the cause of lymphatic disorders. Cancer cells often migrate to nearby lymphatic vessels and nodes and these must be removed during cancer surgery. For example breast cancer surgery routinely involves removing the lymphatic vessels and nodes from the region of the armpit. This has a detrimental effect on the drainage of interstitial fluid in the nearby arm and can lead to the disorder of lymphedema. Edema (of which lymphedema is one type) involves compromised immunity and tissue repair, pain, swelling and disfigurement. Half a million women in the UK will develop lymphedema from breast cancer surgery. Currently the only treatment is applying external pressure, through bandaging or specialist massage techniques.

Figure 1.1: Arm Edema

Compared to the state of knowledge in other areas of biofluids, relatively little is known about the lymphatic system, and there has been little theoretical analysis. The most detailed theoretical analysis was completed by Reddy in 1975 [4, 6, 7] (see sections 3.3.1 and 5.2). Accurate and well validated models could help determine more effective treatment to increase flow during edema, at the least improving manipulation techniques. It would therefore be of great relevance to determine mechanical reasons for the difficulties in recovering from lymphoedema. Quick and

Stewart [8, 9] claim that the best course of action is to induce relaxation in the smooth muscle, allowing passive flow of lymph to dominate and increasing the average radius. However Olszewski [10] reports the necessity of the contractions in edema isolated in the leg. These contractions may be necessary due to the increased gravitational effects in these lower limbs. There are many unexamined phenomena within the field of lymphoedema, only a proportion of breast cancer patients with seemingly identical procedures go on to suffer from lymphoedema. In addition, the condition can remain dormant for years, except for an initial brief bout immediately after surgery, only to resurface years later.

1.1 Current Knowledge

For more than a century it has been known that the lymphatic system is involved with immunological control and tissue drainage [11]. There have been many ultrastructural studies of the system in the last few decades and intravital microscopy has allowed the collection of dynamic data throughout the lymphatic network. According to Gnepp, in situ, there are general similarities among the lymphatics of the different organs, but also some regional differences [12].

A widely accepted overall picture of the mechanisms for lymph transport is still to be established. In many ways, studies of the lymphatic circulation are behind that of the major (or blood) circulatory system. However, an understanding of the mechanics of the major circulation (often called Haemodynamics) is relevant to the functions of the lymphatics and the type of problems that arise are discussed in the next section. A computer model using these techniques would allow greater understanding of lymphedema including prediction of patients at increased risk and to establish what type of medication may help the disorder.

1.1.1 The Complexities of Biofluid Mechanics

Biofluid problems are very different to those found in other areas of engineering and are often far more complicated. James Lighthill [13] details the major points that set internal biofluids apart: the range of Reynolds numbers; the complexity of the branching systems; the nonlinear distensibility of the tubes involved; the complicated fluid properties; and the pulsatility.

The Range of Reynolds Numbers

The Reynolds number (Re) represents the ratio of inertial to viscous forces and is a useful measure for the type of flow involved in all fluid dynamics problems. Within the lymphatic and blood circulation, the small vessels generate slow, laminar flow represented by low Reynolds numbers. The Reynolds numbers for large airways and arteries can range from hundreds to thousands, indicating turbulent or transitional flow. Representing a unified model with such a variety of Reynolds numbers requires a very complex computer program with high processing time [14]. Further modelling complexity is caused by the tendency for turbulence in these vessels to manifest in short 'bursts', in contrast to the fully developed turbulence traditionally analysed by engineers. Even modelling the areas of laminar flow is more involved as fully developed poiseulle flow cannot necessarily be assumed (this is an assumption made for most engineering problems). However, the entry regions, ie the length before the next bifurcation (ie branch), are too short for poiseulle flow to develop fully. Lastly the tubes are sometimes curved, generating the extra factor of centrifugal motion.

The Complexity of the Branching Systems

The branching systems of the circulation and lungs are far from symmetrical and diverge from one to hundreds of millions of tubes. Approximations are often used due to the computational cost involved in representing the spatial positioning and dimensions of the vessels due to the vast numbers of vessels involved and the minute scale of the smaller vessels. The bifurcations of the large tubes cause a significant

distortion to the flow pattern, unlike the smaller tubes (due to their low Reynolds numbers). The branches themselves are rarely symmetrical and flow depends on the area of the daughter and parent tubes, the angle of the branch, the radius of curvature and the Reynolds number and velocity profile in the parent tube. One of the most investigated types of asymmetrical branch is a right-angled branch as shown in figure 1.2. Strong secondary motions are setup as the flow splits. This leads to areas of low and high shear and has undergone much investigation due to the significance with aneurysms etc [14].

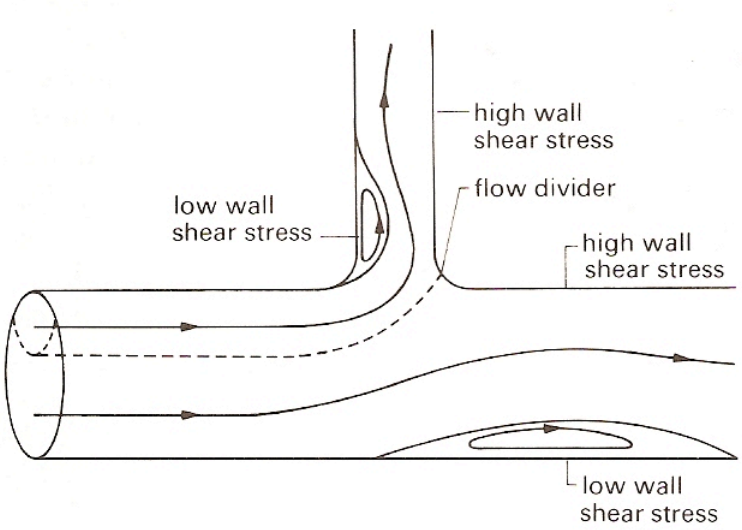

Figure 1.2: Flow in a right-angled branch [1] .

Nonlinear Distensibility of Tubes

Blood vessel walls contain two materials with different elastic properties; collagen and elastin. These influence the combined properties of the material to different degrees at different distensions. This gives a nonlinear relationship during elastic behaviour (rather than the linear relationship usually seen in engineering material). As different material components become dominant, the gradient of the stress strain relationship changes while the material is still able to return to its original shape. There is a viscous time-dependent element which acts as a flow and an elastic compo-

nent which is non- time dependent. . To further complicate matters, the properties of the vessel walls change to suit internal conditions. This includes the vessels' ability to dilate in response to shear stress [15].

Non- Newtonian Fluid Properties

Air (eg in respiration models) and blood both contain particles and these can have a significant effect on fluid properties and flow. Blood is the most complicated fluid found in the body, comprising of 40 to 50% volume deformable bodies and has a viscosity 4 times that of water (0.0008904 Kg/m^2) [16]. The red blood cells have a great contribution to the fluid behaviour in comparison to the other blood particles by effecting the overall viscosity due to the large numbers involved.

Lymph is similar to plasma (blood with the blood cells removed) but contains less protein [12]. Plasma can be viewed as a newtonian fluid, with aslightly higher viscosity than water, around 12 mNm^{-2} at 12 C [1]. There may be some changes in properties as the composition changes e.g. in disease with the addition of more immune cells and during digestion, in the mesenteric lymphatics some nutrients are transported as lipoproteins. During this project the fluid is represented computationally as a newtonian fluid with the properties of water and this is matched in the experimental work of chapter 4.

Newton's Law describes the 'internal friction' of a liquid and can be used to approximate the plasma alone. At a high flow rate this will also be effective if blood cells are included. As the flow slows down however the blood viscosity begins to increase with decreasing strain. Newtons law only holds for laminar flows where the viscosity does not vary with the rate of shear [17]. This 'non- Newtonian' behaviour is due to the propensity of the blood cells to collect together in 'aggregations' at low strains, increasing the resistance to flow.

In smaller tubes the cells tend to move away from the sides of the vessel due to an unequal distribution of forces around any cell at the side of the vessel. This leads to a lubricative layer of fluid at the edge of the vessels, reducing the effective viscosity

[16] of the volume of fluid as shown in figure 1.3.

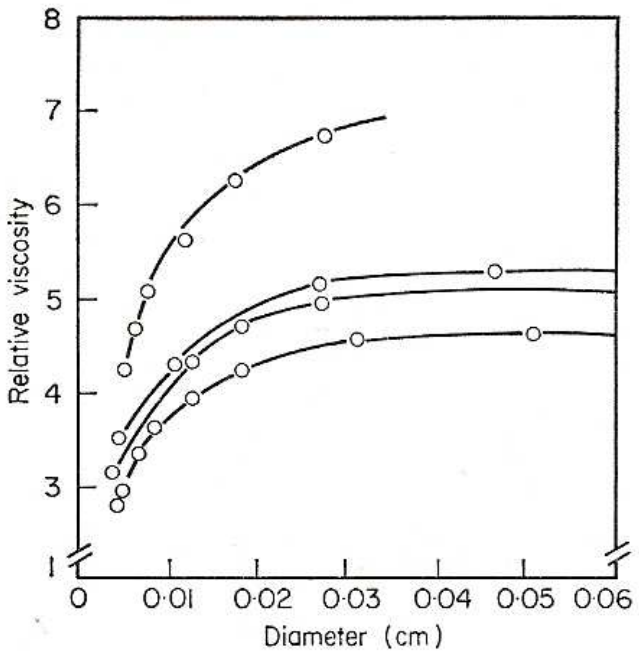

Figure 1.3: The Fahraeus- Lindquist effect means that the effective viscosity of blood is smaller than expected in very small tubes [18]

Pulsatility

The beating of the heart generates a pressure wave, which propagates throughout the arterial network. This soon becomes a very complicated waveform due to the bifurcations and non-linear elasticity. These waves largely die out before they reach the veins and the flow becomes steadier [17, 1].

The following section goes on to discuss the history of understanding of the major circulation, many of the principles that were discovered in the last few centuries for the blood vessels, are now relevant to the lymphatic system today. This is then followed by a section on the history of understanding of the lymphatic system.

1.2 Haemodynamics History

Haemodynamics has been a major area of focus for some time due to its connection to the heart and obviously critical importance to the body. McDonald's book [17] contains an indepth description of the history of haemodynamics.

William Harvey (1578-1657) initiated science in this area after a lengthy stalemate caused by the erroneous Galenical teachings (129-199). Harvey was part of Galileo Gallelei's movement to back up arguments with experiments, but his work into cardiac output was not widely accepted initially. In 1669 Richard Lower continued this work and in 1689 Newton defined the concept of viscosity, which Stephen Hales was able to use in 1733 to show there was pulsatile flow in arteries and smooth flow in veins. Hales found that the minute vessels in the wall of the gut were the main cause of resistance to flow, recording a change in flow rate with different temperatures and brandy! (This can be explained by the later discovery of vasoconstriction attributed to Claude Bernard.)

Many important principles were defined in the 18^{th} and 19^{th} centuries, including Euler's equations (Leonhard Euler 1707-1783) and Bernoulli's law (Daniel Bernoulli 1700-82). The Navier-Stokes equations were composed by Stokes in 1845 as an extension of Euler's equations to allow for viscosity. The doctor Jean Louis Poiseulle (1797-1869) developed a law describing flow in a circular tube including viscous flow and the pressure profiles across tubes with different elasticities. He developed this major law of fluid dynamics in spite of his background orientated in medicine because he needed one to progress his studies into the flow of blood! Young (1773-1829) instigated the Elastic modulus named after him and made important discoveries about the elastic properties of arteries and the velocity of propagation of the arterial pulse in 1808 and 1809. Weber (1825) performed further work involving wave reflections and propagation. In 1878 Moens started work (later continued by Korteweg and Rosal) to give the thin elastic wall equation (for a non-viscous liquid). This method for modelling the wall was later usurped by the thick elastic wall equation [19] as detailled in section 5.

1.3 Lymphatic History

As described by Gnepp, Nishimaru and Swartz [12, 20, 21], the physiology of the lymphatic system really began to make progress in the 17^{th} and 18^{th} century but there is evidence of lymphodema and elephantisis as far back as Ancient Greek and Hebrew literature. Aristotle mentions vessels containing colourless liquid and Hippocrates, white blood. In 300BC arteries containing 'milk' were discovered at the Alexandrian medical school (home of Erasistraties and Herophilus). Then for 18 centuries the Galenical teachings prevented any progress within the lymphatic circulation, in addition to preventing exploration of the major circulation. This was due to the belief that lymphatic vessels were no different to arteries and veins.

Finally in 1622 Asellius (Professor of Anatomy and surgery in Milan and Paris) described finding 'white lacteals scattered thoughout the entire mesentery of a well-fed dog'. This white colour is now known to be due to the absorption of fats into the mesenteric lymphatics during digestion (lymph, the fluid inside the lymphatic vessels is normally clear). This work was corroborated by findings from Pecquet (1651), Van Horne (1652) and Rudbeck soon after.

The lymphatic valves were revealed by Swammerdam's wax injections in the middle of the 17^{th}century. The spread of cancer to the surrounding nodes was discovered by Louis Petit at the beginning of the 18^{th} century.

Rudbeck began to have some understanding of the importance of the lymphatic circulation to the major circulatory cycle believing in the nutrition of the tissues by irrigation. This hypothesis involved the lymph and solid substances passing from the blood vessels, for use in the tissues, while fluid flowed into the blood through the lymphatics. The lymphatics were named in 1653 by Bartholin (Professor of anatomy in Copenhagen). He was one of the first scientists to show that the lymph fluid flows from the thoracic duct to the veins through the lymphatics (also corroborated by Pequet, Rudbeck and Jolive). At the end of the 17^{th} century the basic anatomy became known and improvements in experimental techniques allowed the study of lymph vessels in situ. This experimental method was perfected by Masagni in 1787

and Cruickshank in 1789.

In the 19th century various anatomists studied the distribution of lymphatic vessels by injection techniques. At this time there was much controversy over the origin of the lymphatic vessels and their relationship to blood and tissues and so lymph-capillary exchange became a major topic during the 19th century.

Ludwig and Starling developed techniques for the collection of lymph, from the lymphatic vessels of different parts of the body. Ludwig initiated the idea that lymph was a filtrate derived from blood, which permeated or diffused across the blood vessel walls. This was however opposed by Heidenham, who believed it to be a secretion from the endothelium of the blood vessels.

The filtration hypothesis of Ludwig was later firmly established by Starling. This began in 1898 when Bayliss and Starling pursued Heidenham's experiments and disproved his hypothesis, indicating Ludwig's to be correct. They found the ligature of arteries and veins increased the internal pressure of blood capillaries, also showing that the collapse of blood capillaries increased lymph production. Starling related the hydrostatic pressure of blood in capillaries to the osmotic pressure of plasma proteins and realised that the proteins leak out of capillaries, as quantified by Starling's law of microvascular exchange. Drinker and colleagues from Harvard [22] then showed that a major function of the lymphatic vessels was to return the protein molecules that escape from the circulation. More support for this understanding of the balance of liquid between the two circulations, including the importance of osmotic pressure and the permeability of the vessels has been provided by Krugh (1930) and Landis (1934).

1.4 Lymphatic and Heart Valve History

The function of the valves of the lymphatic system is also very important to this project. There has been little research into the mechanics of lymphatic valves and this is covered in depth in chapter 2. They are often referred to as underdoing similar mechanics to heart valves which have been well explored . This section describes

how progress was made on the physiology of the heart valves as the best example of our understanding of the valves of the body.

Leonardo da Vinci made the first record of a mechanism for the closure of heart valves in 1513. He attributes the closure of the mitral and aortic valves to a hydrodynamical mechanism involving a vortical flow field inside the ventricle chamber and the aortic sinuses. Two hundred years later Valslava in 1740 wrongly stated that the sinuses were present to dissipate the violence of systolic contraction [23]. The early closing of the mitral valve was originally attributed to contractions of the papillary muscles pulling on the chordae tendinae, however these tendons are now believed to simply prevent reversal of the cusps.

Bellhouse and Talbot [24, 25] reexamined the heart valve mechanics mathematically and experimentally. They began to develop the current understanding of the system - that vortices in the sinuses (or surrounding structure) aid efficient closure of the valves. A similar shape behind the valve leaflets is present in the valves of the lymphatic and venous systems. In the venous system it has been indicated by Buxton and Clarke [26] that a similar mechanism occurs so it seems likely this is also true of the lymphatic system

1.5 Thesis Overview

The aim of this thesis is to develop and validate a modern model for the lymphatic vessels, taking into account the fluid flow (using the Navier Stokes equations in 1-d), the wall mechanics and the fluid/structure interaction. Chapter 2 details a description of the mechanics of the lymphatic system and a background in relevant computational modeling is described in chapter 3. Secondly the method and results from an experimental study performed in partnership on this project are included in section 4. Chapter 5 describes a 1 dimensional implementation of Reddy's work (using Matlab) closing with the changes made to the model and the reasoning behind them. In chapters 6 and 7 a study and further modelling of the wall mechanics was undertaken. Chapter 9.2 details the physiological implications of some of the findings

along with future work and conclusions.

This model enables a more accurate, non-invasive exploration of the lymphatic vessels, indicating parametric changes which may be desirable and could be used to improve treatment of the lymphatic disorder.

Chapter 2

Lymphatic Mechanics Background

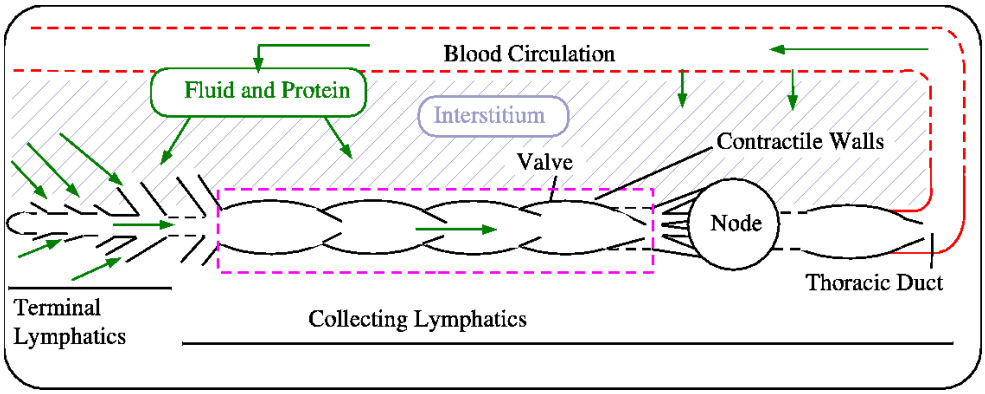

Figure 2.1: A schematic diagram showing the cycle of lymph fluid around the body.

The lymphatic system has two important roles, firstly it is a drainage network and secondly part of the immune system. The drainage is of excess fluid and protein from the interstitium, which has leaked out of the blood circulation is can then returned to the blood system via the thoracic duct as shown in figure 2.1. The capillaries at the origin of the system, which absorb the plasma filtrate, are known as the terminal lymphatics. One way valves prevent fluid from returning to the interstitium and the capillaries converge into larger vessels. These collecting lymphatics act like mini-hearts pumping the liquid in sequence as a propagating wave, with the aid of the further one way valves at intervals along the vessels. The distribution of these larger vessels is show in figure 2.2 and typical parameters are shown in tables 2.1, 2.2 and

2.3.

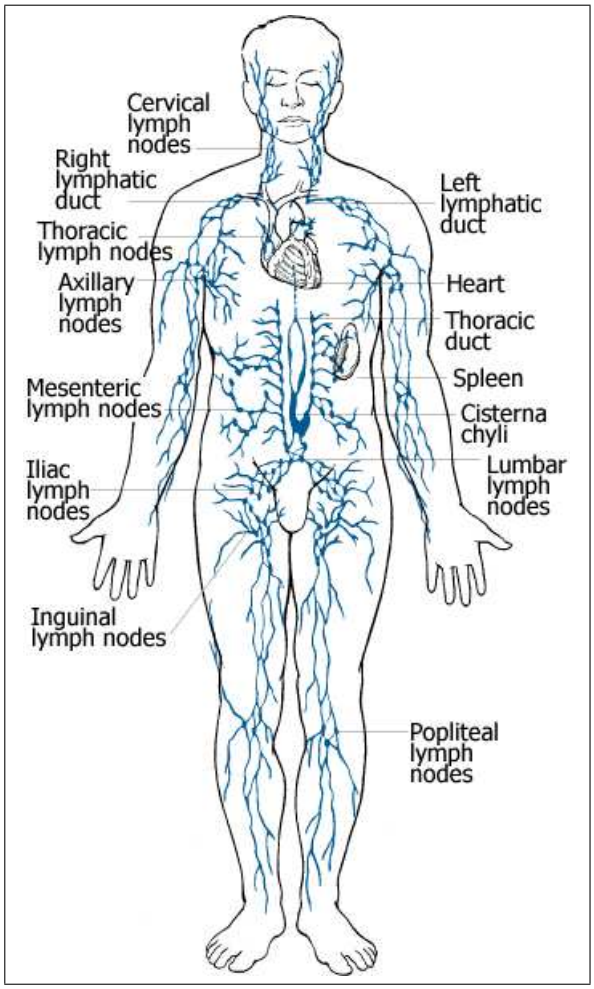

Figure 2.2: The distribution of the major lymphatic vessels around the body [2]

Fluid transport in the lymphatic system is also aided by the surrounding external muscles, eg moving a limb can help generate flow. This external pumping is the only well substantiated method of transport within the terminal lymphatics although there is some investigation of the possibility of osmosis acting across the boundary between the interstitium and the terminal lymphatics [11, 12]. This could potentially create a high pressure at this end of the network which is the only way flow could be generated without the use of any muscles. On route to the thoracic duct the fluid passes through nodes, which act as part of the body's immune system. These can filter out bacteria and abnormal cells, but the ability to then contain the

Parameter	**Value**
Radius (mm)	1 - 2
Pressure (Pa)	100 - 1200
Peak Flow (ml/min)	6
Velocity (mm/s)	0.2

Table 2.1: Typical parameters within the bovine mesenteric lymphatics

Rel D μ**m**	**Rel P Pa**	**Con D** μ**m**	**Con P Pa**	**Contraction freq. no./min**	Δ **P** %	Δ **D** %
55	300	35	550	8	83	-36
55	600	27	900	30	50	-51
60	250	20	200	6	180	-67
90	650	60	1400	15	123	-33
90	800	50	1600	12	100	-44
100	950	62	1150	10	21	-38
143	400	100	700	30	75	-30
200	900	160	1200	30	26	-32
260	500	200	700	15	40	-23

Table 2.2: The Pressures during spontaneous contractions of the mesenteric lymphatic vessels of the rat, taken from [27], where P = Pressure , D = diameter, Con = contracted and Rel = relaxed

Location	**Proximal Pressure Range (Pa)**	**Mean**	**Distal Pressure Range**	**Mean**	**Δ Pressure (Pa)**
Terminal Lymphatic	0-250	130			
1st Valve	100-400	230	300-500	360	130
2nd Valve	300-700	360	400-800	550	180
3rd Valve	400-800	480	500-900	680	200
4th Valve	600-900	600	700-900	12	100
5th Valve	500-1000	810	800-1100	1050	250
6th Valve	800-1600	1030	900-1800	1270	270

Table 2.3: The Pressures across valves in the mesenteric lymphatic vessels of the rat, taken from [27], where the valves are numbered distally from the terminal lymphatics.

disease depends on the person [12]. Some lymph nodes may contain disease in this way indefinitely while others transfer and even accelerate the spread of disease.

An effective flow profile in the lymphatic system maintains healthy tissue and allows the most efficient transport of immune cells. Currently there is little that can be done to improve flow; with modern treatments consisting mainly of specialist massage and bandaging techniques [28].

This section has covered the basic mechanics of the collecting vessels to show they can be modelled as a contraction wave moving the fluid along an elastic tube, broken periodically by valves. Any external pumping can be modelled by varying external pressures. The mechanics of the terminal lymphatics involves flow in smaller tubes with no intrinsic contractions. When more than one tube is modelled, the fluid mechanics surrounding bifurcations also become important as discussed in chapter 1. These have been shown to be areas of high wall stress in the cardiovascular system, although the high Reynolds numbers that make this important are unlikely to be reached in the lymphatic system. For the cardiovascular system, the effects at

these divisions of the non-newtonian fluid and asymmetry has also been examined in work by Chen, Wang et al 2004 [29] and Lu, Wang et al 2002 [30].

2.1 The Anatomy and Physiology of Lymphatic Vessel Walls

There are three major factors which should be considered relating to the effects of the walls. The mechanical properties of the walls, the effects of the surrounding structure and the tethering effects of the anchoring filaments. This study concentrates on the mechanical properties of the wall. It is logical to start with the simplest factor to study first, however there is not much known about any of them. This section starts with the anatomy of lymphatic vessels, containing a brief description of the anchoring filaments but concentrates on the properties of the walls themselves, the focus of this part of the project. This is followed by a description of the physics of the lymphatic vessel walls in section 2.1.2.

2.1.1 Anatomy of Lymphatic Vessels

The walls of lymphatic vessels exhibit elastic properties and contain smooth muscle as shown in figure 2.3. Smooth muscle is also found in the arteries and the gut and is able to keep contracting without tiring. Lymphatic vessels are more similar to veins than arteries (arteries are thicker in order to withstand higher pressures).

According to [31] the combination of materials in the lymphatic vessel walls is an unusual one, containing not only cardiac smooth but also skeletal muscle and protein isoforms (these are slightly different versions of the same protein). In man the smooth muscle is positioned in parallel bundles, with a circumferential orientation. However this alignment does vary in other animals [12].

In lymphatic vessels larger than 0.2 mm diameter, 3 different layers of the wall become apparent; the intima, media and adventitia. The inside of the vessel consists of raised endothelial cells on top of an elastic lamina (which becomes a basement

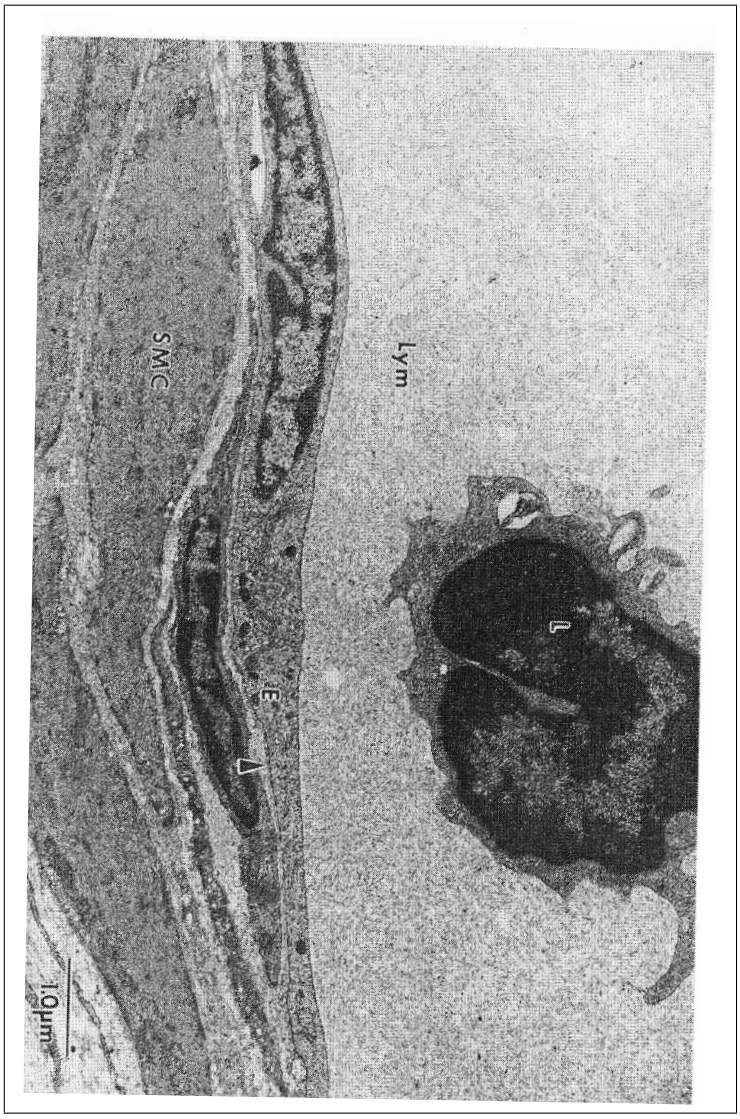

Figure 2.3: Microphotograph of a cross section of a collecting lymphatic from a sheep's lung from Schmid-Schonbein's review [11]. **SMC** shows the layer of smooth muscle cells, the arrow shows the discontinuous basal lamina and **E** shows the layer of long thin endothelial cells at the inner edge of the wall. **Lym** shows the lymph fluid contained in the vessel and **L** a lymphocyte.

membrane in smaller vessels). In between this and the media is a layer of randomly orientated collagen and elastin fibers. The media contains layers of smooth muscle cells. In larger vessels there is a clearer distinction between a longitudinal outer layer and a circumferential inner layer; except for the valve area which has less or no smooth muscle. The external layer of advential contains collagen, elastic fibers, blood vessels and nerves. The inner layer contains dense collaginous fibers and elastic tissue and the outer contains loose fibroadipose tissue.

Anchoring Filaments

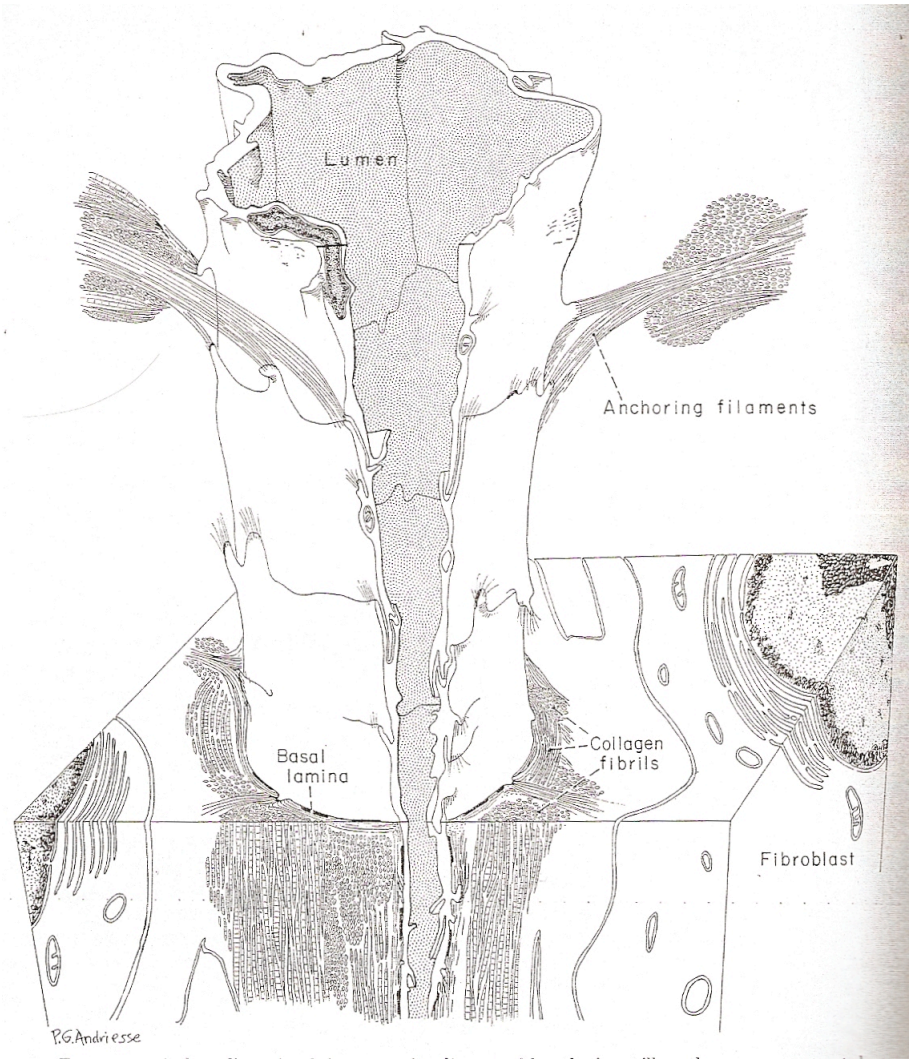

Figure 2.4: The anchoring filaments of lymphatic vessels [3]

There are reports by Casely Smith [32] that the anchoring filaments (shown in figure 2.4) hold the vessels open even during Edema. Leak and Burke [3] submitted that perhaps the vessel is capable of opening itself and according to [33] the filaments act like springs. It is known that they are a binding mechanism for firm attachment of the lymphatic capillary wall to adjoining collagen fibres and cells of the connective tissue. They are similar to microfibrils of extracellular space and seem to originate from endothelial cells [3] and are constructed from the same material the eye is suspended by. As discussed above this project concentrates on the properties of the walls themselves and leaves representation of the anchoring filaments and the rest of the surrounding structure to future work.

2.1.2 Physiology of Lymphatic Vessels

There is a similar mixture of materials in blood vessel walls. Collagen, elastin and smooth muscle determine the stiffness of the walls via different ratios under different conditions [34]. This leads to an alinear stress strain relationship during elastic deformation (i.e. during the period of reversible deformation) see figure 2.5. When the vessel is relaxed the wall stresses are predominantly taken up by the elastin and parallel collagen fibres. When the muscles are contracted it is predominantly the smooth muscle and series collagen which dominate the material properties.

Intrinsic Pump

The larger collecting lymphatic vessels exhibit an intrinsic pumping mechanism even when removed from the body [35]. If we return to the image of a contraction wave passing along an elastic tube broken by valves, as described at the beginning this chapter. Each chamber or area between two valves can be seen as a mini-heart, with the chain pumping in sequence. A single such chamber was termed a lymphangion by Mislin and Schipp [36]. A contraction follows a twisting peristaltic wave travelling along the vessel, within and between these chambers, travelling at about 4-5 mm/s [37]. This sequential pumping can be reproduced in isolated perfused lymphatic

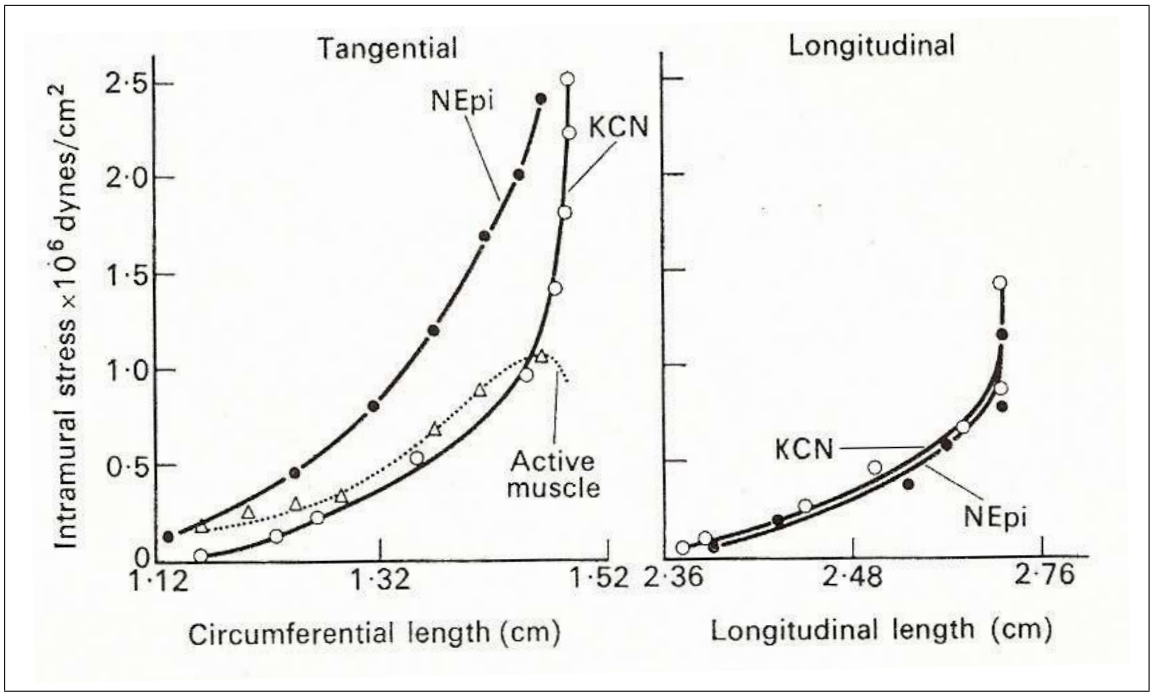

Figure 2.5: The alinear elastic stress strain relationship of relaxed blood vessels caused by the mixture of collagen, elastin and smooth muscle dominating at different stresses taken from [17]. KCN- muscle tone is abolished using potassium cyanide , NEPi- During strong contraction due to norepinephrine

vessels [35]. Bovine mesenteric lymphatic vessels are the largest lymphatic vessels which are easily obtainable. This basic contraction wave, found during experiment can be altered in magnitude and frequency by changing various parameters (e.g. the inlet and outlet pressures). Zweifach and Prather speculate that the contraction cycle naturally waxing and waning [27] in frequency.

The pumping sequence has been found to travel both in the direction of flow and against it, in fact McHale (private correspondence) has found it is most likely to travel against the direction of flow. The mean flow was found to be the same whether the wave propagates backwards or forwards, in vivo and in vitro, suggesting this is a normal form of propagation [38, 39]. This is also examined using our model in section 7. If the contraction wave follows the direction of flow, some waves would have to stop at a branch and wait for the other converging waves in order to

maintain co-ordination, losing efficiency due to the loss in propulsive momentum. We submit a new hypothesis that a contraction wave against flow, propagated from the larger vessels to the smaller, would allow for greater synchronicity when passing bifurcations. With correct timings and the presence of one way valves, it seems likely that this type of propagation would not be detrimental to flow and may aid it when the entire network is considered. Furthermore there are areas where breaks in the normally good synchrony of the wave occur, due to isolated areas of poor connectivity of nerves and muscles [40]. An interesting study might investigate whether the position of these breaks in synchrony have any relationship with the position of branches and the mechanical issues of propagating a wave though a network.

Although contractions were initially thought to be pressure or stretch driven, recent evidence suggests that the contractions are predominantly initiated by an electrical signal while radial stretch only modulates the amplitude and frequency of contractions [41].

The original theory of contraction initiation assumed the endothelial response to a certain triggering pressure to be graduated between cells to facilitate coordination [42, 37]. Each cell was considered to be triggered by a pacemaking response to high pressure and stretch. This is related to the excitability rate of pacemaker firing in lymphatic smooth muscle as it is in the sino-atrial node in the heart and in other types of smooth muscle [38]. The possible placement of pacemaker cells in the immediate vicinity of the inlet valve has been submitted by Zhang [43]. Endothelial cells throughout the chamber are also part of the pacemaking process. They are known to respond to shear stress in the walls of blood vessels by emitting nitric oxide, which effects the dilation of the vessel and there are similar control mechanisms in lymphatic vessels. Gashev et al [39] also found that imposed flow (therefore shear stress) inhibits the muscular pumping action and exposure to nitric oxide partly mimics the effects of flow.

Pacemaking is still credited with initiating a small portion (and the magnitude) of the contractions but a lymphatic vessel can pump without any need for a transmural

pressure difference. McHale [40] found a good correlation between electrical and mechanical activity and during retrograde wave propagation the triggering cannot be related to the local transmural pressure and so must be due to electrical activity [39, 38]. McHale and Meharg [38] found that in 80% of cases there was little or no correlation of lymphangion contraction and pressure maxima, using different temperature water baths to effect the behaviour of different areas of the vessel. A cold bath was found to slow the frequency of that area while increasing the frequency in an adjoining unaltered segment. This showed that the electrical stimulation of contractions was dominant. The segments remained synchronised, except there were two contractions in the normal segment for every one in the cold segment. The muscles do not appear to relax completely even during the relaxed stage of the cycle as described in section 3.1.

The Branching Network

The branching of the vessels cause further complications to the propagation of the contraction waves, as discussed above in section 2.1.2 and also can lead to areas of high shear stresses.

There is some discussion as to whether there are inherent differences in the mechanics of the vessels at different points in the network. According to McHale and Meharg [38] the inherent contraction frequency does not appear to be different depending on the position in the body the vessel comes from. Conversely, Gashev et al [44] conclude that there are different strengths and sensitivities of pump to pressure and flow, relating to the resistance at that point in the body.

Gashev [45] found differences in pumping capabilities of the larger vessels of the mesentery and thoracic duct in studies on 4 legged animals. The mesenteric lymphatics were found to be strongly pumping, able to withstand high output resistances, with increased contraction frequency and work to high pressures of 500 Pa (5 cm H_2O). The thoracic duct was found to be more sensitive to flow and principally a conductive vessel which has a maximum pressure of 200-300Pa (2-3 cm H_2O). The

thoracic duct returns lymph fluid to the blood stream and a simple conductive vessel is all that is required. It follows that this area should have different properties but this does not necessarily indicate that other areas of the lymphatic system differ to this extent. It is possible that the lymphatic vessels can adjust to the conditions they are submitted to (McHale, private correspondence), becoming more sensitive at lower flows.

Causes of Resistance Within The Lymphatic System

Resistance of the lymphatic system has been shown to drop with flow [46, 47]. This is due to the ability of the vessels to dilate with shear stress. The coordination of the contraction and therefore variation in diameter with time will also be important. Areas with more complicated flow profiles e.g. branches and bends will be likely to cause greater resistance.

Auckland and Reed [47] discuss whether the pressure drops after passing through a node [48] or continues to steadily increase as the flow progresses further down stream (ie up the network) [27]. The resistance of nodes was found to be 50-200 times greater than the resistance of the main vessels by Papp et al [49] and this is supported by other reports [47]. It is however possible that in these experiments the nodes were not fully perfused due to cannulation of only one of the afferent vessels, which could lead to a falsely high resistance.

The valves should also be considered as a factor causing resistance even when open. To understand the valves contribution to resistance at different pressures and flows it is important to know how the valves work as discussed in the next section.

2.2 The Lymphatic Valves

The lymphatic valves can be considered to be similar to those of the heart, in terms of mechanics, efficiency and the importance of flow behind the valve leaflets. The main differences are the dimensional scales, the range of speed of the liquid through

the valves and the details of the structure of the valves themselves. The bulbous areas that can be found behind the lymphatic valve leaflets have been suggested to be sinuses by Leak and Jamuar [50]. We speculate that these act in a similar manner to the sinuses in the heart valves, encouraging recirculation and aiding efficient closure (see chapter 8). Further efficacy may be gained by endothelial extensions on opposite leaflets [51], which form a tight seal in the closed position allowing the valves to withstand high retrograde pressures.

The lymphatic valves can also be compared to those in the venous system. However the differences in the networks cause different distributions of damage in the two networks [52]. the lymphatic valve damage appears to be more widespread where it occurs. The lymphatic valves do however have a remarkable ability to withstand retrograde pressure [51]. The maximum flow and pressures that can be borne before damage to the valves occurs is highly relevant to cases of edema.

The type of flow makes a difference to the stresses that may be expected within a valve. Steady laminar flow has been indicated in studies by Gnepp and Green [53] from observations of the endothelial lining of the lymphatic vessel walls. They found that the endothelial cells are long and thin, lining up with flow; indicators of laminar flow (in turbulent flow the cells are likely to be shorter and less aligned). Laminar flow is likely to cause far less damage to the materials involved.

It is agreed that the valves are all one way valves and are opened or closed passively, requiring a positive pressure gradient downstream in order to open. There appears to be little or no muscle in the wall near the valve [53] or in the cusps or elastic fibres [54] indicating that this is a passive mechanical component. The anatomy of lymphatic valves is discussed further below but the physiology is detailed in chapter 8 as it informs the valve modelling detailed there.

2.2.1 The Anatomy of Lymphatic Valves

There is some disagreement within the literature as to the structure of lymphatic valves. The postulated alternatives are a simple bicuspid description ([55] Gnepp

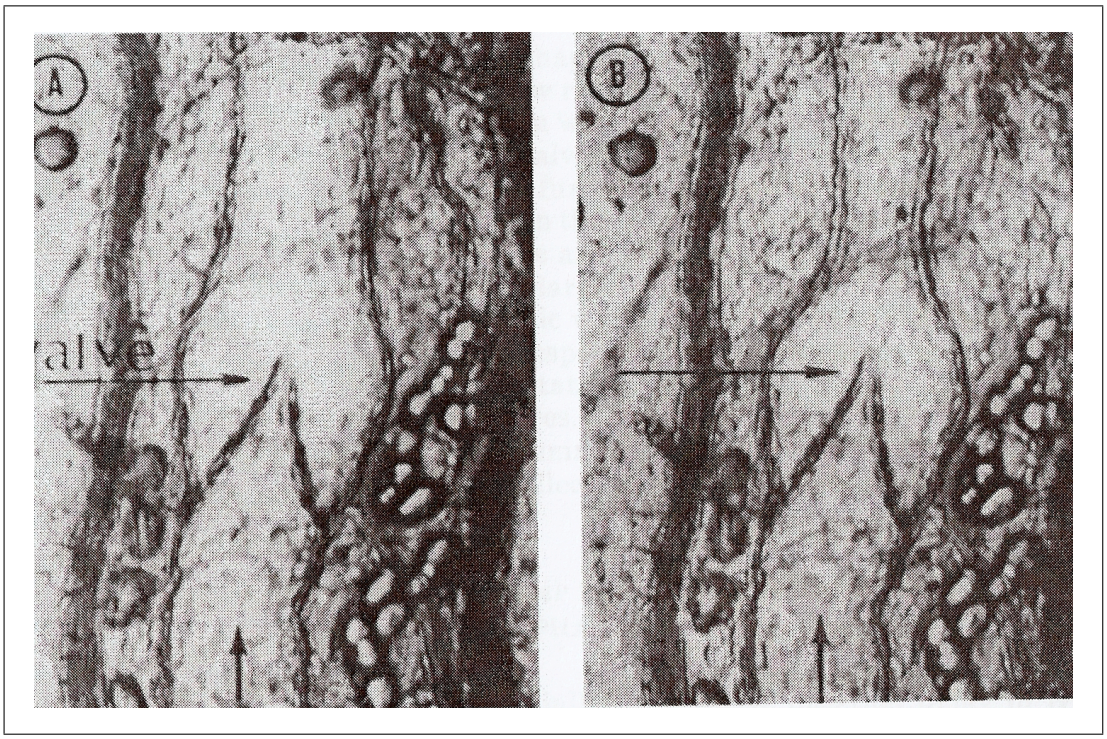

Figure 2.6: Cat mesenteric lymphatic valve taken from [27] relaxed (A), pumping (B); scale × 183

[12], [53]) and a funnel-like structure. The funnel-like structure was reported by Lauweryns [56, 57] in the lung lymphatics (a similar aperture structure was also found by Gruntzig et al [58] in the conjunctiva of bovine eyes). Lauweryns found 25 out of 26 valves were funnel shaped and extrapolated this basic structural pattern throughout the body.

The biscuspid structure is however much more widely reported. Mazzonni [55], reports the presence of bicuspid valves in the skeletal muscle, McHale (private correspondence) in the mesentery and Gnepp performs further such analysis [12], [53]. Gnepp considers Lauweryn's [56] extrapolation unwarranted and concludes that the conical or truncated structure is not part of the large collecting lymphatic channels and thoracic ducts. He does however conjecture on the possibility of two different structural patterns for valves.

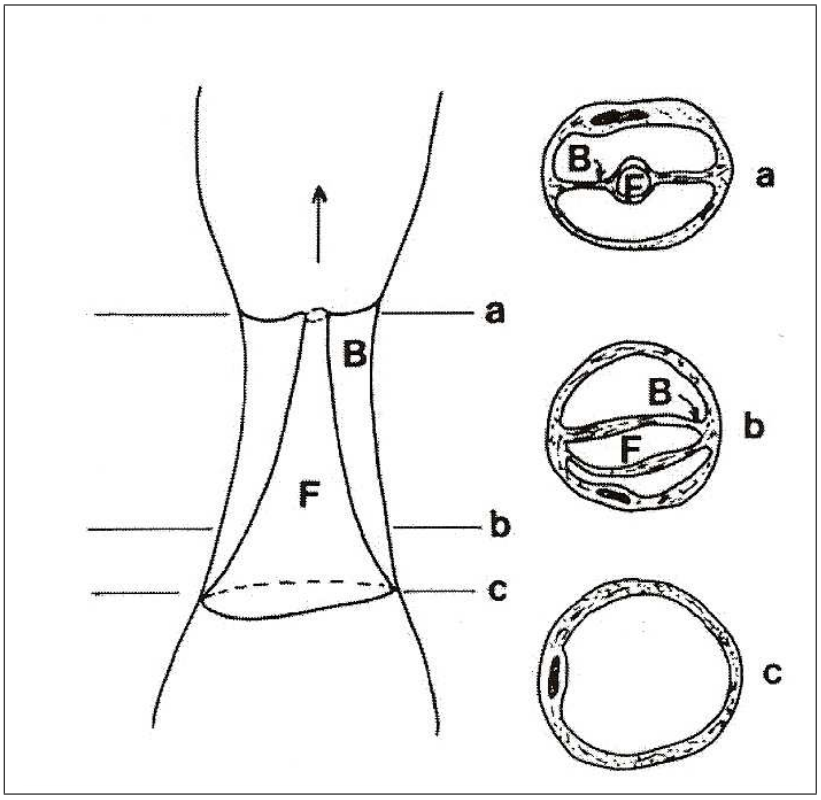

Figure 2.7: Lymphatic valve schematic by Schmid-Schonbein [11]. This is likely to be referring to the microlymphatic valves

The shape described by Schmid-Schonbein's review of the lymphatic system [11] shown in figure 2.7 is similar to the funnel shape but has the addition of buttresses attaching this funnel to the surrounding tube. Schmid-Schonbein's review centres around the microlymphatics so it seems most likely that he was representing microlymphatic valves by this schematic, which would explain its difference to those most often described in larger vessels. It is unclear whether this shape has been observed from experiment or is intended as a general shape from a literature survey. Schmid-Schonbein particularly mentions that the funnel-like shape works well in soft tissues and viscous flow even with irregular channel shapes and low flow rates. This would lead to particularly efficient closing on small back flows and the funnel-like valves can operate under extraordinarily low flow rates without regard to the shape of the channel in which they are embedded. The efficiency can be increased by increasing the funnel length or decreasing the diameter as found in the initial lymphatics. To follow this conjecture on, one could assume that the aperture section of the valve is only required in the smallest vessels, and becomes smaller as the vessels increase in size, eventually disappearing altogether.

We speculate that a basic valve structure could look like any of the shapes reported if the dimensions of the funnel, leaflets and buttresses are altered depending on the required sensitivity and ability to withstand back pressure. It would make sense if the dimensions were altered in different positions within the body to cope with different surrounding tissues conditions, size vessels and in order to be more sensitive in the areas of low pressure gradients. An examination of the valves' efficiency, sensitivity and retrograde pressure stamina in different positions of the body would enable improvements of models of the entire network.

In the current study (based on the bovine messentery) the valve structure is assumed to be the bicuspid shape. The valves in the bovine mesentery have been extensively investigated by McHale (private correspondence) and can be described as 2 pouches on opposite sides of the vessel. See figure 2.8 of a schematic of such a valve developed in collaboration with McHale.

Indeed there has been no contradictory evidence from experiments based on the

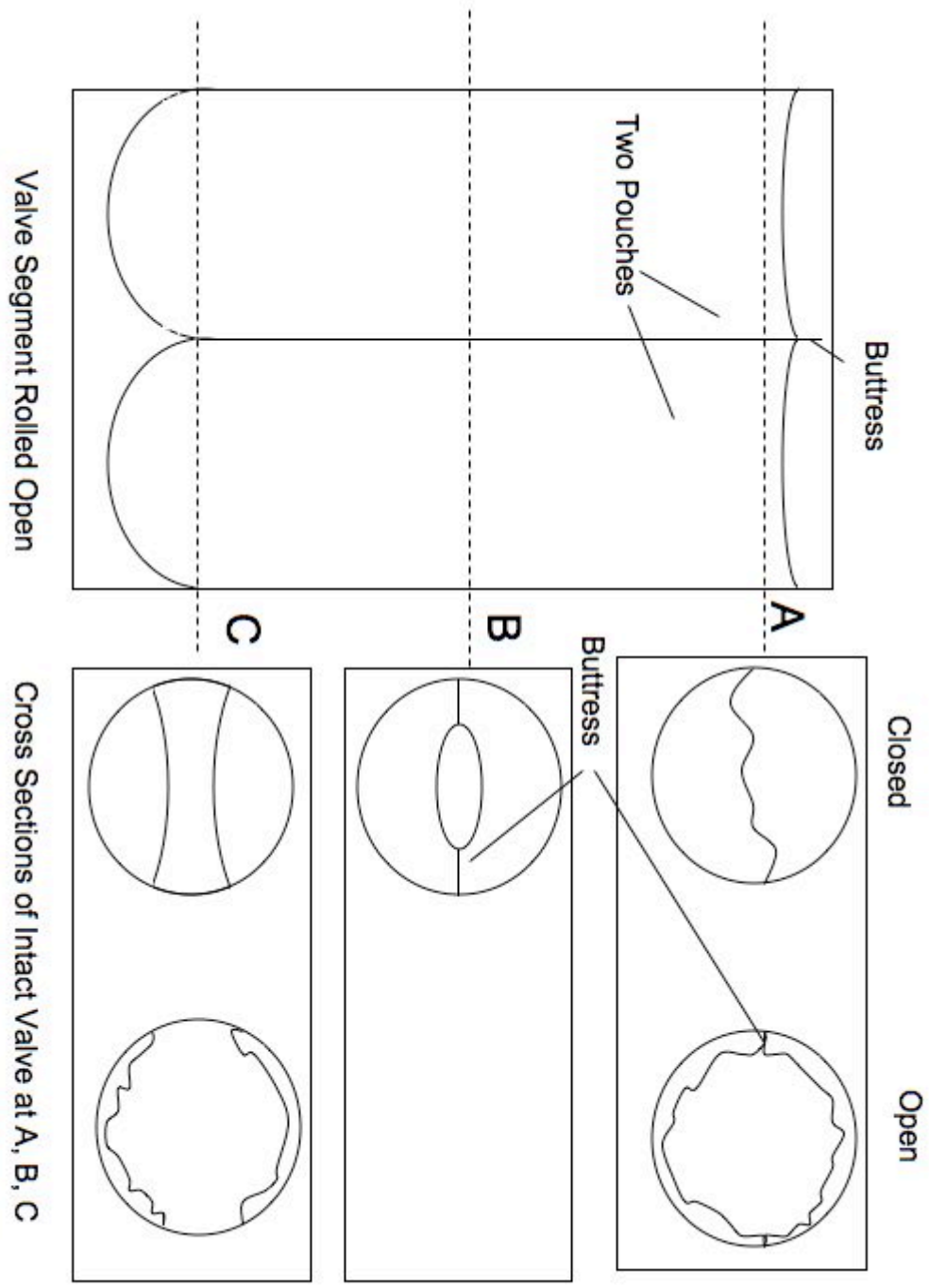

Figure 2.8: Schematic (developed with McHale) of valves constructed from pouches found in the bovine mesentery

collecting lymphatics of the mesentery. Measurement of dimensions of lymphatic valves can be performed from published micrographs eg [59, 53, 50].

2.3 Terminal Lymphatics

The microcirculation of the lymphatic system has many unanswered questions but is not the focus of this project so only a brief overview is included. The main difference between the terminal and collecting lymphatics is that the vessels do not contract, apart from that the mechanics can mainly be considered to be a scaled down version of those in the collecting lymphatics.

On passing from the interstitium to the lymphatic system tiny valves have been found and described as flaps of endothelial cell, overlapping the neighbouring cell [37]. Trzewik [60] fixed sections with the valves open and closed and observed fluorescent microspheres passing through the endothelium into the lymph vessels. These microspheres could not be forced out again by increasing the internal pressure. (Also see section 2.2.1 which speculates on the variation of valve shape to suit the conditions in a particular vessel.)

There is much speculation about how the liquid is moved into and along the microlymphatics, where the walls are not able to contract. There are 3 main theories regarding the transport mechanisms involved:

1) Uptake by osmosis

If a solution of protein (volume 1) is seperated from a volume of water (volume 2) by a perfect semi-permeable membrane, the smaller water molecules will be 'drawn' into the protein solution to level out the concentration of the two solutions, increasing the volume of 1. This osmotic pressure is an important method of transport in the body. However the lymphatics need to also drain the larger proteins. If the semi-permeable membrane is not perfect it will also let through some of the larger molecules, however the osmotic pressure will be lower. Curry et al [61] are currently

investigating the endothelial glycocalyx in the blood circulation for its possible effect in creating an osmotic pressure for absorption. Perhaps there is a similar mechanism in the lymphatic vessels.

2) Squeezing of exterior muscles

Moving an arm or leg compresses the lymphatic vessels in that region thereby acting as a pump. This would not however contribute to fluid propulsion during night rest and the system does not stop entirely at this time.

3) Pressure drop further up network

As described in [11] the contraction cycle further up the system could cause a large enough pressure difference to generate flow. This would require a negative pressure in order to create the necessary back pressure. There is little evidence to support the vessels' ability to keep open against an external pressure although the filaments may help with this (see section 2.4).

The only method of propulsion in the terminal lymphatics that has been universely agreed upon is the contraction of the external muscles. It does however seem incredible to this Author that at these low pressures; firstly the fluid gets into the microlymphatics and secondly, goes anywhere within them.

2.4 Edema

During edema the lymphatic system is unable to drain enough interstitial fluid to keep the quantity of fluid in the intersitium within the normal limits. This may be due to a compromised lymphatic system (due to surgery or disease), a larger amount of fluid in the interstitium (due to excessive leakage from blood vessels) or both. Certainly each can cause the other. Edema can be very hard to recover from; it is unclear how much of this is due to damage to the system from the disorder, or from mechanical effects inherent to the system. The lymphatic vessels

are abnormally full but the contractions are irregular and of low amplitude [10]. An already failing lymphatic system is further disabled by the resulting disorder due to the effects of the high pressures. The lymph capillary pressure goes from around 8 mm Hg (1066 Pa) to 15 mmHg (2000 Pa) in edema [62]

Overstretching (due to high pressure) of the blood vessel walls is well know to cause damage to the elastic properties of the walls, the muscles in the walls and the valves (causing such disorders as varicose veins). Therefore in the lymphatic system one would expect it to have similar detrimental effects on the elasticity of the walls, integrity of the valves and the ability of the muscles to pump.

According to Picard [52] when lymphatic valve damage occurs it is usually widespread throughout the system rather than just in the peripheral circulation as found in veins. During studies into the development of edema Olszewski [63, 10] noted that overloading of the lymphatic vessels lead to dilation of the vessels throughout the effected limb and therefore damage to the vessels and the valves, leading to valve incompetency .

In healthy collecting lymphatics the pumping of the vessels themselves - the intrinsic pump - is the primary method of transport. This is very important during night rest, anesthesia and immobilization as well as for those with damaged peripheral motor neurons. This mechanism becomes less effective in lymphedema because it is not able to produce a high pressure difference and the valves are either damaged or are not efficient at these low gradients [10].

Lymphoedma can remain dormant for years with a brief bout immediately after surgery only to resurface indefinitely years later. Perhaps this is due to a tendency for incomplete re-growth of lymphatic vessels over damaged areas [64] which are inadequate for the volume of drainage needed. A smaller regrown vessel would be under strain more of the time as it would be overloaded. This could lead to a gradual build up of damage to the elasticity and the vessel's ability to pump, even effecting the competency of the valves. Alternatively, such a vessel is more at risk from a build up of pressure, causing the disorder itself and possibly damage which would further exacerbate the disorder.

The delayed onset of Edema was observed in experiments on dogs by Olszewski [63]. After an initial onset of edema some regrowth of vessels occurred and the edema went away. Scars began to form and lymph stasis began to occur 8 months to years after the original edema. There were two different routes associated with this. For the first fibrosis of the lymphatics occurred causing loss of permeability of the terminal lymphatics. In the second route the lymph vessels were dilated causing valve incompetency, overly compliant vessels and ineffective muscular pumps.

There is some speculation as to whether contractions are detrimental to flow during lymphoedema, simply adding resistance to an already high flow (this may depend on the gravitational contribution to flow). Returning to the principle that during a contraction cycle the vessel never fully relaxes; artificially causing complete relaxation of the vessel could decrease resistance, conserve energy and increase flow if the pressure gradient is in the right direction. It may also reduce damage to the muscles and valves which would otherwise be submitted to a higher strain. The system would act as a conduit with a larger radius according to [8, 9] (see chapter 9.2). This is supported by the experimental findings of Pippard and Roddie, that the addition of isoprenaline to a perfusate of saline causes reduction of resistance, indicating that the muscle tone and/or spontaneous active contractions impede flow [46, 47]. Olszewski however [10], showed that flow only occurred in leg lymphedema when there were contractions.

Various effects should be more thoroughly investigated before advising relaxation of the vessels during lymphoedema. These include gravitational effects, the effects of a chain of lymphangions, a more realistic network and the possibility of transient waves when the vessel is completely relaxed. Also see sections 2.1 about the mechanics of elastic tubes and section 9.2 which discusses the major current model by Quick, Stewart and colleagues which suggests the use of relaxation of the vessels during edema.

Chapter 3

Computational Modeling Background

This project centers around a 1-d model of a section of collecting lymphatic vessel. This uses the 1-d Navier Stokes equations coupled with valve and wall models. This modelling technique was chosen as a balance between CPU time and the detail of the flow. This unit could later be taken to form larger areas of lymphatic network but even at this level begins to show the variation within different parameters which can be used to inform treatment of the disorder.

Computational Modelling techniques within fluid dynamics have made many notable advances in recent years. This has been possible as a result of the increase in computational power available. These techniques have been applied extensively to the cardiovascular system and other areas of the body and can be modified to suit the lymphatic system (where there has been little or no such application). In modelling aspects of the lymphatic system; useful parallels can be found representing the elastic walled tubes, valves, contraction waves and branching networks. There has been work worth comparison within the heart and venous valves, blood vessel walls, bifurcating tubes and their networks (eg in the lungs or blood circulation) and the peristaltic-like contractions for the transport of urine [65, 14] (this also involves an intrinsic contraction travelling along an elastic tube).

Representing the fluid 'lymph' is more simple than modelling blood due to the absence of red blood cells, which have a major effect on the properties of the fluid. Lymph is a mixture of plasma and proteins [12, 17] and can be assumed to have properties very similar to water at the current level of modelling detail as described in section 1.1.1 .

This chapter goes on to discuss the modelling of flow phenomena in collapsible tubes, the setup of various computational techniques and the previous applications within this type of problem. In this project the properties of the walls are examined in 1 dimension (1-d) representing a circular tube (see chapters 5 and 6) and the valves are examined in 2-d (see chapter 8) giving greater accuracy for this more complicated shape. This could then be used to inform the 1-d model.

3.1 Modelling Flow Phenomena in Collapsible Tubes

Various phenomena have been found to present at different levels of inflation of a partially collapsed tube [66, 67, 14, 68] and have proved challenging to model computationally. These include flow seperation and flow induced oscillations. The full 3-d solution (using the Navier Stokes equations coupled to the equations of large displacement shell theory) is just not practical for most biological tube problems [67]. This led to the development of 1-d methods including various adhoc assumptions.

One of these is the tension term, first described in the land mark paper by Cancelli and Pedley [68]. This allows the representation of self-excited oscillations but cannot show some other types of oscillation or energy losses due to departure from stream line flow.

When investigating the major circulation, the compressive force from external pressure P_{EXT} can cause the tube to buckle, going from a circular to elliptic cross section. In blood vessels the possibility of transient waves and the characteristic shapes at different pressures have been extensively explored. In this model of the Lymphatic system however, it is assumed that no transient waves or buckling occurs (see sections 2.1 and 2.4). The radius simply decreases during a contraction,

maintaining the circular shape of the vessel. In reality transient waves are likely to be negated by the contractions although verification of this is left to future work.

In the lymphatic system it appears that the collecting lymphatic tubes are always partially contracted, generating an internal pressure which makes it less likely that collapse will occur. The vessels remain partially contracted even at the relaxed phase of the cycle. Muthuchamy [69] found the diameter in relation to the passive diameter going from 60 % during systole to 90 % during diastole. This was also confirmed by the experimental work accompanying this project see section 4. A very small pressure is required to inflate these vessels, in fact they will inflate simply floating in a glass of water. Collapse - and therefore these phenomena - are more likely to occur in completely relaxed vessels; so for the lymphatic system possibly in cases of edema. Olszewski [10] mentions the presence of superimposed waves in cases of lymphedema. This phenomena should be thoroughly investigated before artificially inducing complete relaxation of the smooth muscle during edema and their effects included in any models which recommend this course of action (eg the model of Quick, Stewart and Collaborators discussed in section 3.2, also see the section on edema 2.4).

In the experiments by Arkill in chapter 4 and all of the computational work during this project, the external pressure is lower than the internal pressure. We can therefore state that we were not representing any conditions that collapse would occur in, but the inclusion of the damping (γ) and tension (T) coefficients in the model should allow for representation of some of the phenomena involved, should such investigations prove relevant in the future. A 1-d model using these two terms is now generally considered the limit to how far a 1-d model of an elastic tube can usefully be modified [14].

Much of the modelling work in this area has been done representing a setup similar to the Starling Resistor.

A collapsible tube is mounted between two rigid tubes, while the pressure drop $P_1 - P_2$ causes flow Q and radius' a_1 and a_2. P_{EXT} can also be used to vary the radii and flow. This arrangement has been used extensively to investigate oscillations in

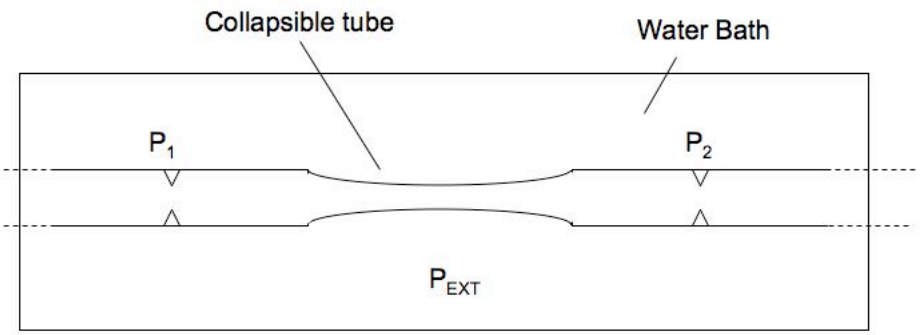

Figure 3.1: The Starling Resistor type setup is often used to model elastic tube behaviour

collapsible tubes (as the Starling Resistor) but the same setup is useful for examining elastic tubes in general. This method is still used for in vitro experimentation (see chapter 4), so it is useful to try to replicate the conditions in a model to match the parametric configuration. In this experimental set up, contractions can be induced or prevented and various parameters investigated (including the dynamics of the walls). Flow can be manipulated using the upstream and downstream pressures, in order to examine the passive wall properties. For example, as the downstream pressure increases, just the radius increases as the vessel stretches, without initiating flow as the valve holds.

In choosing the level of detail for the model , various different modelling methods were explored from lumped parameter, 1-d, 2-d and 3-d representations. Most existing models of the lymphatic system are lumped parameter models [70, 71], except for the model by Reddy from 1975 [4]

3.2 Lumped Parameter Models

0-d or lumped parameter models use electric circuit analogies to represent a system, these are often based on a setup like the Starling resistor. They are beneficial in

modelling large complicated systems in combination with other techniques in order to save on processing time and power. However some lumped parameter models of the lymphatic system are of small sections of vessel. Work in cardiovascular mechanics [14] has shown this type of modelling is limited for looking at the detail of biological systems but has advantages in representing large networks where speed is required and the parametric detail has already been found from more precise techniques. Current lumped parameter models of the lymphatic system include work by Lambert and Benoit [71] and Quick, Stewart and colleagues [8, 9, 70, 15, 72].

The model by Lambert and Benoit is a simple model describing a series of contracting pumps seperated by valves. The rate of lymph flow is decided by the Starling relationship and the pressure gradient allows filling of the first segment, while pressure or volume can be set to trigger ejection. Valve competence is adjustable and interstitial volume provides the driving force for lymph filling. There is a choice of a passive or active network (ie just external contractions or the addition of intrinsic contractions).

The most up to date and extensive lumped parameter model of the lymphatic system comes from Quick, Stewart and colleagues [70]. This uses blocks of an electrical analog model and was published from 2003 onwards. These blocks are connected in series to form a 'crude transmission model' using a technique developed in [73] for modeling vascular haemodynamics and introducing the 'time-varying elastance' in the wall. This time varying elastance concept was originally used to model the behaviour of the heart by Suga and colleagues in 1972 to 1974 (see [70]) but has also been used to model sections of the arterial tree [74, 73]. This model has provided significant physiological insights but as a lumped parameter model has its advantage in larger areas of network and analyse the interaction between the fluid and elastic walls. It would benefit from a greater understanding of the lymphatic vessel mechanics from experiment and 1 (or higher) dimensional models such as the work presented in this thesis. Currently some details of the wall behaviour such as the passive relaxation of the wall and the radius peak at the start of contraction are not presented by this or other lumped parameter models. The variability with time

in contraction period and magnitude are not included.

The model was first used to describe a single lymphangion [70], but was developed to represent several lymphangions and has now been used to investigate various properties including incomplete relaxation in [15], the benefits of the vessels acting as a conduit rather than a pump in edema in [70] and the necessity of coordinating contractions in [72]. Their work is discussed further in comparison to our work and the literature in section 9.2.

3.3 1-d Models

1d models introduce 1 spatial dimension in addition to the time dependence already considered above. They can provide significant insights that are missed by 0-d models by including spatial resolution and therefore the interaction between the fluid mechanical and elastic forces. There are many examples of 1-d models in flexible tubes [14], some introduce terms to represent additional factors such as the tension and damping in the walls as shown in equation 3.9. For the detail of modelling useful in this project a 1 dimensional analysis should be adequate to examine the behaviour of the walls due to the simple flow involved at this stage (e.g. so we do not need to model flow separation or turbulence). However 1-d models can fail to represent some conditions in more complicated flows. If an elastic tube begins to collapse the shape of the vessel becomes more complicated, with a 'dip' at the centre. This causes the flow to separate and the resistance will not be accurately represented using only 1 spatial dimension. Secondly different types of oscillations can develop in elastic walls; some unstable modes of such oscillations cannot be represented in 1-d models. Lastly 1-d models cannot show viscous dissipation at high Reynold's number (Re) flows, however the Re numbers for the lymphatic vessels are relatively low.

3.3.1 Reddy

Surprisingly, the most detailed 1-d analyses of the lymphatic system was completed by Reddy as long ago as 1975 [4]. This was based on the Navier Stokes equations, coupled with a wall model in which it was assumed to be a thin walled tube.

The laws of mass and momentum for the axisymmetrial flow of an incompressible Newtonian fluid in a cylindrical tube.

$$\frac{\partial u}{\partial x} = -\frac{1}{r}\frac{\partial (rv)}{\partial r} \tag{3.1}$$

$$\frac{\partial u}{\partial t} + u\frac{\partial u}{\partial x} + v\frac{\partial u}{\partial r} = -\frac{a}{\rho}\frac{\partial [p+\rho g z]}{\partial x} + \frac{\mu}{\rho}\left[\frac{\partial^2 u}{\partial x^2} + \frac{1}{r}\frac{\partial}{\partial r}\left(r\frac{\partial u}{\partial r}\right)\right] \tag{3.2}$$

$$\frac{\partial p}{\partial r} = 0 \tag{3.3}$$

$$\frac{\partial u}{\partial t} = -\frac{1}{\rho}\frac{\partial}{\partial x}[p+\rho g z] + \frac{1}{\rho r}\frac{\partial}{\partial r}(r\tau) \tag{3.4}$$

$$\tau = \mu\frac{\partial u}{\partial r} \tag{3.5}$$

Continuity Equation:

$$\frac{\partial Q}{\partial x} = \frac{-2Q}{a}|_{r=a} \tag{3.6}$$

Momentum Equation:

$$\frac{\partial Q}{\partial t} = -\frac{\pi a^2}{\rho}\frac{\partial}{\partial x}[p+\rho g z] + \frac{2\pi a}{\rho}\tau|_{r=a} \tag{3.7}$$

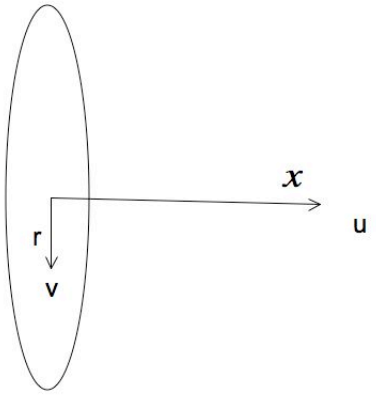

Figure 3.2: The coordinate system used by Reddy [4]

Symbol	**Parameter**
h	velocity in the axial direction
x	axial coordinate
Tr	radial coordinate
τ	shear stress
ρ	density
g	gravity
p	pressure
t	time
Q	flow

Table 3.1: Symbols used by Reddy [4]

where τ is the shear stress, Q the flow, a the radius, P the pressure and x the longitudinal position)

Reddy went on to represent the whole system by extending this model [6]. He used 1 computational cell to represent each lymphangion.

Stembera, Marsik and colleagues [75, 76] actually produced a model of blood vessels; but it is a good example of the progress in one dimensional models and the techniques are easily transferable. Since Reddy's work it has become accepted practice in Biofluids to use 'the tube law', which assumes a thick walled tube. Stembera and Marsik's model also has the addition of a damping term and one to represent longitudinal tension as explained in section 3.3.2.

Using these extra terms Stembera and Marsik describe the thick walled tube equation as below.

$$p - p_e = \phi\left(\frac{A}{A_0}\right) - \frac{T}{D_0}\frac{\delta^2 A}{\delta x^2} + \gamma\frac{\delta A}{\delta t} \tag{3.8}$$

3.3.2 General 1d Method

This section outlines a general method for modelling elastic tubes based on the work of Reddy and using additional terms from Stembera and Marsik (which are also mentioned in Grotberg and Jensen's review [14]) .

In the most recent one dimensional wall models of flexible tubes, partial differential equations - the Navier Stokes equations - are used representing mass and momentum conservation as described in section 3.3.1 (also see section 5 for more on their application) .

These Navier Stokes equations are coupled with a pressure/area relation. Reddy's work [4] uses a simplification of the standard 'Thick Walled Tube' equation and assumes a thin walled vessel which does not change in thickness and is a uniform elasticity. A more detailed version of Reddy's work could use this standard thick walled tube model [14, 19].

$$\Delta P = E\Delta a_{out}^2 \frac{(a_{out}^2 - a_{in}^2)}{2(1-\sigma^2)a_{in}^2 a_{out}} \tag{3.9}$$

where E is the Young's modulus, σ is the Poisson's ratio, a_{out} the exterior radius and a_{int} = interior radius.

Flexible tubes can give rise to various interesting phenomena, including elastic jumps, choking and separated flow which can all lead to instability in a 1d computer model. Additional terms have been developed in various 1d models to approximate the consequence of these effects, which are not automatically represented by a 1d model [14]. These aid the stability of the system and prevent singular behaviour. The most important of the additional terms is the tension term T α_{xx}, which approximates the effects of longitudinal tension T, where α_{xx} is the longitudinal curvature of the wall [14]. Further representative terms include bending stiffness, wall damping and wall inertia. Stembera and Marsik [75] use a simple yet effective combination of this tension term and a damping coefficient as shown in equation 3.9.

3.4 2d/3d Modelling

The following section discusses relevant techniques and applications with 2-d and 3-d modelling. These techniques may be required in areas of biofluid research involving more intricate mechanics such as occur during flow seperation and turbulence. Greater resolution may be required in order to represent such phenomena in a stable and accurate manner. There has not been any previous attempts to study the lymphatic system to this detail but these techniques have been used to model valves (including heart valves [77]), buckling, seperated flow and aneurysms [78].

3.4.1 Method

There are various packages available which can be used to model 2 or 3 dimensional flow for example, Fluent (the commercial code chosen for this project). The external structure is first generated using software such as Gambit (commercial code). A

mesh can also be generated using MRI or micro CT scans of the actual vessel material which can be translated to Fluent using software such as Simpleware (commercial code). Most CFD modelling programs use the Navier-Stokes equations in 2 or 3 dimensions.

Firstly this type of model can be static, a freeze frame of conditions taken to convergence. Secondly it can be dynamic, a step by step sequence in time which must be converged at each time step (and is therefore much more time consuming). The static models save on processing time and are therefore ideal for modelling conditions that do not change with time while a dynamic model is necessary for modelling varying conditions.

Fluid Structure Interaction (FSI) can be used to model both the fluid and the surrounding structure (ie the vessel walls) in detail, although there are other ways of approximating these effects. Usually solving FSI problems involves linking two seperate computer codes (although there are programs such as OpenFOAM which are able to perform complete FSI). Usually one program (e.g. Fluent the commercial CFD code) calculates the motion of the fluid to convergence and passes the solution to the other program (e.g. Abacus, the commercial stress analysis program). This second program can then calculate the resulting structural motion of the solid element. The fluid mesh must then be updated to account for this motion. The solutions are thus passed back and forth until there is no further change in either. A third program is usually required in order to control the passing of the information between the first two (eg MPCCI commercial code). Unfortunately full FSI in 2 or 3-d is a very time consuming technique (for example a PhD has recently been awarded for the modelling of a single heart valve leaflet in this manner).

Fluent does however also contain capabilities for approximating the motion of solid materials (without solving the full stress problem) as well as the full solution for the fluid. Either the motion must be prescribed or the fluid can effect the motion of simple shapes based on their moments of inertia. This is termed 6 DOF modelling within Fluent.

For the valve modelling during this project the 2-d approximations allowed within

Fluent are considered to give an accurate enough solution, for the more detailled study of the valve in chapter 8 given the wide scope of this project.

3.5 Multidimensional Modeling of Other Systems

This thesis begins to work towards another focus of modern research within Biofluids; using a combination of the available techniques to patch together information over a larger area (in this case the lymphatic system. Existing examples include larger areas of circulatory networks modelled using 1-d/0-d techniques and informed by more detailed 2-d/3-d models. A research group at Sheffield University have used multi-scaled modelling to represent the left ventricle and the behaviour of a prosthetic heart valve [79]. A particularly extreme example is the 'Physiome Project', an international consortium working towards a whole body system, led by Hunter from Auckland University in New Zealand and described during the Plenary lecture at the 5th World Congress of Biomechanics .

For the lymphatic system it is logical to look at the valves and the walls in detail (2-d or -3d) and then model the overall system using those results in a 1-d or/and a 0-d model.

3.5.1 Heart Valve Models

Modelling of heart valves started with the work by Hung and Schuessler, and Au and Greenfield [80, 81] in the 1970s. Some of these numerical experiments have focused more on evaluating heart prosthetics and designing new ones such as the work by Hose, Narracott et al [82], who developed a model of a single leaflet mechanical valve to evaluate a simple analytical method to aid design of prothetic valves. However this section aims to focus mainly on the work involving modelling the native valves which are likely to perform similar mechanics to the lymphatic valves. In the 1970s, 2-d models were formed using a vorticity-stream function formulation of the Navier-Stokes equations. This proved to be convenient for 2-d but not 3-d analysis. Hung

and Schuessler [80] used this work as an aid to the design of heart valve prosthesis. They were able to include leaflet motion by manipulating the boundary conditions on the leaflet surface.

In order to predict 2-d fluid structure interactions, Peskin [83] developed an immersed boundary method to couple blood flow to the structure of the heart and its valves. They then used it to predict flow through the mitral valve mounted in a straight tube and in the left heart chamber in [84]. They then went on to use it for prosthetic valve modelling. The early model was only valid for a low Re [85] but this was later extended to account for a larger Re, showing no qualitative differences between flow at Re = 20 or Re=200. (Our calculations for Reynolds number from the experimental work in chapter 8 give a value of 56, falling inside this region.) A further 2-d solution was provided by De Hart et al [86] who developed a 2-d fictitious domain finite element code to predict the unsteady flow in the aortic valve.

3-d models began to be developed in the mid to late 1990s. Computer resources allowed research into 3-d simulations of mechanical heart valves. Often this had to be done on only a fraction of the valve due to the computing time involved.

Peskin and McQueen [87, 88] extended their 2-d immersed boundary method to 3-d and computed the flow in the whole heart (although the Re was much lower than in the physiological range. Their method was also applied to heart valves [89]. There are however problems extending this method to predict the turbulent flow that often occurs in diseased or mechanical heart valves.

De Hart et al [90, 91] extended their fictitious domain fluid structure interaction code into 3-d. They used this to predict the flow and motion of a type of prosthetic valve and the native heart valve.

Chapter 4

Experimental Methods

4.1 Introduction

In partnership to this computational project, Kenton Arkill undertook experimental work (see sections 4.2.1 and 4.2.2) to provide input reference data and in vitro data to compare the computational model against. The discussion and conclusions in sections 4.2.3 and 4.2.4 are informed by the group's research and section 4.3 contains a table of relevant experimental parameters from literature and Arkill's experiments.

4.2 Experimental Work

4.2.1 General Method

Collecting lymphatics were excised from bovine mesentery at an abattoir (AIBP, Clones, Co. Monaghan, Ireland or Stillmans, Taunton UK) immediately after death, before the fatty tissue could solidify. The vessels were placed in normal Krebs solution (with 95% O_2, 5% CO_2 gas mix, BOC) and kept at 4 C until warmed for use at 37 C. The vessels were cannulated at both ends and immersed in a purpose-built, Krebs-filled bath at 37 C and connected to pressure reservoirs at both ends. Pressure transducers (RS components) were placed in the inflow and outflow lines.

Typically the vessel segment contained 2-4 lymphangions. A typical vessel is shown in figure 4.1.

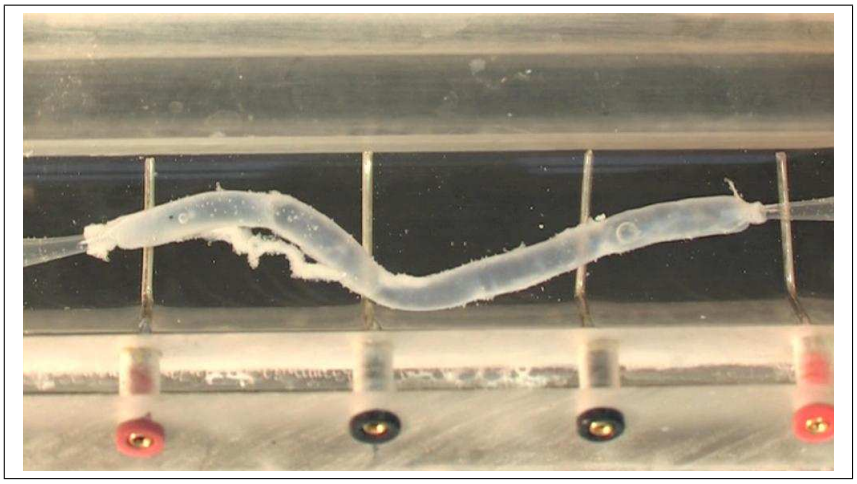

Figure 4.1: An isolated perfused lymphatic vessel scale × 0.71

Static Compliance

L For static compliance measurements the vessels were imaged with a long focal length microscope (adapted Wild 10) with a Nikon Coolpix 4500 camera attached. The external diameter was measured as lumenal pressure was varied between 0 Pa and 1500 Pa, with particular attention to the 0 - 500 Pa range where little previous data is available [92, 5]. The preparation was stabilized before measurement by performing a number of cycles over the full pressure range and images were acquired immediately after each pressure step.

Young's Modulus

The Young's modulus was calculated using the 'thick walled tube' model (see section 3.3.2). The major uncertainty in the calculation was the evaluation of the wall thickness. Several methods of obtaining the wall thickness were investigated (including density measurements, histological sectioning and traveling microscopy). The most consistent method was to add Evans Blue to the lumen after the pressure-

radius measurements had been taken which rendered the inner wall clearly visible and measurements could then be obtained from the digital images.

Dynamic - Radius time Relationships

Pumping vessels were observed using a video camera (Canon XL2 Mini DV) in the same experimental apparatus. Stills were taken from the output video to determine radius-time relationships. Pressure-diameter measurements were taken in the maximum and minimum contractile state.

Damping Coefficient

$$\gamma \frac{\partial A}{\partial t} \tag{4.1}$$

The damping coefficient, γ described in section 5.3.1, was obtained by use of a purpose-made mechanical testing rig. Loops of vessel approximately 1.5 mm long were placed over 2 steel rods (0.8 mm diameter), one fixed and attached to a force transducer and the other to a computer-controlled stepper motor. The vessels were stretched and relaxed 6 times at 0.09 mm/s before force-extension data was taken at extension rates between 0.09 and 0.50 mm/s. γ was calculated, determined as the gradient of the force against strain rate (at constant strain) curve. The area of the sample was defined as the width of the loop. The thickness was determined from photographs being clearly visible around the support wire. The extension was taken within the toe region of the force-extension curve, which covers the physiologically relevant range.

4.2.2 Results/Discussion

Static Compliance

The images were analyzed in Image J (NIH, USA) to derive the diameter at several locations along the vessel. The resolution was 7.5μm per pixel.

Static compliance measurements all showed the same characteristic shape, illustrated in figure 4.2 Initially there is a linear slope followed by a sharp transition to a region where the vessel no longer expands with increased pressure.

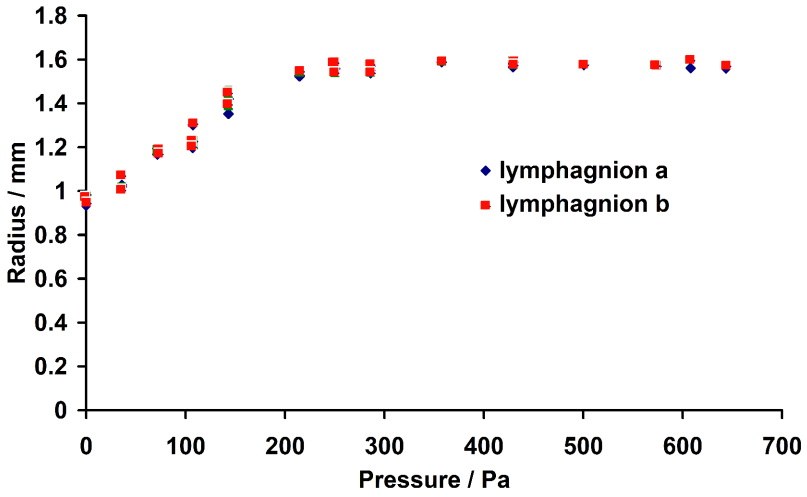

Figure 4.2: Experimental results for static compliance

Young's Modulus

The calculated Young's modulus is (1200± 700) N/m^2 (n = 10 samples measured), which agrees with the results of Deng et al [5], though it is lower than other reports e.g. [92]. The variance in the measurements was largely due to uncertainties in the wall thickness and the initial diameter measurements. The marked increase in Young's modulus occurred at a strain of 1.1 ± 0.4. No consistent pattern of variation in elastic properties along a lymphangion could be established.

Dynamic Characteristics

The effects of mean luminal pressure (with no net pressure gradient along the vessel) on contractability are shown in figure 4.3, which agrees with previous work by Gashev et al [44] and Muthuchamy et al [69]. In relaxed vessels there is an initial

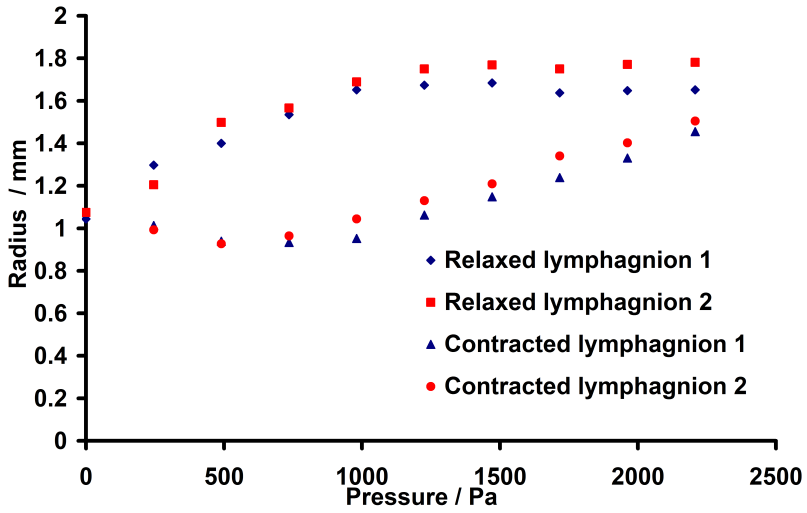

Figure 4.3: Compliance of a pumping vessel from experiment

linear section followed by a pressure-independent region of lower compliance. So the relaxed dynamic results show a similar shape to the static compliance curve. In the contracted vessel an almost converse pattern is observed with an initial pressure independent region giving way to a linear portion. The slopes of the two linear regions are almost identical. The largest contractile radius change occurs at approximately the radius and pressure at which the change in Young's modulus occurs.

The radius-time measurements during pumping as shown in figure 4.4 showed a distinctive 'shark fin' shape over the cycle with a short contractive phase and a longer relaxation phase. The radius variation is slightly greater in amplitude at the mid-point of the lymphangion than at the valve. There is also a sharp increase in diameter immediately before the onset of the contractile phase in the vicinity of the valve, which is not evident elsewhere. In the trace shown in figure 4.4 the contractile wave is in the opposite direction to the flow direction. The pressure therefore peaks at the valve as the fluid is trapped between the contractile wave and the closed valve.

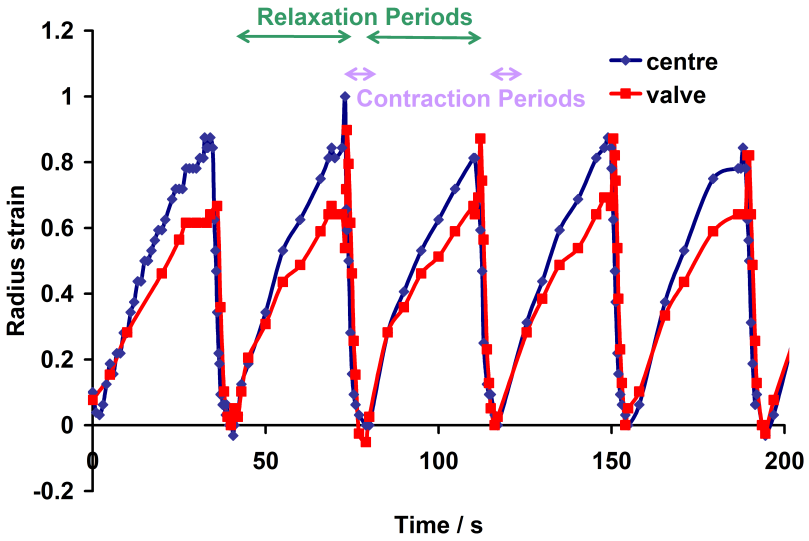

Figure 4.4: Dynamic radius - time from experiment

Damping Coefficient γ

The damping coefficient, γ, has a value of $(7.0 \pm 3.0)10^7$ Ns/m^4 (10 measurements from 5 different vessels). Much of the error arises from the difficulty in determining the point of zero extension as well as the error in wall thickness.

Period

The period was found from the radius time results and varied between 20 and 40 seconds in different vessels.

Speed of Contraction of Wave

A speed of a contraction wave along a 4 cm length of contracting isolated lymphatic vessel was observed using time stills, recording the time for the start of contraction to reach 4 cm along the vessel, was recorded for several repeats. The result of 20 mm/s was intended as a ball park figure for use in the parametric study in chapter 6. From this the phase difference could be calculated, which was used as an input for the 1d model as described in chapter 6. The maximum speed of the fluid was

found to be approximately 20 mm/s. This was also intended as a rough estimate for further exploration in chapter 6. This was found using the video of the pumping vessel and by timing the progress of a bubble inside the vessel, which allowed us to see the rate of flow inside.

Tension

An estimation for the longitudinal tension T in the lymphatic vessel walls was found by using the following equation:-

$$T = kP \tag{4.2}$$

where k=5. This comes from the equation from work by Patel and Vaishnav in [18] :-

$$S_z = \frac{P}{2}\left(\frac{a}{h} - 1\right) + \frac{F}{2\pi ah} \tag{4.3}$$

Where S_z is the longitudinal stress. The effects of longitudinal tethering can be ignored, so the second term $\frac{F}{2\pi Rh}$ can be removed.

$$S_Z = \frac{P}{2}\left(\frac{R}{h} - 1\right) \tag{4.4}$$

Arkill found that the thickness of the wall was approximately 10% of the radius, since $\frac{R}{h} \gg 1$, this can be further simplified to

$$S_Z = \frac{PR}{2h} \tag{4.5}$$

where $\frac{R}{2h}$ is constant therefore $S_z = k_p$ where k=5.

These assumptions give a maximum error of $\frac{50h}{R}$ % [18]. So for a wall thickness of 10% R a maximum of 5% error

4.2.3 Discussion

The physiological measurements showed considerable variations between vessels. We measured the Young's modulus E for static (non-pumping) lymphangions, and also for individual lymphangions during pumping. The average value of E from the static lymphangions agrees with published values; however the values covered a large range. Much of this variation is likely to be due to factors such as vessel size, position within the system, and animal age, which have not been controlled for (age was partially controlled as all samples here were taken from bovines aged 18 - 36 months). In individual vessels the E values measured for the pumping lymphangions were significantly larger. Perhaps coincidentally, the lymphangions that we successfully set to pump tended to be larger in size as well. Further work to quantify this variability would be valuable, but our immediate concern was the difficulties it created in the choice of parameters for modeling, necessitating an investigation of parameter sensitivity. For our standard 1-d model, as described in the following chapters, we adopted the value of $E_{relaxed} = 2500$ N/m^2, being in the middle of the range of our measurements and the experimental values.

Two mechanical parameters that have not been considered previously in the literature for the lymphatic system are the damping coefficient γ and the tension T. These are investigated further in chapter 5 in order to aid stability of the 1-d computational model.

4.2.4 Conclusions

This Experimental Study provides a useful basis and validation for the modelling of a lymphatic vessel in the following chapters.

We found that the pumping of the lymphangion depends on both the passive and active behavior of the wall. Both the passive and contracted elastic modulus E exhibit two clearly distinct phases, with a low E state initially switching to a high-E state at larger strains see figures 4.2 and 4.3. The effect of muscle contraction is to move these states to higher stresses, leading to the curves shown in figure 4.3.These

two different regions of the stress strain relationships are due to a different material (and therefore its characteristics) in the vessel walls being dominant under different loads.

4.3 Parameters

This section contains a survey of the literature to determine previously measured values for the parameters of interest. Table 4.1 contains a summary of this information. When using the literature results for flow, the method used to obtain the lymph flow should be considered. As Quick et al 2007 [70] note, the standard method of calculating lymph flow using the ejection fraction and contraction frequency to calculate lymph flow is a very unreliable method as it does not account for any passive flow.

Author	**Ar** *BM*	**[93, 94]**	**[5]***CT*	**[95]***BM*	**[44]***RM*	**[96]***HL*	**[12]***HA*	**[38]**	**[92]BM**	**[97]***HL*	**[98]**	**[99]**	**[100]** *GP*	**[101]**	**[27]***RM*
E_C (MPa)	1.2		1.2-36						4.2-27						
a (mm)	1-1.7							3-11							0.04-0.2
Δ a(%)	70														$\leq$50
L (mm)	20														
h	10% a_0														
V_E (ml)										1	0.001				
F_E					0.71				0.55						
U (mm/s)		0.18													
U_{max} (mm/s)	20														
U_w (mm/s)	20								4-5						
Q_{max} (ml/min)	5.89									0.027					
Q (x 10^-7 m^3/s)												3-102			
T_P (s)	20-40	20-120										5.5-30		2.4-6	4-5
T_C(s)	20														0.8-1
P (Pa)													480	50-1200	
P_max (MPa)						3.17									1.2-1.8
P_OV (Pa)														98-265	100-150
P_SV(MPa)				16.5					6.67						2.67
Δ P_W (Pa)							4.5-1200				533				200-400

Table 4.1: Table of parameters from literature and the experiments completed in partnership to this project (see section 4.2.2)

Symbol	Description
O	Ovine (Sheep)
H	Human
B	Bovine (cow)
GP	Guinea Pig)
R	Rat
C	Canine
M	Mesentery
T	thoracic Duct
L	Leg
A	All parts of the body
$\mathbf{E}_C$	Circumferential Young's modulus
$\mathbf{a}$	Radius
δa	Change in radius over cycle
$\mathbf{L}$	Length of Lymphangion
$\mathbf{h}$	Wall Thickness
$\mathbf{V}$	Volume
$\mathbf{F}_E$	Ejection Fraction
$\mathbf{U}$	Velocity
$\mathbf{W}$	Wave
$\mathbf{Q}$	Flow
$\mathbf{T}_P$	Period
$\mathbf{T}_C$	Contraction time
$\mathbf{P}$	Pressure
$\mathbf{P}_{OV}$	Pressure to open valve
$\mathbf{P}_{SV}$	Stamina of valve
$\Delta\ \mathbf{P}_W$	Change in pressure due to contraction wave

Table 4.2: The abbreviations used in table 4.1

Chapter 5

1-d Modelling

5.1 Introduction

Reddy's 1-d model [4] could be brought up to date using some of the modern standard practices; for example the 'Tube Law' and additional terms can be added. The model by Stembera and Marsik [75] is a simple but effective combination of the techniques that can be useful to work from which includes extra terms to represent factors otherwise missing from 1d models. Beyond this, further complication of the computational techniques to model the elastic tube behaviour within a 1-d upwind differencing model would lead to little benefit, due to the limitations of 1-d analysis.

The first step in developing a 1-d model of the lymphatic system was to implement and update the most detailed existing model of the lymphatic system introduced by Reddy [4]. This chapter describes this implementation using the finite volume technique and upwind differencing scheme. Further adaptations to increase stability were found to be necessary.

5.2 The Reddy Model

A length of lymphatic vessel was represented in Matlab as a series of computational nodes, one lymphangion (ie area separated by valves) per node. Each cell was

arranged so only positive flow was possible by setting the flow to zero if it became negative, thus representing the opening and closing of the valves. The Navier Stokes equations were used to describe this flow and were simplified to a 1-d version as in Reddy's method, as shown below (see chapter 3 for derivation).

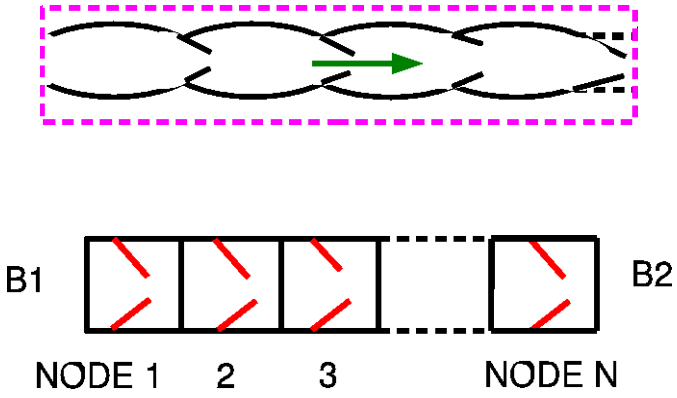

Figure 5.1: Section of a collecting lymphatic vessel and computer model schematic of the same vessel

The mass conservation or the continuity equation was used as shown below.

$$\frac{\partial Q}{\partial x} = \frac{-2Q}{a}|_{r=a}$$

The momentum conservation equation completes the use of the Navier Stokes equations in 1-d.

$$\frac{\partial Q}{\partial t} = -\frac{\pi a^2}{\rho}\frac{\partial}{\partial x}\left[p + \rho g z\right] + \frac{2\pi a}{\rho}\tau|_{r=a}$$

These Navier Stokes equations were then coupled with a pressure radius relationship. To bring the Reddy method in line with standard Haemodynamics modelling techniques the thin walled tube model was replaced with the modern standard; the thick walled tube model (also see chapter 3). The thin walled tube model is derived from the thick walled tube model, assuming the stress is uniform, the thickness is

small compared with the diameter and the internal and external diameters are approximately equal [1]. Therefore the thick walled tube model contains less errors, the thin walled tube model has a maximum error of $\frac{50h}{R}\%$ for circumferential stress as discussed in the previous chapter.

The pressure radius relationship for a thick walled tube was shown by Bergel in [19]

$$\Delta P = E\Delta a_{out}^2 \frac{(a_{out}^2 - a_{in}^2)}{2\,(1-\sigma^2)\,a_{in}^2 a_{out}}$$

where a_{out} refers to the outer radius of the vessel, and a_{in} - the inner. So if h is the wall thickness:-

$$a_{out} = a_{in} + h$$

The use of this equation includes the assumption that the length of the vessel does not vary with pressure. Observations of the in vitro pumping vessels indicate that any longitudinal variation is secondary to the circumferential variation and this may be reduced further in situ by the anchoring filaments. Further exploration of longitudinal variation is left to future work.

5.2.1 Discretisation

Reddy's use of the explicit upwind differencing scheme was followed for the finite volume technique. This will help to stabilise the numerical scheme. The mass conservation equation is discretised to the form:

$$\frac{da_i}{dt} = \frac{1}{2\pi a_i l_i}\left[Q_{i-1} - Q_i\right] \tag{5.1}$$

$$a_i^j = dt\frac{1}{2\pi a_i^{j-1} l_i^{j-1}}\left[Q_{i-1}^{j-1} - Q_i^{j-1}\right] + a_i^{j-1} \tag{5.2}$$

where i-1 refers to the data for the computational cell to the left of the focus cell and j is the current timestep.

The moment conservation equation becomes;

$$\rho\frac{dQ_i}{dt} = \frac{\pi\left(a_i^2 + a_{i+1}^2\right)}{(l_i + l_{i+1})}\left[p_i + p_{i+1}\right] - 4\mu\left(\frac{1}{a_i^2} + \frac{1}{a_{i+1}^2}\right)Q_i - Rv_i \tag{5.3}$$

or:-

$$Q_i^j = \frac{dt}{\rho}\left[\frac{\pi\left(\left(a_i^{j-1}\right)^2 + \left(a_{i+1}^{j-1}\right)^2\right)}{\left(l_i^{j-1} + l_{i+1}^{j-1}\right)}\left[p_i^{j-1} + p_{i+1}^{j-1}\right]\right] \tag{5.4}$$

$$-\frac{dt}{\rho}\left[4\mu\left(\frac{1}{\left(a_i^{j-1}\right)^2} + \frac{1}{\left(a_{i+1}^{j-1}\right)^2}\right)Q_i^{j-1} - Rv_i^{j-1} + Q_i^{j-1}\right] \tag{5.5}$$

Reddy [4] uses the equation below to describe resistance. He explains this is based on experimental results giving the pressure to trigger opening of the valve as 120 dyn/cm^2 (12 N/m). However we have not been able to understand how this equation was derived and the units are inconsistent.

$$Rv_i = 120\left(\pi r_{0i}^2\right) \tag{5.6}$$

where r_{0i} is the resting radius of lymphangion i

He states dimensions of dyn/cm (which are required in order to use this term in the momentum conservation equation). The equation includes a pressure times an area, which would need a further length term to give the attributed units. It is not clear whether this was a mistake in the units or the equation.

In order to try and retain the spirit of this way of modelling the valve we used Reddy' s equation with a constant k_r representing the opening threshold as below:-

$$Rv_i = k_r\left(\pi r_{0i}^2\right) \tag{5.7}$$

The constant k_r was varied between 12 and 1200 and this did not have an effect on the results as the resistance was very low using this range of values. A possible improvement for modelling the valve resistance is discussed in chapter 8, where decreasing gap, increases the resistance, unlike this original equation.

Thick Walled Tube Equation:

$$P_i^j = \left(\left(a_i^j\right)^2 - \left(a_i^0\right)^2\right) E \frac{\left[\left(\left(a_i^0\right)^2 + h\right) - \left(\left(a_i^0\right)^2\right)\right]}{2\left(1-\sigma^2\right)\left(a_i^0\right)^2\left(a_i^0 + h\right)} - P_0 \tag{5.8}$$

where a_i^0 is the radius at pressure P_i^0 and P_i^0 is 0 Pa.

The contraction is added by attributing a sine wave to each node. The phase difference ϕ determines the wave speed by effecting the relative position in the cycle of each computational cell at any one time. A_{amp} is amplitude of the wave, t is time, f frequency and x can be E or A_0 depending on the method of the driving function as described in section 7.3.

$$x\left(t\right) = A_{amp} sin\left(2\pi f t + \phi\right) \tag{5.9}$$

Reddy included a second sine wave to represent breathing, which dominates his results. We wished to compare the model to in vitro results and so omitted breathing from the model.

5.2.2 Results/Discussion

The low frequency elements in Reddy's results shown in figure 5.2 can be ignored as they are the representation of breathing, which we have omitted as explained above. The high frequency elements of Reddy's work, which are not going to be effected by the low frequency breathing, demonstrated a very similar magnitude to the oscillations in our results. (see figure 5.3 graphs a to c). They are however

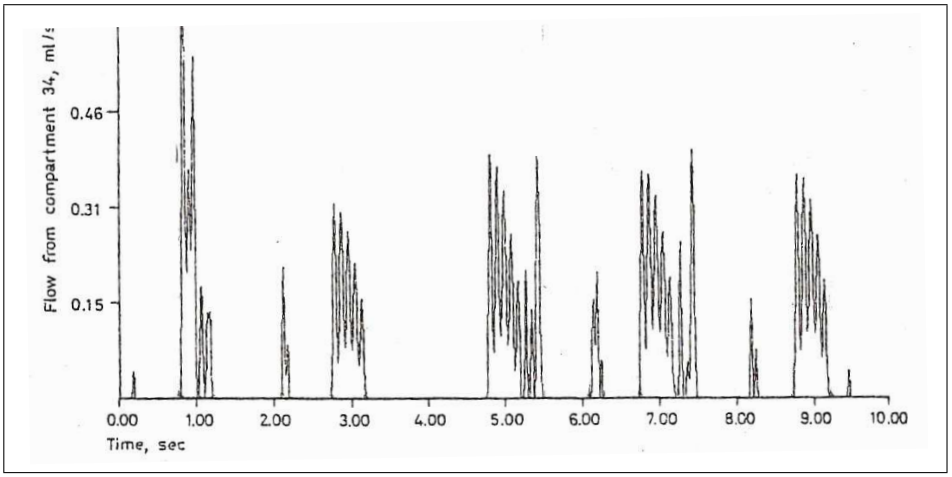

Figure 5.2: Results for flow in the 39th lymphangion taken from Reddy's model [4], where the low frequency elements represent breathing (which has been omitted from the current study) and the high frequency elements resemble the computational instability in our results. To compare with graphs of our results in figures 5.3 and 5.4 the units must be converted from ml/s to mm^3/s by a factor of times 1000)

reminiscent of computational instabilities. Therefore these investigations lead on to an examination of the stability of the model.

5.3 Adaptions to the Reddy model

5.3.1 Stability

Our implementation reproduced Reddy's results see figures 5.2 and 5.3 a-c. Please note that the units on Reddy's graph are in ml/s rather than mm^3/s (which are the units on our results). The timestep was then varied in order to find the highest value which did not effect results. Unfortunately at the time step Reddy has used the size and magnitude of the oscillations was found to be effected by varying the timestep. Such instability at this magnitude of timestep has been found to be one of the drawbacks of the use of a 1-d explicit scheme in modelling elastic tubes. This type of instability depends on the Deborah number (D_e), which measures the fluidity of a

material. This is a ratio of the relaxation time scale (t_c, characterizing the intrinsic fluidity of the material) and the time scale of observation (t_p e.g. the time scale of an experiment or a computer simulation). For a smaller Deborah number the wall material appears more fluid [102].

$$D_e = \frac{t_c}{t_p} \tag{5.10}$$

As discussed in chapter 3 techniques have been developed to improve stability of such schemes with a combination of additional terms, appropriate timesteps and by graduating any changes within the program.

Larger timesteps were shown to give more frequent and larger oscillations, sometimes causing a divergence to infinity. Therefore the timesteps were reduced until the size no longer affected the results. However this significantly affected the processing time. Various other measures to improve stability were investigated. After implementing these measures the timestep could be increased, improving the processing time.

The initial transience presented by the computational model (i.e. the larger oscillations found at the start of some runs during settling) and the rate at which changes were imposed, transpired to have a large importance in terms of the eventual stability of the case. The model was therefore altered so there were no sudden, sharp changes imposed on the system. Gradual changes reflect the physiological situation much more accurately than the sudden sharp changes of the original setup. The starting pressures along the vessel were set to values from a standard, settled run to minimise any initial transience. Any changes imposed on the vessel during a run were ensured to happen smoothly, so the contractions were modelled using a sine wave. The valves were set up to gradually open or close (rather than instantaneously) using a slope calculated from the expected maximum and minimum. There is no data available on the opening/closing times of the lymphatic valves and the only

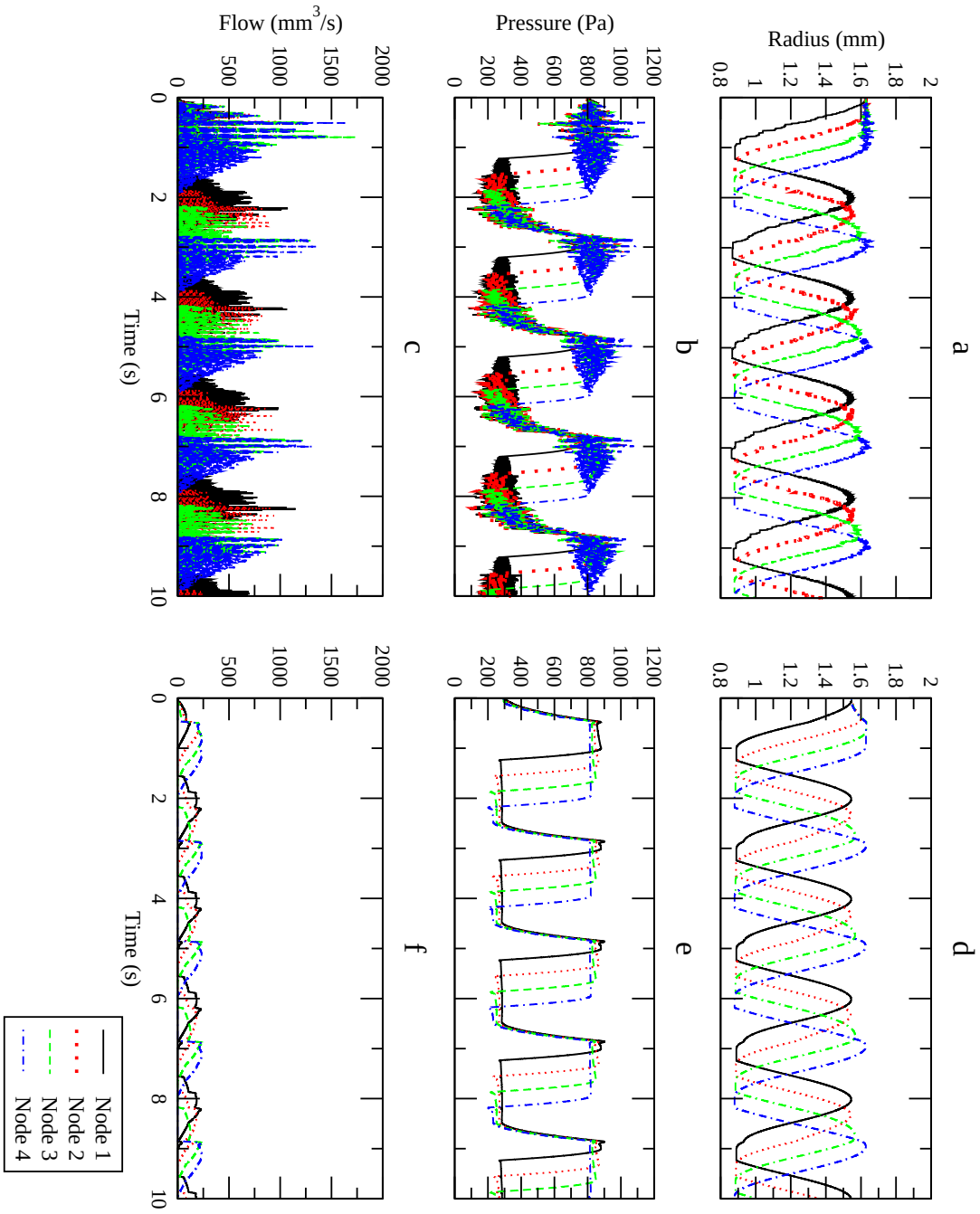

Figure 5.3: Implementation of Reddy's model at various positions along the segment (lymphangions 1-4). With (d radius time, e pressure time and f flow time) and without (a radius time, b pressure time, and c flow time) stability measures (these include a smaller timestep, imposing only gradual changes within the program and the addition of the damping (γ) and tension (T) terms). The magnitude of the spikes are similar to those found by Reddy in figure 5.2 once the change in units is performed (for mm^3/s to ml/s divide by 1000)

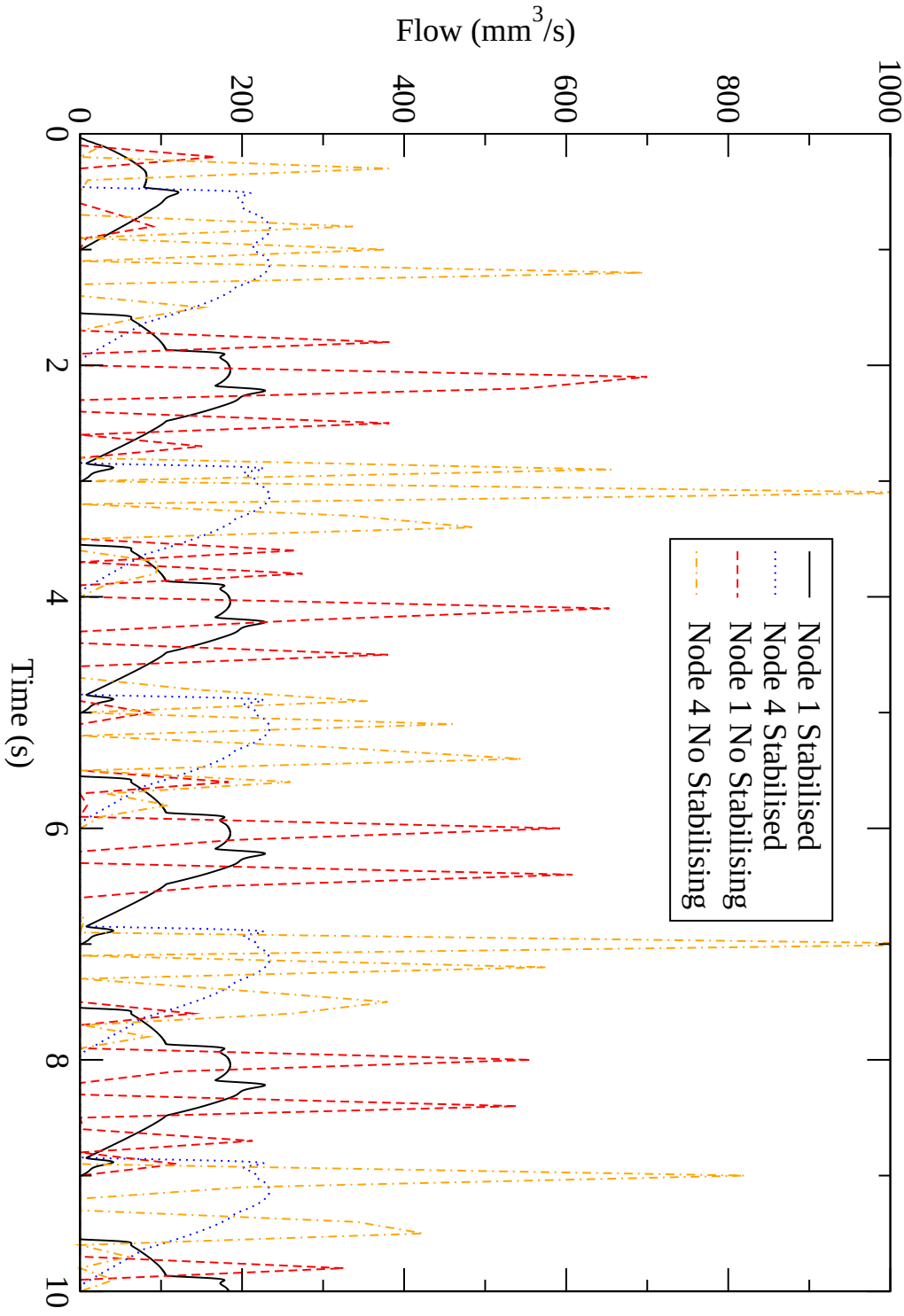

Figure 5.4: Implementation of Reddy's model at lymphangions 1 and 4 showing flow against time with and without stability measures (which include a smaller timestep, imposing only gradual changes within the program and the addition of the damping (γ) and tension (T) terms)

Parameter	Symbol	Standard	Range
Time Step(s)	dt	0.000002	0.01-0.0000001
Number of nodes per lymphangion	1		
Number of Lymphangions	4		
Young's Modulus (N/m^2)	E	5000	-
Radius (unstretched) (mm)	A_0	1.25	-
Damping Coefficient (Pa s m)	γ	7 x 10^7	7 x 10^5 - 2 x10^8
Tension (Pa/m)	T	kP	see k
Tension factor	k	5	0.2 - 5
Phase (radians)	ϕ	$\pi/40$	-
Amplitude (%)	a_{amp}	0.838	-
Valve opening/closing time (ms)	T_v	20	0-20
Valve Triggering Pressure (Pa)	P_v	10	2 - 100
Period (s)	T_p	2	-
Contraction Time (s)	T_c	1	-
Length of lymphangion (mm)	L	2	-
Pressure in (Pa)	P_{in}	500	-
Pressure out (Pa)	P_{out}	800	-
Pressure difference (Pa)	dP	300	-
Viscosity (Kg/m^3)	μ	0.0008904	N/A
Density (Kg/m^3)	ρ	998	N/A
Poisson's Ratio	σ	0.5	

Table 5.1: The variables used for the Reddy implementation, where the number of lymphangions excludes the two boundary nodes

reference point we have is the heart valves. The literature reports the heart valves taking between 20 and 160 ms to open or close [103, 23]

The model uses 10000 timesteps which translates as 20 ms for a standard run, the lowest of these values. This value was also large enough to prevent instabilities caused by the valve opening or closing too fast and seems to be physiologically possible when compared to the heart valves.

These measures were found to reduce the initial transience of the system, increase the likelihood of a successfully convergent solution and cut out large numbers of oscillations leaving the radius profiles looking much more like those found in practice. It was also possible to increase the size of the time step a little and retain the same stable solution.

The Valve Setup

In addition to graduation of the opening and closing of the valve (as described above) it was also found to be necessary to set the opening pressure for the valve higher than the closing pressure. Without this the valve tended to flutter, opening and closing in short succession. This also fits with the mechanics of the heart valves, which have a higher pressure to open than close. The pressure during closing of the heart valve rises above zero but remains lower than the pressure required to open the valve 'the opening threshold' . If the opening threshold was too low this increase during closing would trigger another opening, before it was fully closed. It seems likely that a too low opening threshold was causing fluttering in the lymphatic model. Also see chapter 8 which examines the behaviour of the valve in further detail.

On testing a very high triggering pressure, this prevented flow as the pressure produced by the contraction was not high enough to over come this.

A pressure of 10 Pa was set as the opening threshold and the closing pressure was set to zero for the standard set up. This differential of 10Pa between the opening and closing pressure was large enough to avoid fluttering. Any larger values simply made the pressure peak at the beginning of the cycle larger and had little effect on

the rest of the cycle as long as the contraction produced enough pressure to over come it.

Damping Constant

A damping term was added as used in the work by Stembera and Marsik [75], using the damping constant γ found in chapter 4.

$$\gamma \frac{\partial A}{\partial t} \tag{5.11}$$

This is added to the Thick Walled Tube equation, which becomes:-

$$\Delta P = E \Delta a_{out}^2 \frac{(a_{out}^2 - a_{in}^2)}{2(1-\sigma^2) a_{in}^2 a_{out}} + \gamma \frac{\partial A}{\partial t} \tag{5.12}$$

which is discretised to become

$$\left(\gamma \pi 2 a_i^j\right) \frac{\left(a_i^{j+1} - a_i^j\right)}{dt} \tag{5.13}$$

This damping term can be thought of as the inertia of the wall and begins to account for the viscoelasticity of the material. Our experimental work found a value for this term (see chapter 4) to be 7 x 10^7 Pa s m^{-2}. This was higher than the value found for blood vessels by Stembera and Marsik [75](1 x 10^6 Pa s m^{-2}), this difference can be accounted for by the difference in material properties of the two types of vessel [31], also see chapter 2 . Initially a value of 1 x 10^9 Pa s m^{-2} was required as the damping constant in order to damp out all the oscillations but as other measures were included this became less important and could even be taken below the value found for experiment without causing instabilities. The effect of varying γ is investigated further in section 6.2. γ is not the only cause of instability but can be artificially increased to improve stability.

Tension Term

A tension term Tα_{xx} was also added using the tension T calculated in chapter 4. This term can be thought of as contribution of the longitudinal tension in the vessel wall and may be especially important when a wave front distend a vessel wall.

$$-\frac{T}{D_0}\frac{\delta^2 A}{\delta x^2} \tag{5.14}$$

The term T can be found as the longitudinal stresses due to the intraluminal pressure are essentially only dependent on the ratio of the radius to the thickness of the walls [18]. As found in chapter 4

$$S_Z = kP \tag{5.15}$$

where S_z = T and k=5.

This is also added to the Thick Walled Tube equation, which becomes:

$$\Delta P = E\Delta a_{out}^2 \frac{(a_{out}^2 - a_{in}^2)}{2\left(1-\sigma^2\right)a_{in}^2 a_{out}} + \gamma\frac{\partial A}{\partial t} - \left[\frac{T}{D_0}\frac{\partial^2 A}{\partial x^2}\right] \tag{5.16}$$

This is discretised to become:

$$2T\pi a_i^j \frac{\left[\left(a_{i+1}^j\right)^2 - 2\left(a_i^j\right)^2 + \left(a_{i-1}^j\right)^2\right]}{l^2} \tag{5.17}$$

Grotberg and Jensen [14] suggest this is the most important of all the additional terms for models of the cardiovascular system.

An experimental value for Tension T was found to be approximately kP, where k is 5 and P the pressure, also see the experimental work in chapter 4. A larger k was required for stability, if this was the only stabilizing measure included. As for γ an artificial increase improved stability.

The constant k was varied between 0.2 and 5 in the parametric study in section 6.2 .

Optimum Set Up

The optimum modelling set up was considered to be the set up which allowed stability with the largest time step without effecting the results. Each of the measures was incorporated on its own one at a time, using the experimental values for γ and the tension constant k. These measures were then varied until stability was reached using that measure alone; at this point both the value for the damping constant γ and tension constant T were higher than the experimental value. Secondly all of the measures were added at once.

The optimum set up was found to be when all of the stabilizing measures were included. The tension T and damping γ terms became more flexible once the other measures were included and could be lowered to match those found during experiment without detrimental effects to the stability.

This optimum set up is compared to that of the initial Reddy implementation in figures 5.4 and 5.3 windows d-f. This shows the removal of all the high frequency components found in a-c and the results look much more like the results found during experiment in chapter 4.

5.4 Model Validation

Poiseuille's law describes flow in a stiff tube with uniform radius [1]

$$Q = \frac{\pi}{8\mu} R^4 \frac{\delta P}{L} \tag{5.18}$$

Where Q is flow, μ is viscosity, P is pressure, L is length and R is radius. We wanted to use this relationship to check our code was behaving as expected. In order to do this the elasticity of the vessel was increased dramatically to approximate a stiff tube, without any drastic changes to the code and to minimise the variation in radius along the tube. The same number of computational cells were used but

the valves were removed and passive flow was set up with a pressure drop of 300 Pa along the vessel.

As can been seen in table 5.3, the flow output from the model was the same as the flow calculated by the Poiseuille equation demonstrating that the code is working as expected. At this high Young's modulus the radius in the model remained the same to within 3 significant figures.

The Poiseuille equation can be extended to account for elasticity in the walls of the vessel as described in the following equation [104]

$$Q = \frac{\pi}{20\mu\alpha L}\left[(a_1)^5 - (a_L)^5\right] \tag{5.19}$$

where, α describes the pressure radius relationship,

$$\alpha = \frac{2\,(a - a_0)}{dP} \tag{5.20}$$

where a_1 is the radius at the inlet of the vessel if it starts off at pressure P_1 and the pressure at the downstream end is then reduced to P_L if $P_L < P_1$ causing flow, where L is the length of the vessel. The results are shown in table 5.5. The results from the model are taken when the system has settled.

5.5 Model Refinement

In order to provide better resolution of the behaviour, the model was split into several computational cells per lymphangion as shown in figure 5.5. Firstly we used 4 cells per lymphangion, giving a cell length of a similar magnitude to the radius. This set up was then used for the following 1d modelling unless otherwise stated.

The Courant number or Courant-Friedrichs-Levy (CFL) Condition requires that for an accurate solution in an explicit time-marching computer simulation the time step has to be smaller than the time for a certain event. In compressible fluids this is the time for a sound wave to cross one of the boxes of the discretisation. The Courant number C (shown in equation 5.21) and needs to be below the CFL (which

Parameter	Symbol	Value
Young's modulus (N/m^2)	E	500000
Dynamic viscosity (Pa.s)	μ	0.0008904
Length (m))	L	0.025
Radius (m)	R	0.001252
Pressure variation along length L (Pa)	δP	300
Time Step(s)	dt	1×10^{-6}
Number of Nodes	n	4
Radius (unstretched) (mm)	A_0	1.25
Gamma (Pa s m)	γ	7×10^7
Tension (Pa/m)	T	$k \times P$ (also see k)
Tension factor	k	5
Phase (radians)	ϕ	N/A
Amplitude (%)	a_{amp}	0
Valve opening/closing time (ms)	T_v	no valves
Valve Triggering Pressure (Pa)	P_v	no valves
Period (s)	T_p	no contractions
Contraction Time (s)	T_c	no contractions
Length of cell (m)	L	0.005
Pressure in (Pa)	P_{in}	800
Pressure out (Pa)	P_{out}	500
Density (Kg/m^3)	ρ	998
Poisson's Ratio	σ	0.5

Table 5.2: Table of values used for a comparison of flows between the model representing a stiff tube and the poiseuille equation

Results		
Flow output from model (m^3/s)	Q_m	1.3×10^{-5}
Flow from equation (m^3/s)	Q_a	1.3×10^{-5}

Table 5.3: Table of flow results for the model representing a stiff tube and the poiseuille equation

Parameter	**Symbol**	**Value**
Dynamic viscosity (Pa.s)	μ	0.0008904
Length (mm)	L	24
Radius at 0 pressure (mm)	a_0	1.05
Pressure in (Pa)	P_{in}	800
Pressure out (Pa)	P_{out}	500
Number of Nodes	n	6
Gamma (Pa s m)	γ	7 x 10^7
Tension (Pa/m)	T	kP (also see k)
Tension constant	k	5
Time Step(s)	dt	1×10^{-6}

Table 5.4: Parameters for use with the Poiseuille equation when modified to account for the elasticity of the vessel wall

Conditions	Parameter	Symbol	Value
if E=E_1	**Young's modulus (N/m^2)**	E	7000
	Radius at point 1(mm)	a_1	2.42
	Flow output from model	Q_{ME1}	1.21×10^{-4}
	Flow from calculation (m^3/s)	Q_{CE1}	1.2×10^{-4}
if E=E_2	**Young's modulus (N/m^2)**	E	4000
	Radius at point 1(mm)	a_1	2.79
	Flow output from model	Q_{ME2}	2.15×10^{-4}
	Flow from calculation (m^3/s)	Q_{CE2}	2.06×10^{-4}

Table 5.5: Results with the Poiseuille equation when modified to account for the elasticity of the vessel wall

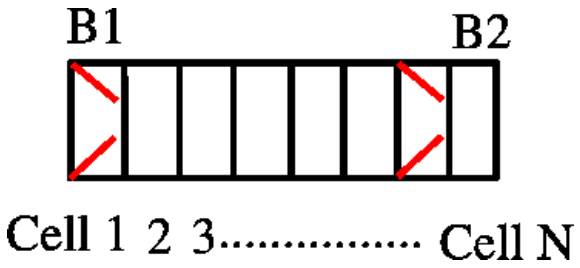

Figure 5.5: More Detailed Model of the Lymphatic System.

varies for different types of problem) for convergency to occur. For models of blood flow, the CFL is usually taken as 1, as in [105].

$$C = \frac{U}{\frac{\partial x}{\partial t}} \tag{5.21}$$

The Courant number was calculated; firstly using the fluid velocity U, based on the flow Q and radius a, to give the Courant number C_f (shown in table 5.6). Secondly the wave speed of 0.02m/s (approximated by Arkill in chapter 4) was used to give a Courant number as shown in table 5.7.

In the experimental studies by Arkill in chapter 4, the wave speed was found to be roughly 0.02m/s. This would give the following Courant number with 4 cells per

Symbol	Parameter	Value
Q_{max} (m^3/s)	Maximum Flow	2.25 x10^{-7}
a (m)	Radius at Max Flow	3.93 x10^{-3}
U (m/s)	Velocity at Max flow (Q/a)	5.73 x10^{-3}
∂ x (m)	Cell Length	0.005
∂ t (s)	Time Step	2 x 10^{-6}
$\frac{\partial x}{\partial t}$		2500
C_f	Courant number	2.3 x 10^{-6}

Table 5.6: Table to calculate the Courant number C_f for the 4 cell per lymphangion model based on the fluid velocity

Symbol	Parameter	Value
∂ x (m)	Cell Length	0.005
∂ t (s)	Time Step	2 x 10^{-6}
U m/s	Velocity	0.02
$\frac{\partial x}{\partial t}$		2500
C	Courant number	8 x 10^{-6}

Table 5.7: Table to calculate the Courant number C_w for the 4 cell per lymphangion model based on the wave speed

lymphangion:-

The value of 8 $\times 10^{-6}$ for the Courant number for the wave velocity C_w, and the values for the Courant number for the fluid velocity C_f (2.3 x 10^{-6}), are all well below 1 so the convergency due to the discretisation cell size should not be a problem.

5.6 Modelling the Intrinsic Pump

Reddy used a simple sine wave to represent the contractions in his model by varying the wall stress. We initially replicated this method using a sine wave to vary the Young's modulus. The method for driving the contraction wave is examined further in chapter 7 to investigate the differences between methods for representing the contraction using a sine wave variation either in the radius or Young's modulus. This represents the difference between a contraction driven by a change in elasticity or muscle fibers moving towards each other. Throughout this thesis the Young's modulus is used to drive the contraction unless otherwise stated.

This basic type of input gives a similar basic sine wave output for the radius with time graph radius output as shown in figure 5.6. Our experimental results (see graph 4.4) give a roughly 'shark fin' shape radius with time profile as confirmed by Zweifach and Prather [27]. In vitro observations of a contracting vessel appear to show a passive relaxation phase where the muscle has stopped contracting and it simply behaves as an inflating balloon. Armenio and colleagues [93, 94] also noted that diastole (filling) is always significantly longer than systole (emptying). If it is assumed that in terms of the muscular activity the active contraction takes as long as the active relaxation, this would lead to the conclusion that there must also be a passive relaxation phase. This also appeared to be the case when observing the contracting vessel.

Passive relaxation was added to the model by inserting a pause between each peak of the sine wave. The length of this delay in comparison to the period of the whole cycle was approximated to be half the total cycle time after observing the pumping vessels and examining the behaviour of the model using different values.

As shown in figure 5.6 the sine-pause model allows the shark fin type shape found by experiment in chapter 4 figure 4.4 to emerge.

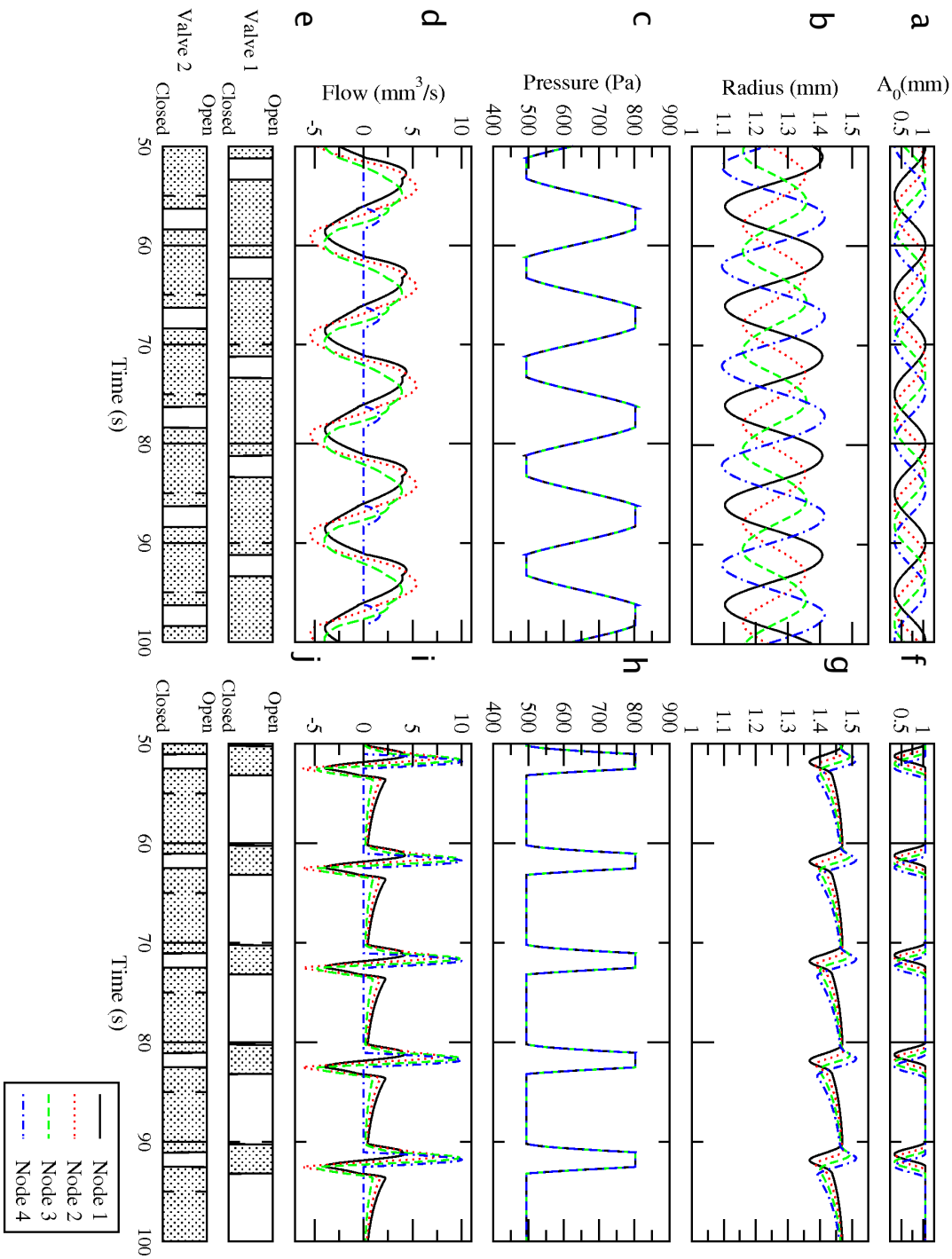

Figure 5.6: Comparison of model with (f-j) and without (a-e) the delay in the sine wave driving the contraction function. With the delay the radius-time graph shows the shark tooth shape found in experiment. Boxes a and f show the Young's modulus variation which drives the contraction , b and g show the radius time output of the model, c and h show the pressure time , d and i show the flow time and e and j show the timings of both valves in the two different runs

Symbol	Parameter	Value
Q_{max} (m^3/s)	Maximum Flow	2.25 x10^{-7}
a (m)	Radius at Max Flow	3.93 x10^{-3}
U_f (m/s)	Q/a Velocity of Fluid at Max Flow	5.73 x10^{-}3
U_w (m/s)	Velocity of Wave	0.02
∂ x (m)	Cell Length	0.00333
∂ t (s)	Time Step	2 x 10^{-6}
$\frac{\partial x}{\partial t}$		1667
C_f	Courant Number for the Fluid	3.44 x 10^{-6}
C_w	Courant Number for the Wave	1.2 x 10^{-}5

Table 5.8: Table to calculate the Courant number for the 6 cell per lymphangion model based on the wave speed and fluid speed

5.7 Further Refinement of Model

The model was then set up with 6 cells per lymphangion, in order to verify the accuracy obtained with the 4 cell model or show if greater resolution was required. The Courant numbers, 3.44 x 10^{-6} for the fluid and 1.2 x 10^{-}5 for the wave, were also well below 1 so the discretisation cell size should be appropriate.

Graph 5.7 shows the difference in results between the 4 cell per lymphangion model and the 6 cell per lymphangion model. The average flow for both set ups was 6.8 mm^3/s. Showing that the effect of either model set up is the same. There is one apparent difference in the flow profile but this is due to the number of cells presented on the graph. The maximum appears much lower for the 6 cells model but this graph only shows the results for the 1st 4 computational cells and not the last two. The peak flow from the 4 cells model is in the cell just in front of the next valve. The results from this position have not been printed for the 6 cell model.

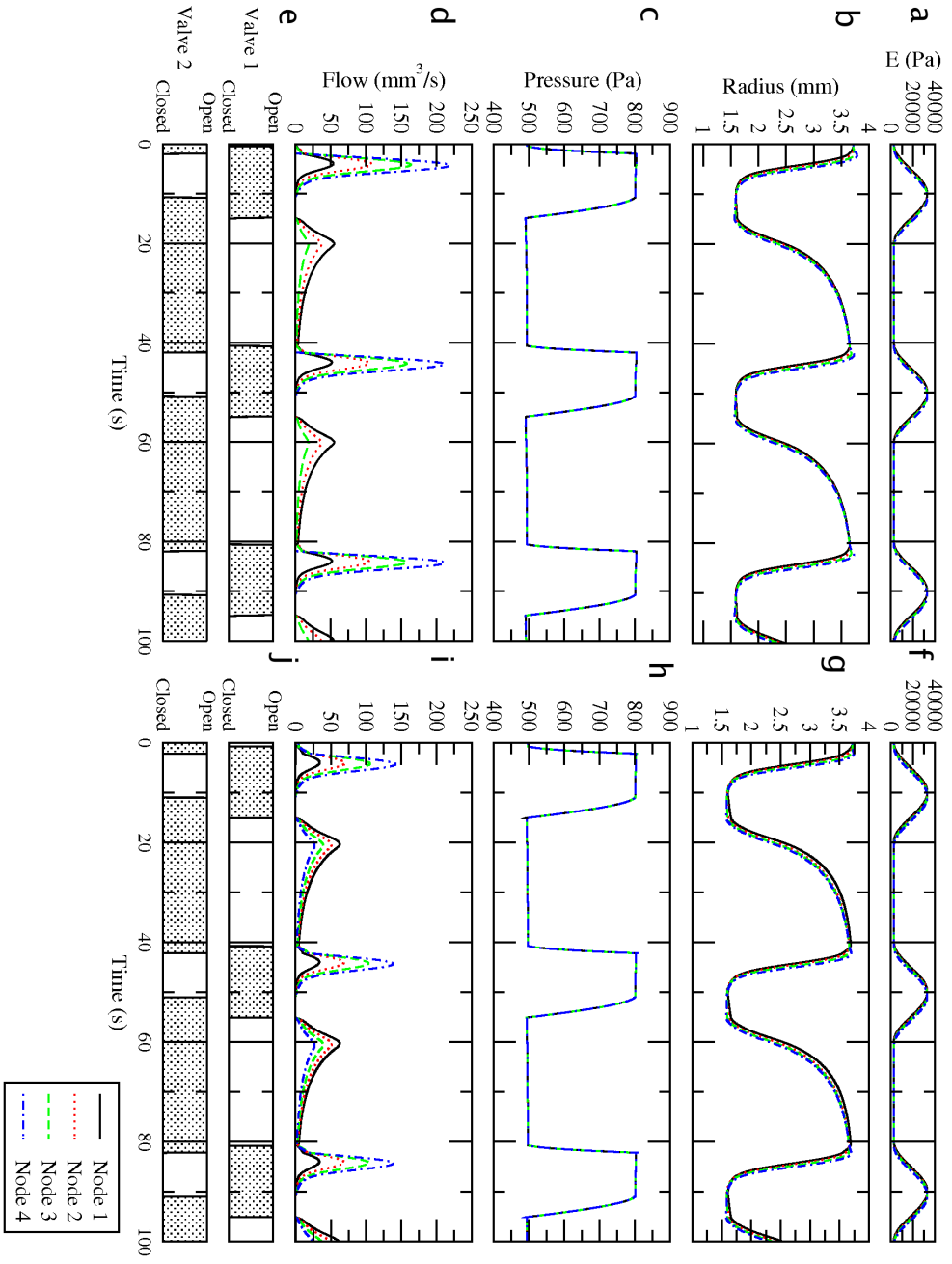

Figure 5.7: There is a negligible effect from varying the number of cells per lymphangion. Windows a-e: the model using 4 cells per lymphangion, f-j: the model using 6 cells per lymphangion. Boxes a and f show the Young's modulus variation which drives the contraction, b and g show the radius time output, c and h show the pressure time output and i show the flow time output and e and j show the opening and closing of the two valves in both models

5.8 General Characteristics of The Stabilised 1-d Model

Graph 5.8 shows a typical run inorder to observe the general characteristics of the model developed involving 4 computational cells per lymphangion and the sine with delay for the contraction cycle. The following section will discuss the variation with time of different parameters and what this means in relation to the mechanics of the vessel.

5.8.1 Radius

As shown in figure 5.8 the radius decreases as a contraction starts, (the values for each node are staggered, as the contraction wave moves along the vessel) (point (i) graph 5.8). A minimum radius is reached once the smallest relaxed radius A_0 value is passed (strongest point of the contraction). The radius then stays at that level even though the Young's modulus continues to decrease. The ejected fluid accounts for all the increased forces on the vessel. The contraction begins to ease off in an active relaxation stage (ii) to (iv) but the radius remains the same until the pressure drops low enough to open valve one. The vessel begins to fill (iii) to (v) and continues to do so even when the contraction has finished in a passive relaxation (or inflation) phase. The vessel has not quite returned to its original radius and the vessel continues to refill from the previous lymphangion, evening out the pressure difference. The length of time taken to passively relax depends on factors like the elasticity, with a larger elasticity the shape takes longer to return to normal.

The radius time graphs typically show a peak just as the contraction starts. This is due to the nodes contracting in sequence. As the first node contracts and pushes the fluid out, the volume of fluid in subsequent nodes is increased, inflating the vessel. As the second node contracts this further increases the inflation of the remaining relaxed nodes. The last node to contract thus ends up with the largest radius before it too contracts in turn. This effect was also seen in the experimental

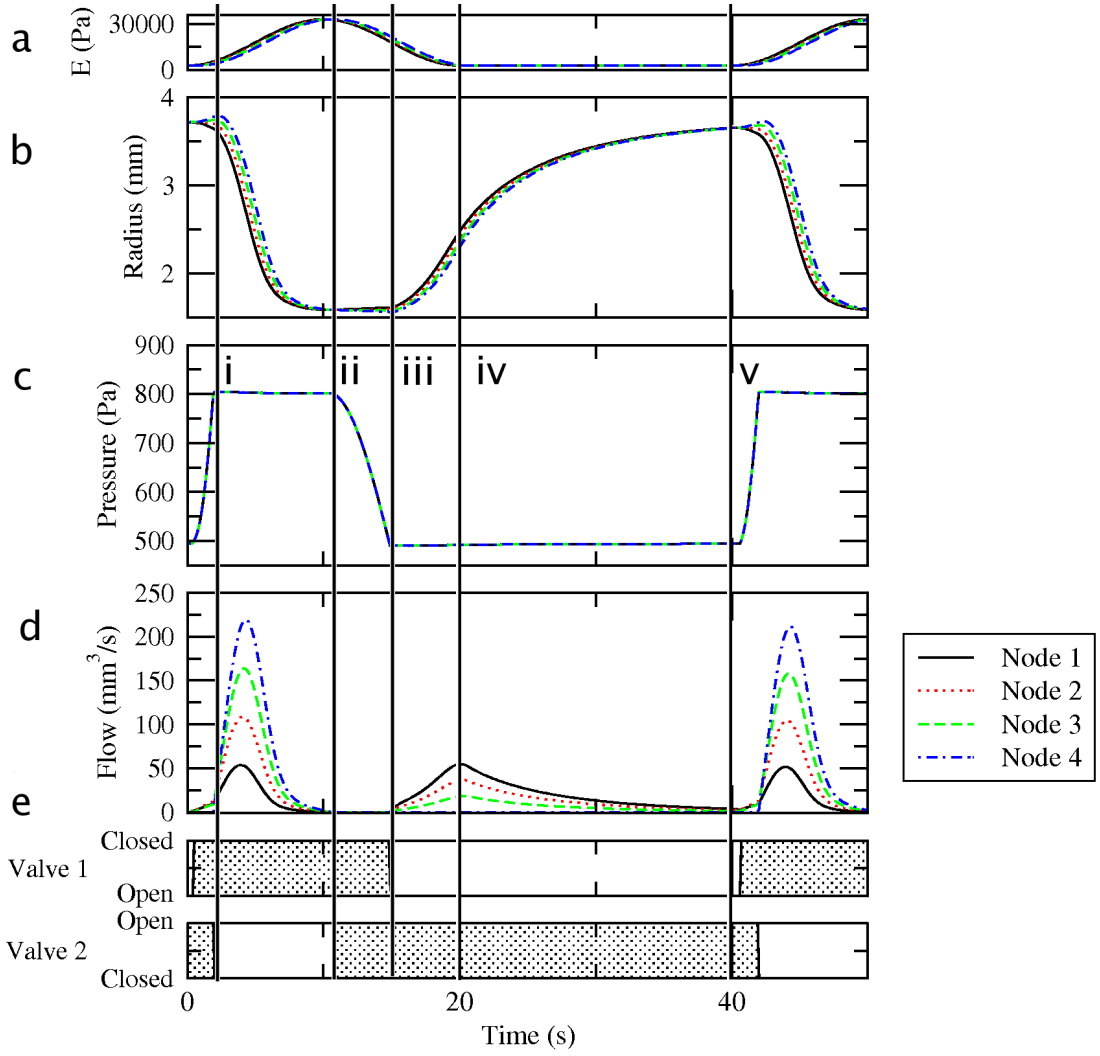

Figure 5.8: General characteristics of the stabilized run, the roman numerals indicate significant stages in the cycle discussed in the text. Box a shows the Young's modulus variation which drives the contraction, b shows the radius time output, c shows the pressure time output d shows the flow time output and e shows the opening and closing of the two valves in both models

work in chapter 4.

There can also be a negative peak towards the centre of the contraction, as the first node to contract begins to actively relax, the other nodes can contract further by pushing more of the fluid into that area. The last node to relax can therefore achieve the lowest radius.

Both of these peaks become larger as elasticity increases as it becomes easier to move the walls and work the pump.

5.8.2 Pressure

The pressure increases as the contraction starts until enough pressure is achieved to open the outlet valve (point (i), graph 5.8). Then the pressure drops to just above the outlet pressure until the contraction reaches its peak. As the pressure begins to drop, the outlet valve closes (at point (ii)). The pressure continues to drop until it is below the inlet pressure and this positive pressure gradient opens the inlet valve (at point (iii)). The pressure then increases at a very slow rate until the next contraction, remaining below the inlet pressure until all flow ceases.

There is a small pressure peak as the outlet valve first opens (i) due to the opening time of the valve and the positive pressure gradient needed to open the valve (the triggering pressure). The pressure must reach this higher value to open the valve, once open the pressures level out along the vessel, but the valve remains open.

The pressure inlet and outlet are set in the model, so the pressure profile does not vary much unless a parameter concerning the pressure is changed (for example changing the triggering pressure).

5.8.3 Flow

There are typically two flow peaks with a period in the middle with no flow:-

Ejection

The first peak is the ejection stage (i-ii graph 5.8) and typically reaches a higher value but for a shorter length of time compared to the second peak (this can be explained by the inclusion of passive relaxation in the second peak). The width is dependent on the length of time for an active contraction, which is kept constant through all the experiments unless the period is being changed. With some properties (eg lower elasticity) the peak is effectively thinner, with the majority of the ejection happening more quickly except for a longer 'tail' stage at the end with a slower flow.

As the vessel ejects, the inlet valve is closed, the second opens with enough pressure and the node nearest to the second valve has the largest flow as the fluid from all the other nodes must pass through there too. Flow stops when the inlet valve closes due to insufficient pressure (ii).

Central Stage

The pressure drops as the active relaxation phase begins (ii-iii). Both valves close, causing a cessation in flow until the pressure is high enough to open the inlet valve.

Filling

The second peak (iii-v) is the filling stage and takes longer but reaches a lower maximum flow. At the beginning of this peak (iii) the outlet valve remains closed but the inlet valve opens and the flow is slower than during the ejection phase, due to a smaller pressure difference. The vessel's contraction cycle is over at point (iv) and the vessel begins to passively relax, causing flow until the pressure is insufficient to keep the inlet valve open. The width of this peak is dependent on the passive relaxation time as well as active relaxation, so with increased elasticity the peak is wider and the vessel takes longer to return to normal size.

5.9 Conclusions

On implementation of Reddy's model of a lymphatic vessel, we discovered that computational instabilities were present in our results. The same instabilities appeared to be present in Reddy's results. The computational instabilities were confirmed by the fact that reducing the timestep changed the results.

Various stabilizing methods were introduced; the inclusion of all of these methods produced an improved model allowing a larger timestep. These measures involved using a damping and tension term, smaller timesteps, graduating any changes within the system and the timings and pressures involved in valve function. The damping term can be thought of as the inclusion of viscoelasticity, moving away from the purely elastic model. Alone, each of these stabilizing precautions required a smaller timestep or artificially high value to produce stability than the combination of all the methods leading to the supposition that the optimum model should include all of them.

The model was set up so changes were imposed gradually (avoiding instantaneous changes). This included an intial setup of a settled run and the gradual opening and closing of the valve. Physiological changes are very unlikely to happen instantaneously, so these measures made the model more realistic aswell as aiding stability. Changing the opening pressure of the valve to be greater than the closing pressure is also justified as this is a characteristic found in the similar valves of the heart. The damping and tension terms have not been used in previous models of the lymphatic system although they have in cardiovascular models. Their stabilizing contribution in these results and the experimental validation indicates that these mechanical parameters are transferable to the lymphatic system.

In modeling the contractile behaviour we find that the best match to the experimental data is given by short contractile pulses interspersed with longer relaxed intermissions, rather than a continuous variation of the contraction function. During these relaxed periods the behavior of the system is governed by the passive behavior of the wall, i.e. its elasticity and inertia. Thus, the complex time-series

behavior of the system is actually generated by a contractile pulse of very simple form. Note that although the myogenic response of smooth muscle (smooth muscle cells contracting in response to stretch) generally occurs over a relatively long time, an electrically stimulated contraction can occur much more quickly [1].

A variation in computational cells size was begun in order to find how small the cells need to be for an accurate solution. The 6 and 4 cell models gave the same results, showing 4 cells is sufficient. The Courant number was calculated and all of the models explored have a suitable ratio between the cell length and time step to allow convergence. A Poiseulle flow study was undertaken using a relaxed but very stiff vessel, with a pressure gradient in the direction of flow. Secondly vessels with two different elasticities were modelled and compared to a modified Poiseuille equation to allow for the elasticity of the vessels. These calculations matched the model results indicating that the computer program was representing Poiseulle flow as expected.

The valve mechanics such as timings and threshold pressures were found to be very important and further investigation of these are discussed in chapter 8.

Chapter 6

Parametric Study

6.1 Introduction

As physiological values undergo large fluctuations between patients, the next two chapters examine the effects of variation of the wall parameters. At this stage it is more useful to find the sensitivity and effects of various parameters across the board than try to represent an individual case. There are reports that the direction of the wave (with or against flow) does not make a a difference to flow and this is investigated in section 7.2. The pressure radius graphs show that the material properties change after a certain threshold, giving two different gradients. Although the physiological range is mainly below the threshold, a model to reflect this gradient change is explored in chapter 7. Further examination of the contraction mechanism is also undertaken in section 7.3 to determine if driving the wave using the Young's modulus E, or the unstretched radius A_0 effects the results.

This chapter concentrates on a parametric study and describes an analysis of the wall model and modelling strategies investigated to produce an improved model of the lymphatic vessel walls. Various factors are considered; including the Young's modulus E, wall thickness h, wall inertia, longitudinal tension, amplitude, contraction wave speed and period.

6.2 Parametric Study Methodology

6.2.1 Method

The effects of various parameters were investigated, based on the model developed as described in the previous chapter, using a varying Young's modulus to drive the contraction wave. The standard values used and range are shown in the table below. The damping coefficient γ and the wall tension T were also varied. These are also discussed in section 5.3.1.

Parameter	Symbol	Standard	Range
Young's Modulus (N/m^2)	E	5000	2750-7500
Radius (unstretched) (mm)	A_0	1.25	0.75 - 1.8
Gamma (Pa s m)	γ	7 x 10^7	7 x 10^5 - 2 x10^8
Tension	T	$\frac{P}{5}$	0.01-0.4
Phase (radians)	ϕ	$\pi/40$	0.04-3.14
Amplitude	a_{amp}	0.838	0.375 - 0.838
Valve opening/closing time (s)	T_v	20	0-20
Valve Triggering Pressure (Pa)	P_v	10	2 - 100
Period (s)	T_p	40	10-40
Contraction Time (s)	T_c	20	50-100%
Length of lymphangion (mm)	L	2	3 - 9
Pressure in (Pa)	P_{in}	500	-
Pressure out (Pa)	P_{out}	800	-
Pressure Gradient	dP	300	- 50 - 300
Amplitude (E wave)	E_{amp}	5.5 E_0	
Viscosity (Kg/m^3)	μ	0.0008904	N/A
Density (Kg/m^3)	ρ	998	N/A
Amplitude (E wave)	E_{amp}	5.5 E_0	
Poisson's Ratio	σ	0.5	

In this section, the standard length of an actual contraction T_c is chosen to be twenty seconds long, half of the entire contraction cycle T_p. The remaining time (as the vessel continues to return to its original shape passively) is termed in this thesis - the passive relaxation phase. This passive relaxation time can indicate the shape for the radius time profile as it depends on how long the vessel takes to relax after the contraction is finished. With a longer passive relaxation time the shark fin shape Arkill found in the experiments in chapter 4 is able to emerge.

6.3 Results/Discussion

This section examines the effects of varying the stiffness (E or h), relaxed radius (A_0), damping coefficient (γ), tension (T), the wave amplitude A_{amp} and period (T_p). The contraction wave speed was also varied by changing the phase difference between the contraction waves associated with each different nodes. In particular the effects on the passive relaxation phase and characteristic radii and flows were examined and the sensitivity of the model to variation of these parameters observed.

6.3.1 Elasticity

The stiffness of the vessel walls can be increased, by increasing the Young's modulus E or increasing the wall thickness h. In this model the wall thickness of the lymphatic vessels is calculated as a percentage of the unstretched radius. Our experimental findings give a thickness of roughly 10 percent of the unstretched radius see chapter 4, although Deng et al, [5] found the thickness to be 3.5 percent of the unstretched radius. For the model we used 7.5 percent as a compromise between the two.

The passive relaxation stage is shorter with a stiffer material (i.e. higher Young's modulus) so the forces pulling the vessel back to its original shape are stronger. See graph 6.1 (e) which shows how a vessel returns to within 1% of its relaxed radius faster if it is stiffer. Also see graph 6.2 (b) and (g) which shows the radius for a low value of Young's modulus (E) and a high value of E. In graph 6.2 (b) with low

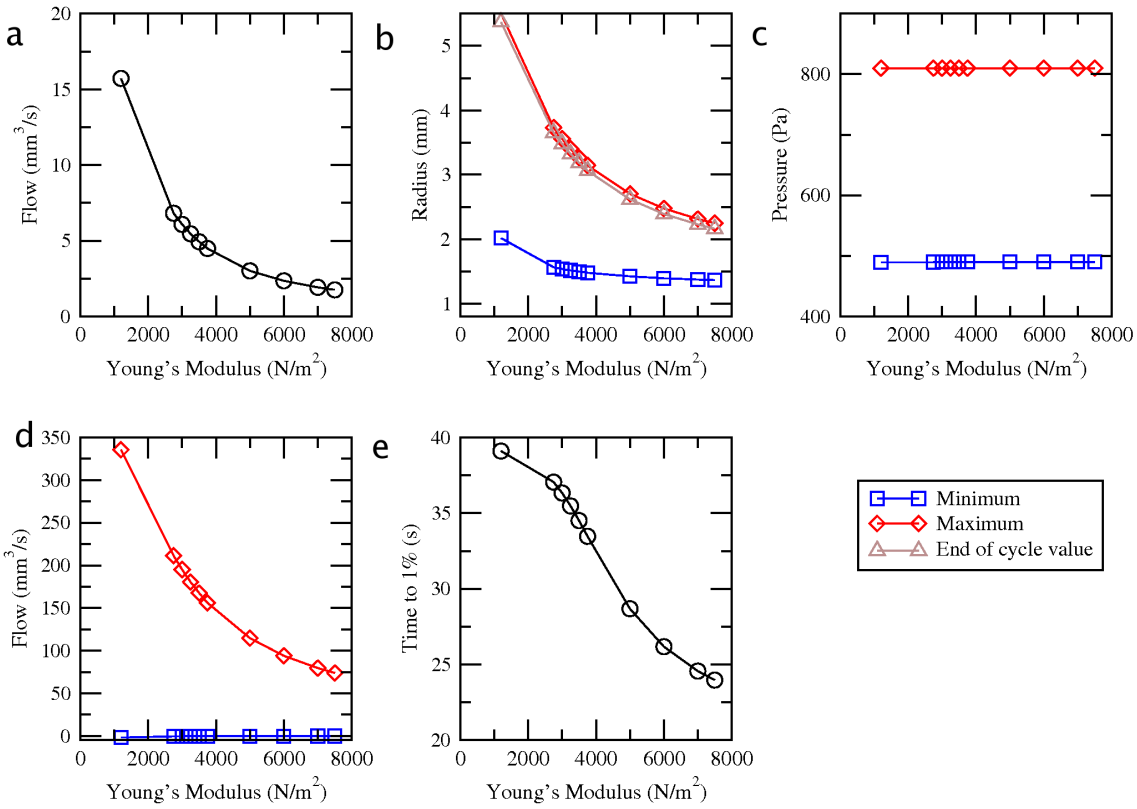

Figure 6.1: Increasing Young's modulus reduces flow. The effect of varying Young's modulus is shown on (a)Average Flow, (b) Radius, (c) Pressure, (d) Maximum and minimum flows, (e)The passive relaxation time

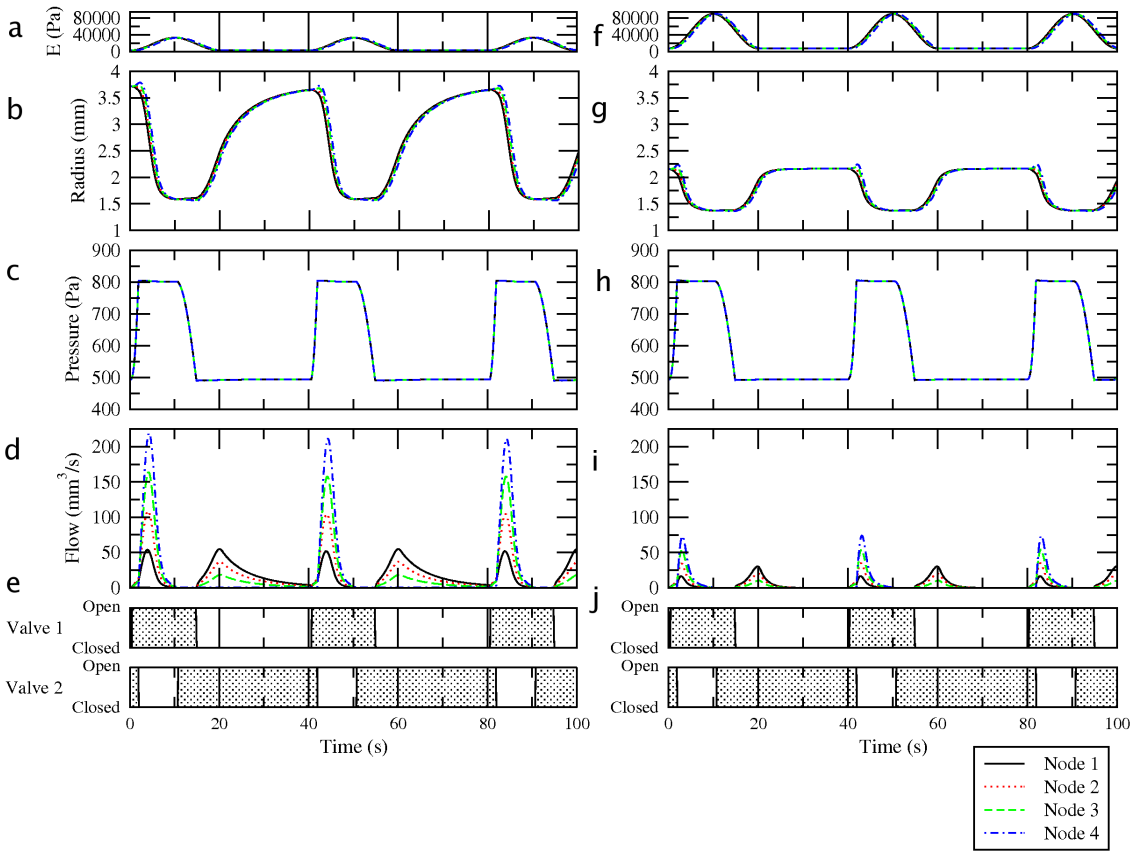

Figure 6.2: Results for a low Young's modulus ($E = 1250$ N/m^2 panels (a)-(e)) compared with a high Young's modulus ($E = 7500$ N/m^2 panels (f) - (j). Panels (a) and (f) show the low and high Young's modulus with the driving function, (b) and (g) the radius output, (c) and (h)pressure, (d) and (i) flow and (e) and (j) the valve timings

elasticity the slower passive return of the vessel generates a shark fin radius time profile.

The maximum, minimum and end of cycle radii decrease in size with a stiffer material. Furthermore the total change in radius (due to a contraction) decreases as more force is required to produce the same amount of movement. See graph 6.1 b which shows how the maximum and minimum radius are closer together for stiffer cases ie with a high value of E. The minimum radius is at a certain positive pressure and is undergoing some stretching. There is a limit to how low the minimum radius can reach (at around 1.5 mm) as this approaches the passive relaxed radius A_0. For a more elastic vessel the radius time profile is more like the shark fin shape from experiment as found in chapter 4, see graph 6.2 b and g.

The average flow decreases with a stiffer vessel due to the smaller aperture it must flow through, and the pumping force becomes smaller as the work to move the walls is increased (see graph 6.1 a). The flow peaks become shorter and thinner as it becomes harder to induce flow as shown in graph 6.2 d and i for flow in a case with low E and high E.

Increasing the wall thickness has the same effect as increasing the Young's modulus as they both represent different ways of increasing the stiffness of the material, as shown in graph 6.3 in comparison to graph 6.1.

6.3.2 Increasing Unstretched Radius

The unstretched radius A_0 was also varied. This can also be thought of as the radius at zero pressure. The standard was chosen as 1.25 mm, the radius recorded by Arkill in section 4. Increasing A_0 has the effect of increasing the time to passively relax because there is a greater distance for the walls to travel, see graph 6.4 e.

If the unstretched radius increases, so does the radius at any other point in the cycle as they are all referenced to this point, see graph 6.4 b. The change in radius increases as shown by the increasing difference in the maximum and minimum radii in graph 6.4 (b). The radius peak is not affected by a change in A_0 as shown by the

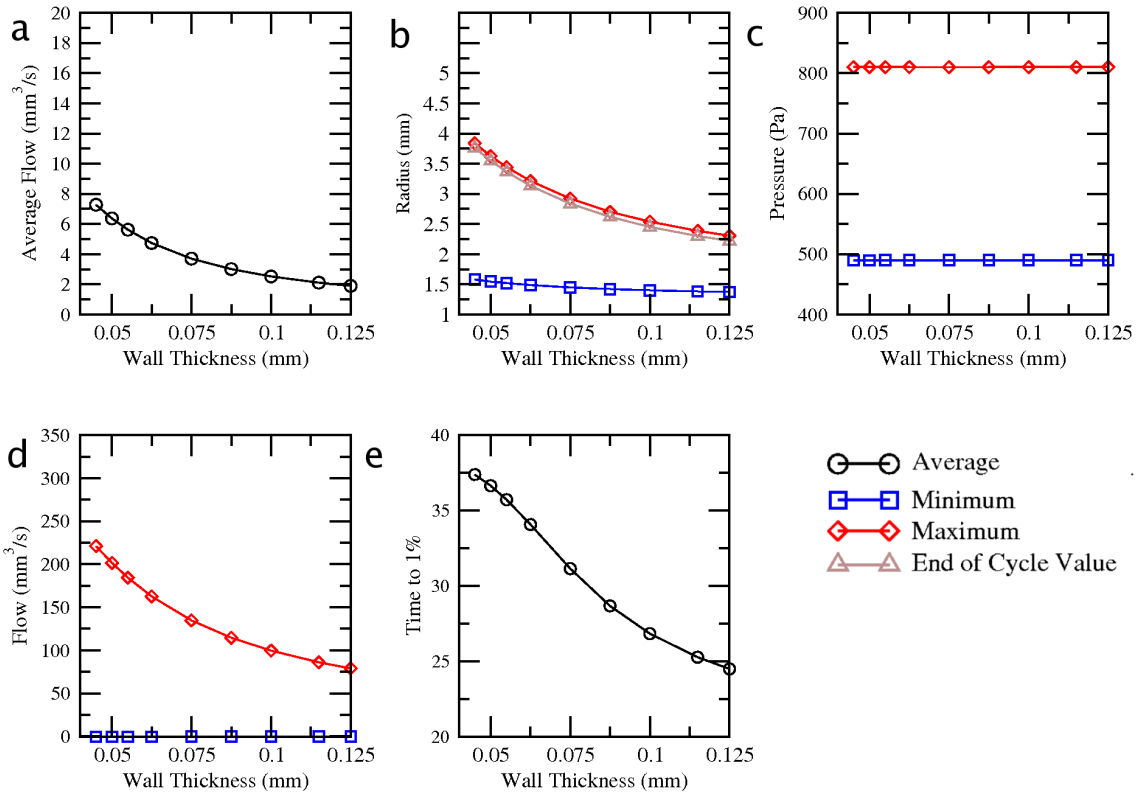

Figure 6.3: Varying the wall thickness is a different way of changing the stiffness of the vessel. Panels show the effect of varying wall thickness on Q, R, P and the passive relaxation time

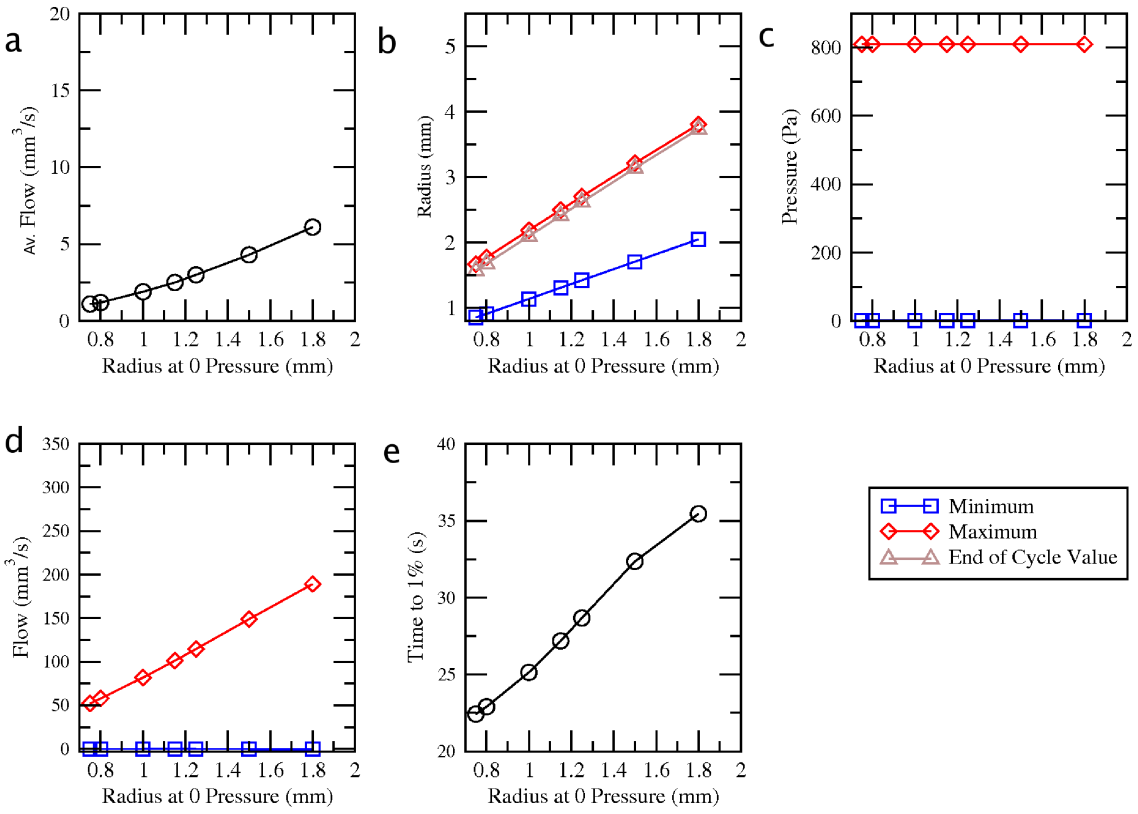

Figure 6.4: Increasing the unstretched radius increases flow. Panels show the effect of varying the unstretched radius on Q, R, P and the passive relaxation time

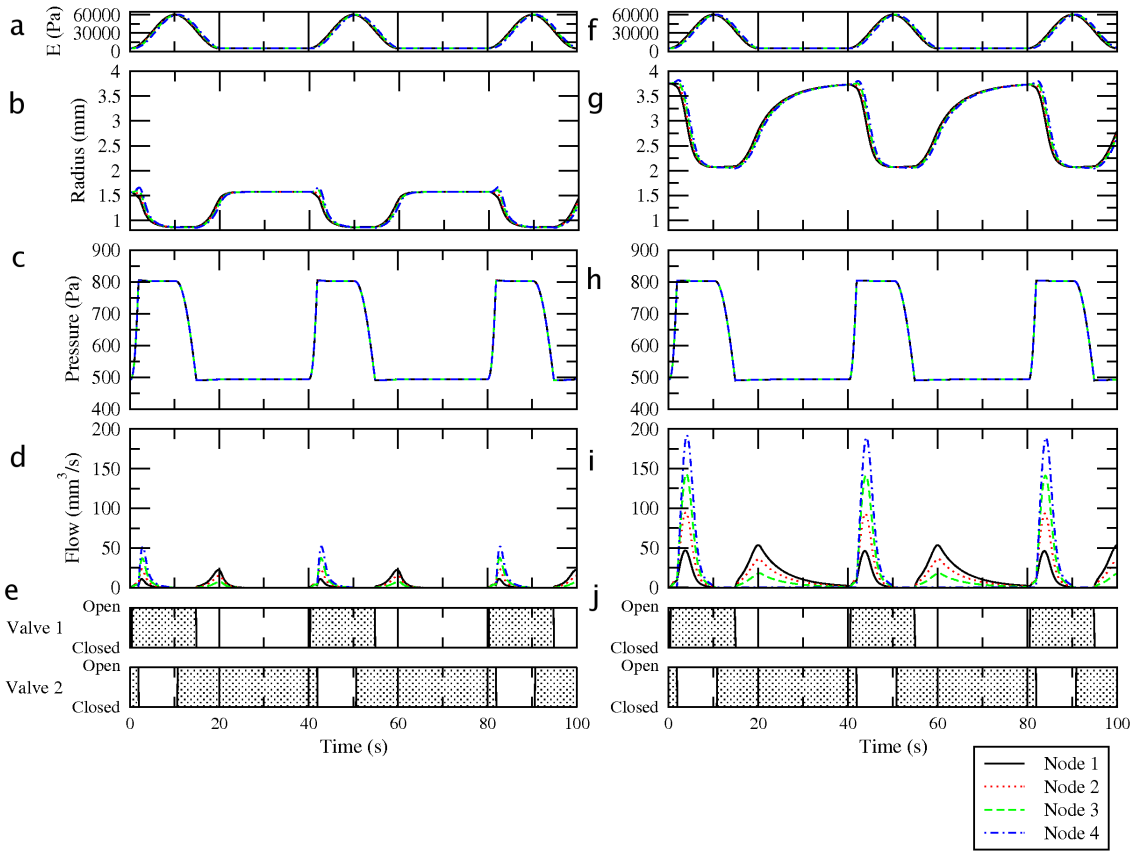

Figure 6.5: Results for a low unstretched radius (A_0), panels (a) to (e) $A_0 = 0.75$ mm and high A_0 panels (f) - (j) $A_0 = 1.8$ mm. Panels (a) and (f) show the driving function, (b) and (g) the radius outputs, (c) and (h) the pressure, (d) and (i) the flow and (e) and (j) he valve timings

constant difference between the maximum and end of cycle radii in graph 6.4 (b). The material properties have not changed so the same force is required in order to stretch the vessel by the same percentage of the original unstretched radius.

The average and maximum flows increase (see graph 6.4 (a) and (d)) because of the increase in change in radius it acts as a larger pump. Both the ejection and refilling flow peaks increase in width and height (see graphs 6.5 (d) and (i)). This is due to a greater volume change and therefore greater possible flow at every point in the cycle, with a greater cross sectional area and smaller relative contribution of resistance from the walls.

This variation in the relaxed radius shows the effect of the scale of the vessel on flow i.e. the position in the network. A lower flow is present in the smaller vessels and they also have a shorter passive relaxation stage, which may have physiological implications.

The flow appears to be directly proportional to the relaxed, unstretched radius. In a conduit we expect a the relationship flow $\propto A^2_{passive}$. So for a system presenting flow $\propto A_{passive}$, the pumping must be more efficient in smaller vessels negating some of the detrimental effect of the increased resistance. In smaller vessel the pressure is great enough to cause flow with only a small change in volume, so flow can start earlier in the cycle and continue for longer.

6.3.3 Gamma

The magnitude of the damping constant γ (also discussed in section 5.3.1) was also varied, effectively changing the damping effects of the wall.

Increasing gamma (γ), means the passive relaxation phase is longer, ie it takes longer for the walls to react passively, see graph 6.6 e and graph 6.7 (b) and (h) which shows the shark fin shape emerges with a high gamma.

The maximum radius is slightly higher for a low γ, giving a larger initial radius peak as shown by figure 6.7 (b) compared to (h). This is due to a faster response of the walls to the pressure of the fluid. As the contraction begins the pressure is

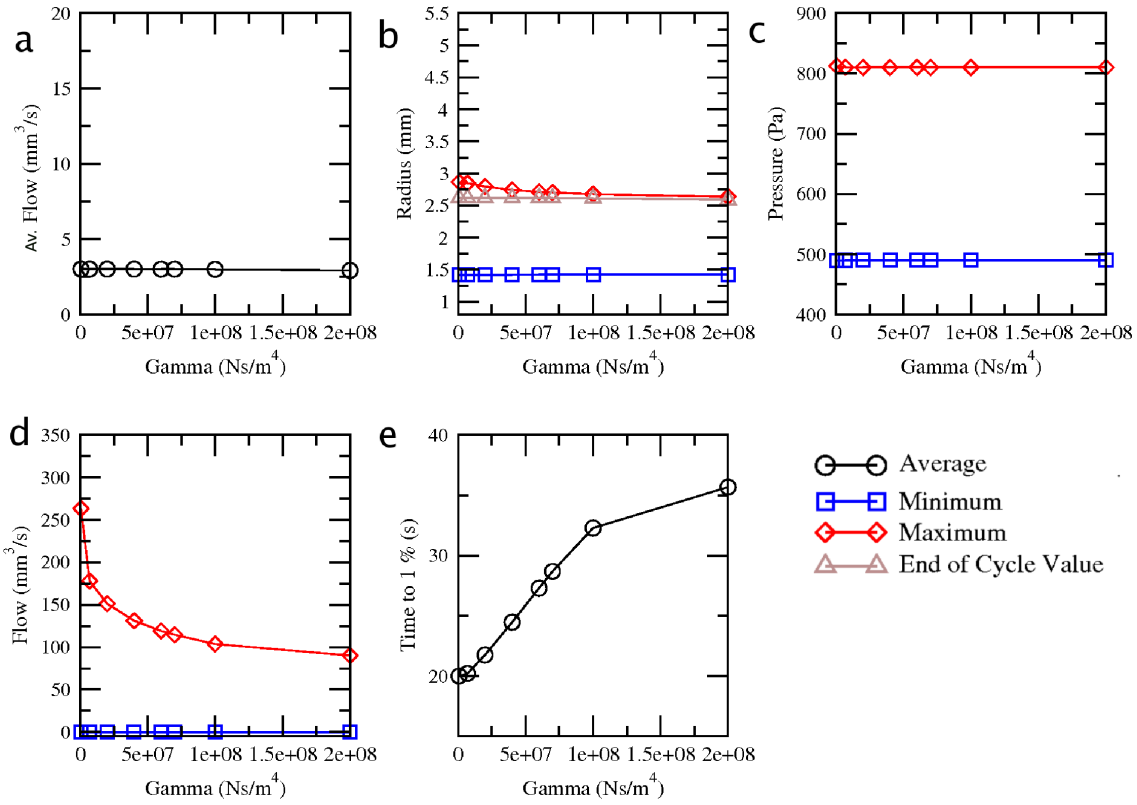

Figure 6.6: The effect of varying γ on Q, R, P and the passive relaxation time. γ has a minimal effect on flow.

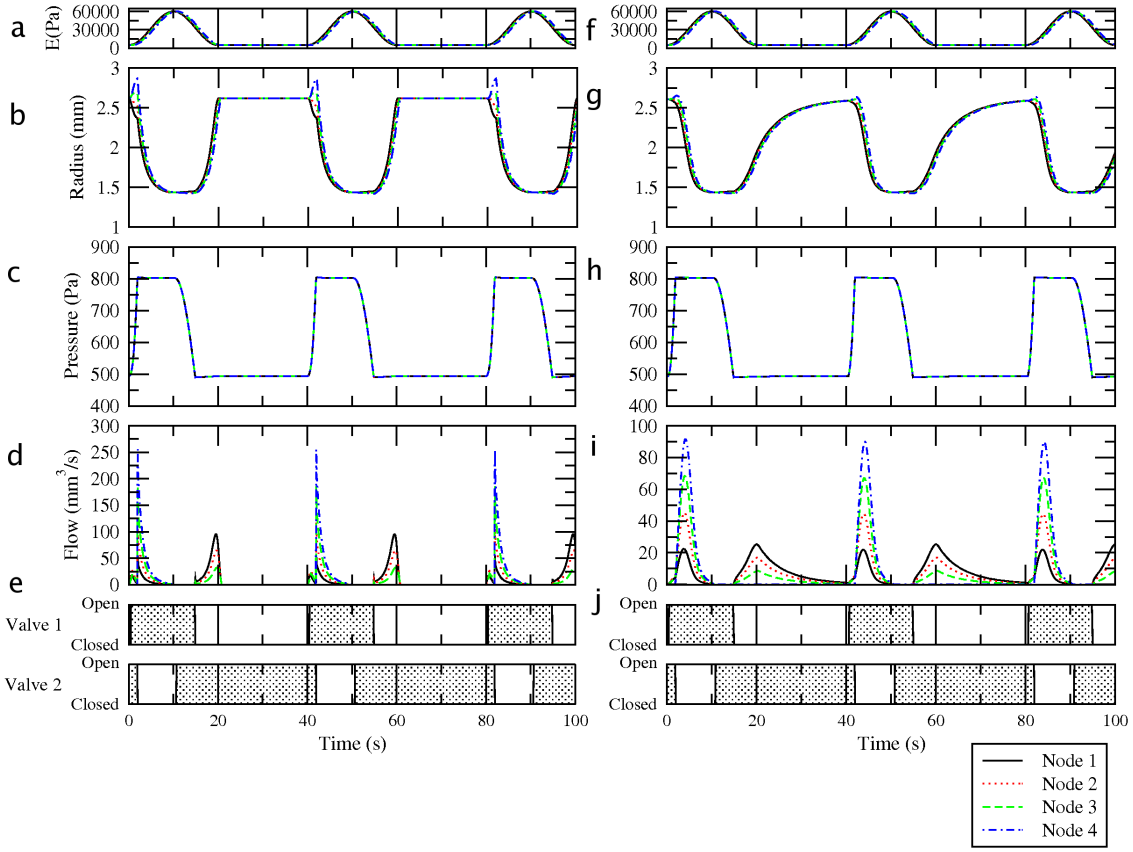

Figure 6.7: The damping constant γ effects the stability of the results. Panels show results for a low and high γ, low (a - e) γ = 7 x 10^5 (Ns/m^4) and high (f - j), γ = 2 x 10^8 (Ns/m^4). Note the different scales on the flow graphs and the flow reaches a value 3 $\times$ higher with a low γ.

transferred from the nodes which have already started contracting to those which are still relaxed, causing inflation. With a larger γ, the walls do not have long enough to react as strongly. There is little comparative change in average flow (see graph 6.6) even though the maximum flow is very high for a low gamma. This is due to instability at low gamma values, the fluctuations even out to the same average flow. A lower gamma does however give a much larger peak flow and some instability, see graph 6.6 (d) and graph 6.7 (d) and (i). With a low Gamma the flow peaks are high, thin and sharp, with a sudden jump at the start of emptying and the end of filling, as there is nothing to stop the walls from snapping into their new positions.

6.3.4 Tension

The Tension T was also varied using the relationship $T = kP$ where P is pressure and k is varied. T is included in the Tension term and this accounts for the longitudinal tension of the vessel. Within the values examined, the Tension T has a minimal effect on the magnitude of these results as shown in graphs 6.8 and 6.9.

6.3.5 Speed of Contraction/ Phase Difference

The speed of contraction can be analysed by looking at the phase difference ϕ between the nodes. The contraction wave speed of 0.02 m/s was found in chapter 4. With a lymphangion length of 0.02 m, period of 20 s, 4 nodes and time to travel across the lymphangion of 1s; this gives a phase difference ϕ of $\pi/40$.

$$x\left(t\right) = E_{amp} sin\left(2\pi ft + \phi\right) \tag{6.1}$$

where E_{amp} is the amplitude of the contraction driving function, which works by varying the Young's modulus.

As the phase difference increases, the contraction wave becomes slower. With a slower wave, the pressure increase caused by the squeezing of one cell inflates the

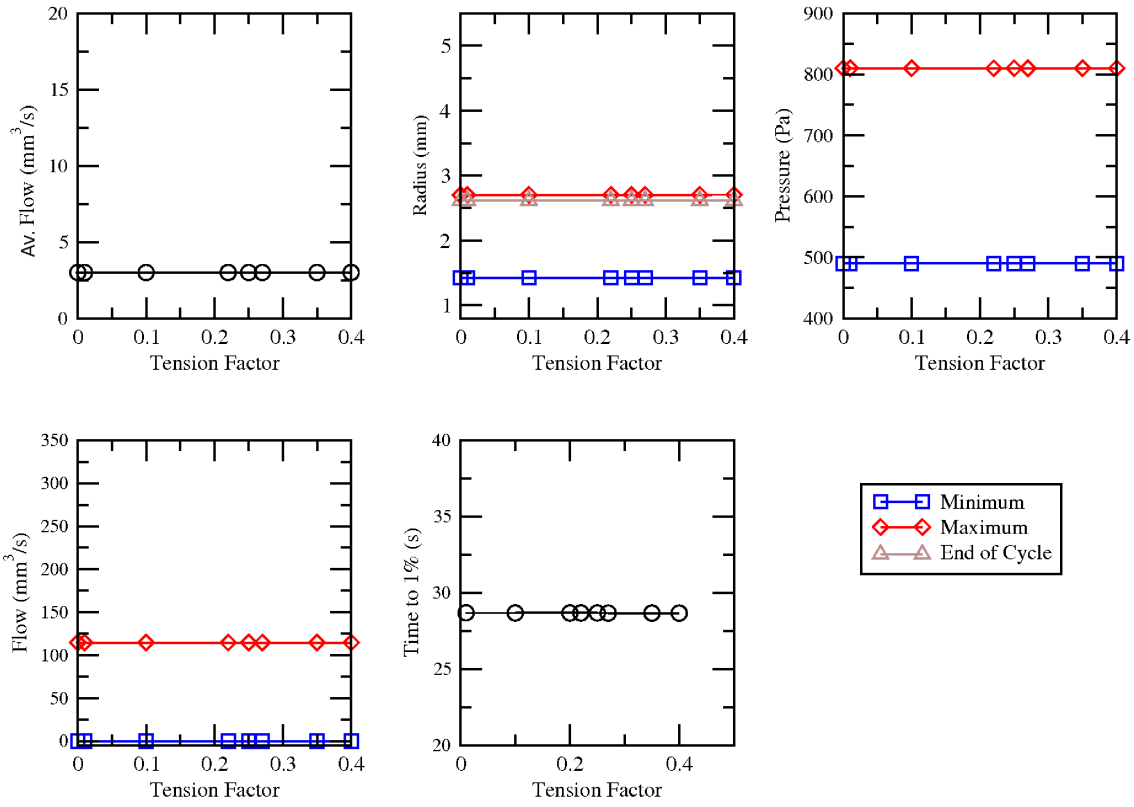

Figure 6.8: The effect of varying tension factor k on Q, R, P and the passive relaxation time. Tension has a minimum effect on flow for the setups investigated.

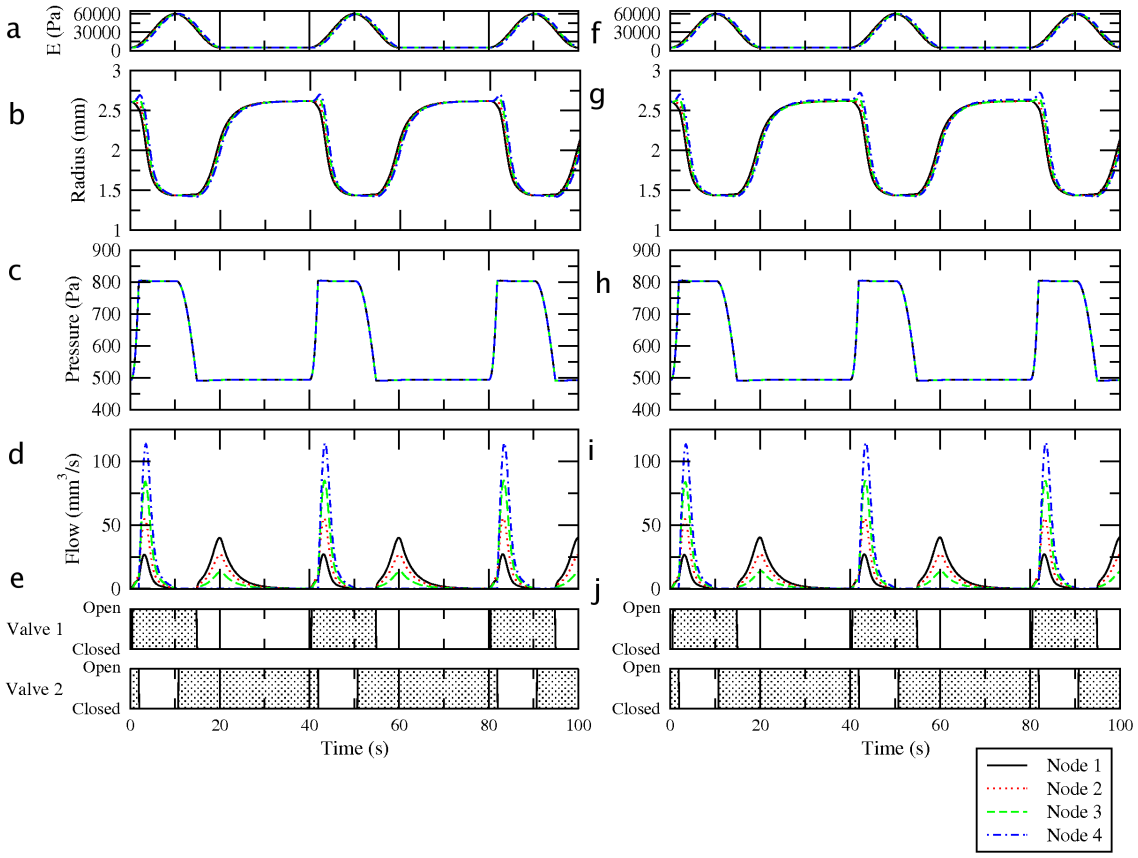

Figure 6.9: Comparing the outputs for a low and high tension factor k. Low (a - e) $k = 0.01$ and high (f - j) $k = 5$

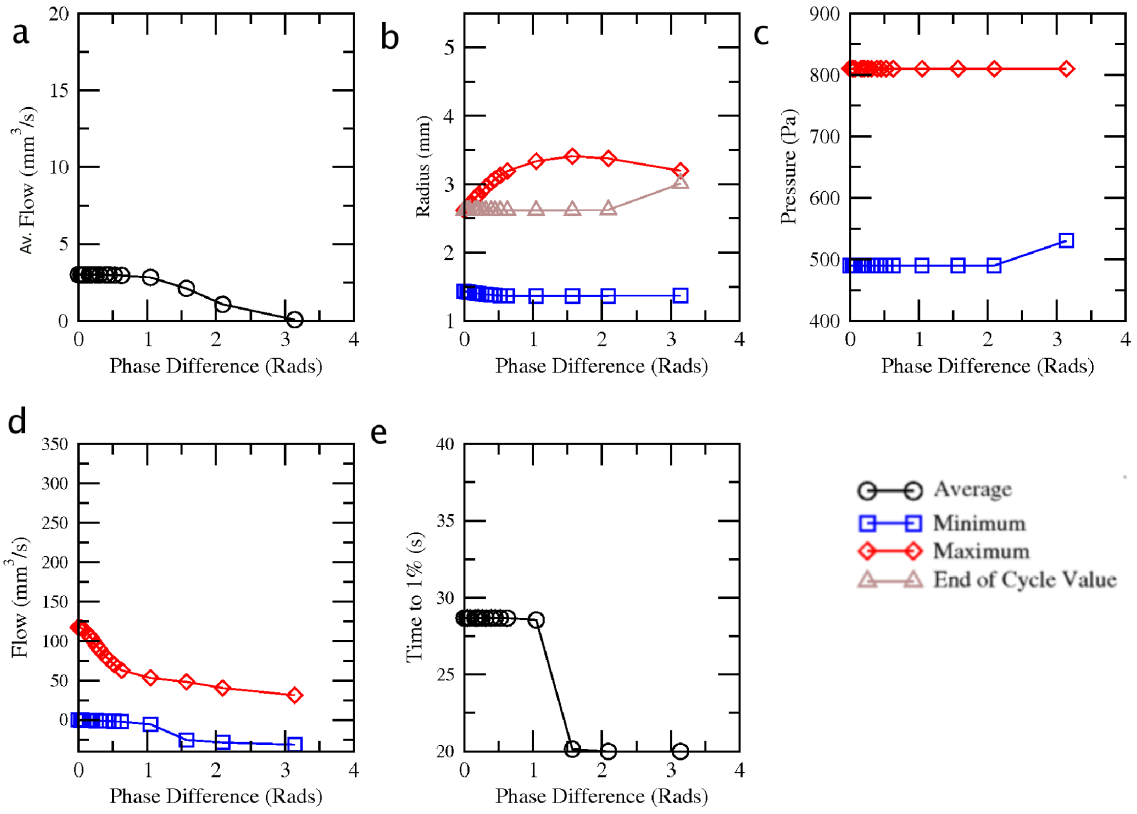

Figure 6.10: Increasing the phase difference generates a slower contraction wave velocity and therefore reduces flow.

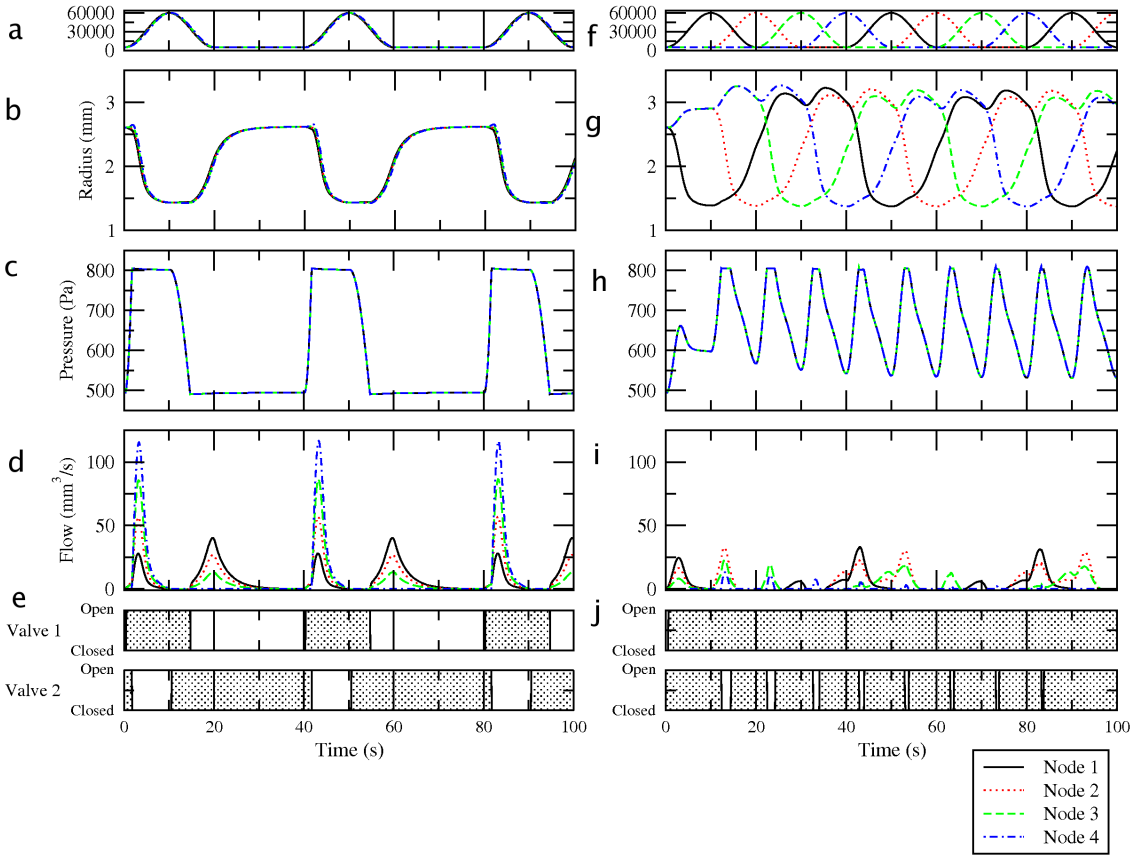

Figure 6.11: Results for a low phase difference ϕ (i.e. contraction wave velocity), panels (a) to (e) ϕ =0.0393 radians and high, panels (f) - (j) $\phi = \pi$ radians.

neighbouring cells (which are relaxed) for longer and to a greater magnitude. There is more time before the next cell contracts, and the 1st cell gets further in its cycle, generating a larger force before the next cell contracts. This leads to a larger radius peak at the start of each contraction see graph 6.10 and 6.11 (b) and (g) (and larger difference between the maximum and end of cycle radii). More of the effort of the contraction goes into inflating neighbouring cells rather than propelling the fluid out of the tube.

With a slower wave, the maximum flow is smaller (see graph 6.10 d) due to the work of the contraction being used to increase the radius of the rest of the tube rather than generating a propulsive force for the initial fast ejection of the fluid out of the tube. For a phase difference above π the wave effectively reverses direction, so π is the largest possible difference between nodal contractions and the slowest speed of propagation possible for the wave.

It is interesting to look at the speed of contraction as a factor for optimising the pump; too fast and damage may occur. Too slow and the previous segment will have relaxed again simply causing the fluid to slosh back and forth. If the segments all contracted simultaneously there would be the same pressure on both sides of the valve at any one time so no pumping activity would be generated. An optimised solution would mean that the segment 'catches' the wave just at the right point. In some ways it would make sense that this would be of a similar order of magnitude to the speed the fluid travels at. This would support Arkill's findings in chapter 4 that the wave speed is similar to that of the fluid during a contraction, behaving a little like squeezing toothpaste out of a tube. Pedley and Luo [106] however, note that there is a difference between the speed of the contraction wave and the average fluid velocity in the blood vessels and the magnitude of this difference is important to the mechanics. The rate of change of cross-sectional area is given by

$$\frac{dA}{dx} = -\frac{RuA}{c^2 - u^2} \tag{6.2}$$

where c is the speed of the wave and u is the speed of the fluid. As the difference between c and u decreases $\frac{dA}{dx}$ becomes more negative. If they are equal $\frac{dA}{dx} = -\infty$.

This point is referred to as choking and steady flow will have broken down. It has been suggested this is the prime mechanism for unsteady behaviour such as self-excited oscillations.

6.3.6 Contraction Amplitude

Next we will discuss the effect of varying the strength of contraction on the results. The amplitude of contractions can be altered by changing the amplitude of the input function. This study was performed using the changing relaxed radius as the driving force for the contraction wave (also see section 7.3). The magnitude of the change in radius was varied around a standard value of 67% of the unstretched radius, which gives a similar change in radius to the results of Arkill (see chapter 4). This means that the maximum A_0 (the relaxed unstretched radius) remains the same but the fully contracted value for A_0 becomes smaller.

As the radius change is larger with an increased contraction amplitude, there is a small increase in relaxation time as it has further to travel as shown in figure 6.3.6. This does not however increase relaxation time enough to generate the curve during return and the shark fin shape found in experiment (6.3.6).

As the amplitude of contraction increases, the minimum radius decreases, while the maximum and settling radius values remain the same. This represents a stronger contraction with a larger pumping effect.

The larger amplitude of contraction leads to a higher maximum flow (as well as minimum and average flows). The increase in maximum and average flows are due to the larger propulsive force of the contraction because of the larger change in volume between relaxed and contracted states.

6.3.7 Period

The length of time a segment contracts for was varied by altering the period. The pause in between contractions was kept as 50% of the total cycle time.

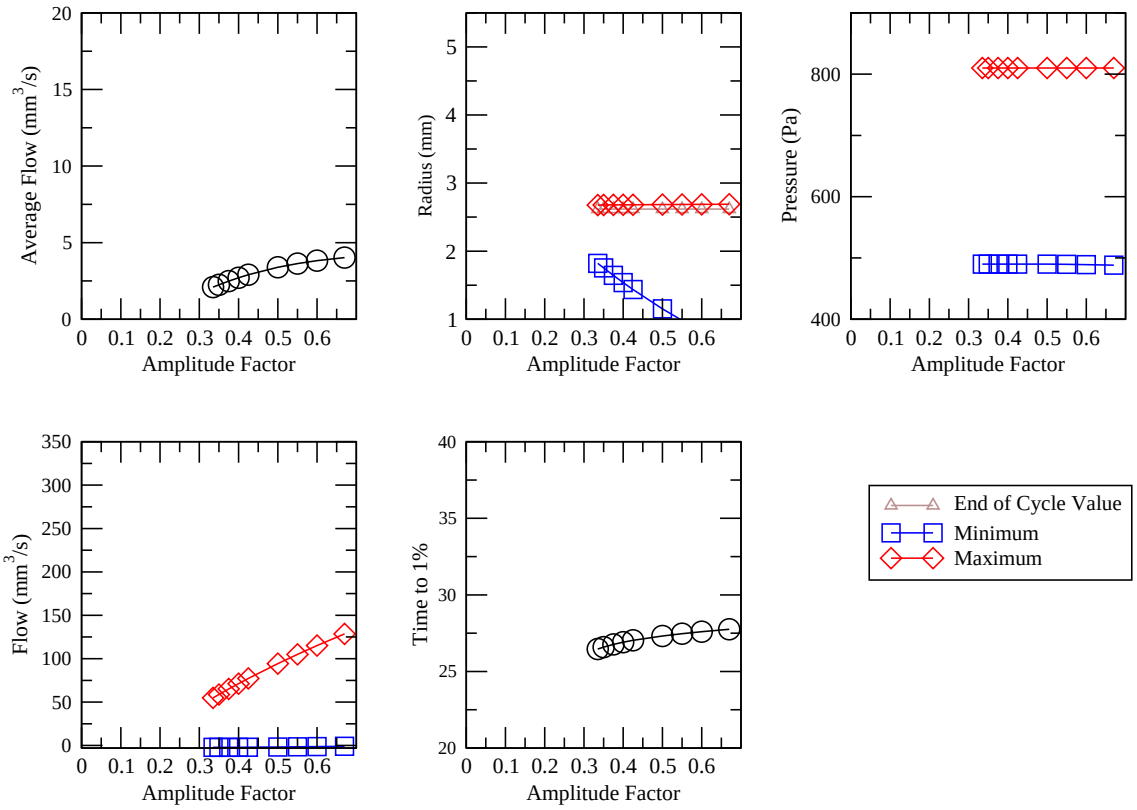

Figure 6.12: Increasing the contraction amplitude increases flow. Panels show the effect of varying the contraction amplitude on Q, R, P and the relaxation time

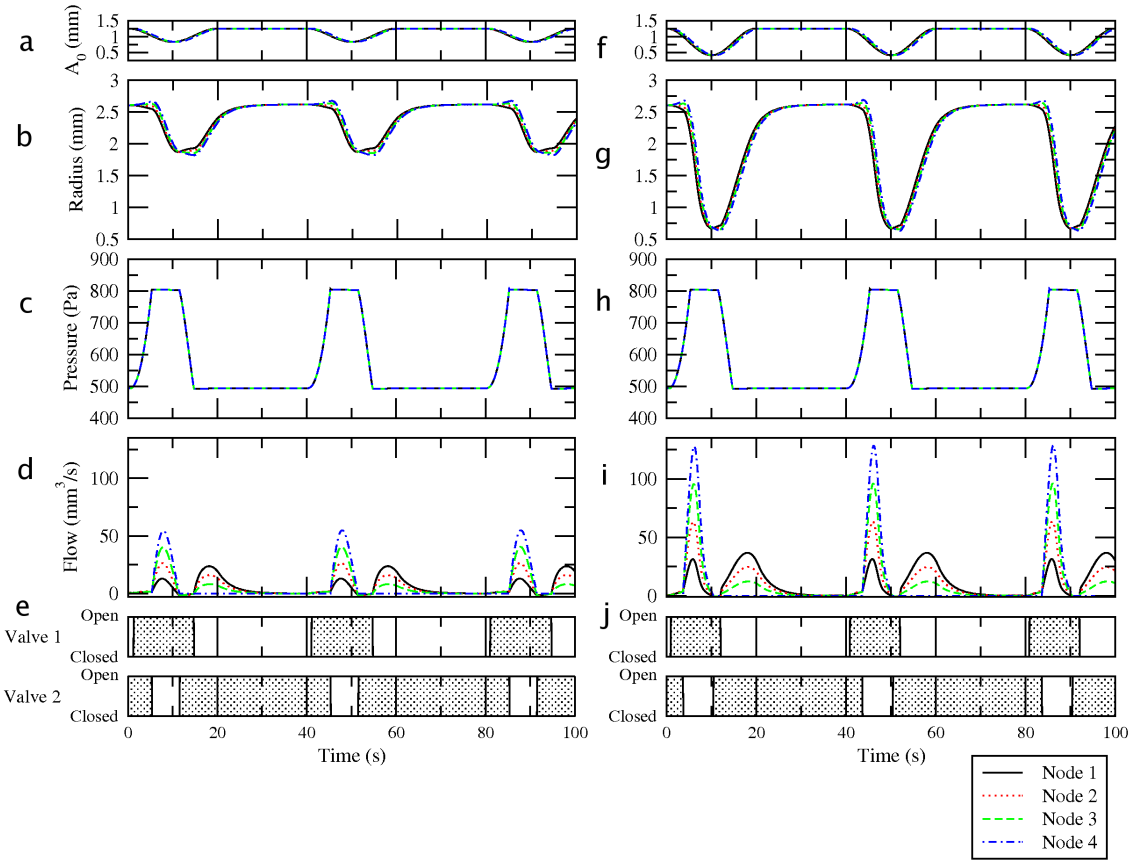

Figure 6.13: Comparison of model outputs using a low (a - e) and high (f - j) contraction amplitude

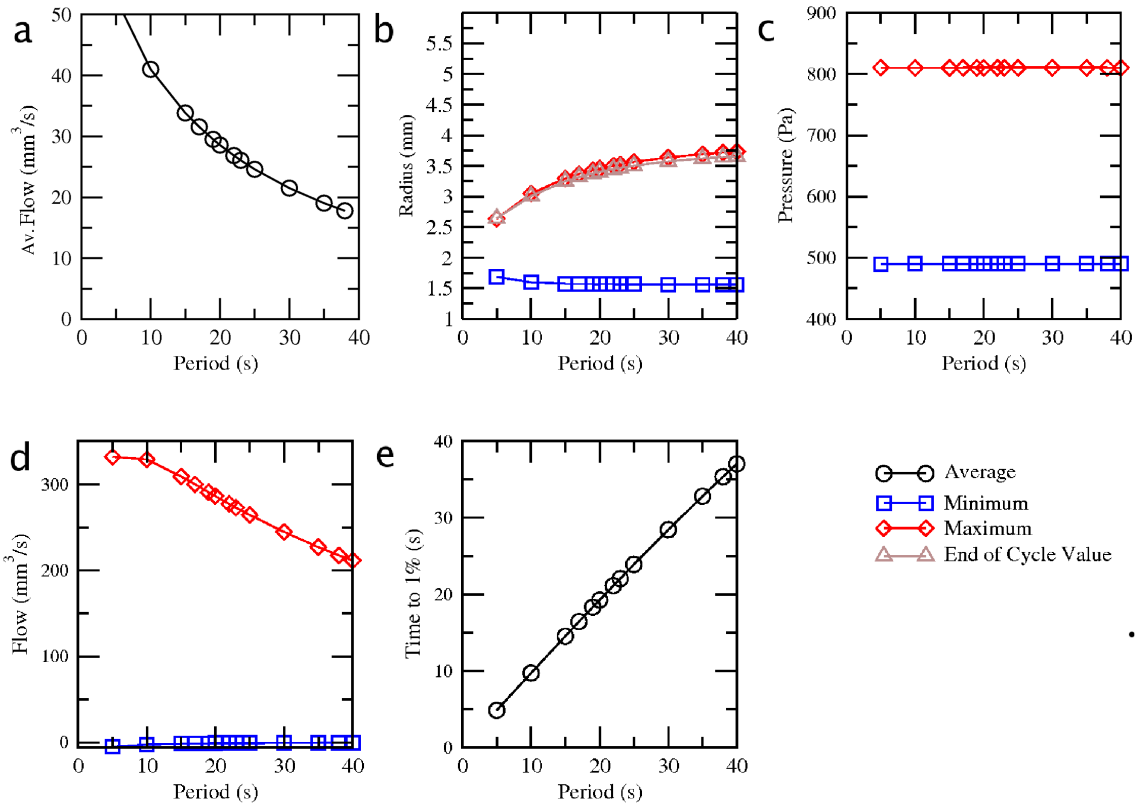

Figure 6.14: The effect of varying the period (T_p 5s to 40s) on Q, a, P and passive relaxation time. Where $E = 2500$ N/m^2 and contraction time $T_c = \frac{T_p}{2}$. Increasing the period reduces the flow as the contraction frequency is lower.

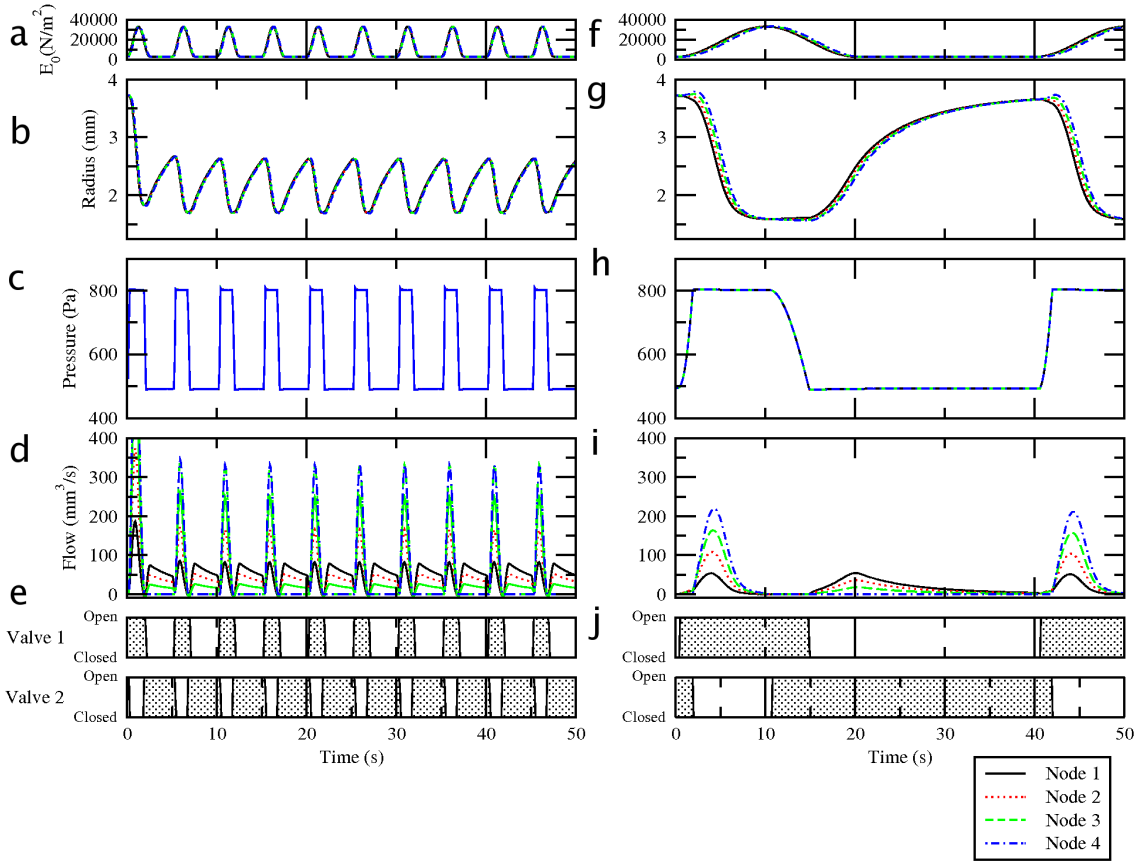

Figure 6.15: Results for a low period (T_p), low (a) to (e) $T_p = 5$s and high (f - j) $T_p = 40$s. For both $E = 2500$ N/m^2 and Contraction time $T_c = \frac{T_p}{2}$

The time to within 1% of the radius just before a new contraction is not a perfect method for quantifying the shape for these results. At a shorter period the radius does not have time to return to its original shape, as the passive relaxation is not fast enough.

The radius range is smaller (see figure 6.15) for a shorter period, as the vessel cannot relax completely. The maximum radius is larger for a larger period as in figure 6.14.

The average flow decreases with a longer period (see graph 6.14 a). The flow peaks are higher and thinner for a small period see figure 6.15. When the period is too short however the flow will decrease again as the vessel will not have time to completely relax before the next contraction occurs.

6.3.8 Pressure

Variation of the outlet pressure was examined to see the effect of pumping with or against a pressure gradient. The inlet pressure was kept at 500 Pa and the outlet was varied from 300 Pa to 600 Pa.

As shown in figure 6.16, using this larger pressure gradient in the direction of flow (i.e. 300 Pa output) completely changed the shape of the flow time relationship. The valve was open all the time and the flow went up to a maximum of nearly 2000 times the flow compared to pumping against a gradient (i.e. 600 Pa output). The flow output from the lymphangion was very similar for the 600 Pa outlet and 500 Pa outlet (so with a negative or zero pressure gradient).

The effect of adding or removing the contractions to a vessel undergoing a pressure gradient in the direction of flow was also investigated as shown in figure 6.17. The inlet pressure used was 500 Pa and outlet 300 Pa.

The flow output was greater for the case without pumping. At these high pressures the reduction in amplitude of the vessel due to pumping restricts flow to a larger extent than the pumping contributes to flow. However, how high does the pressure between two lymphangions in series really get in edema? An important

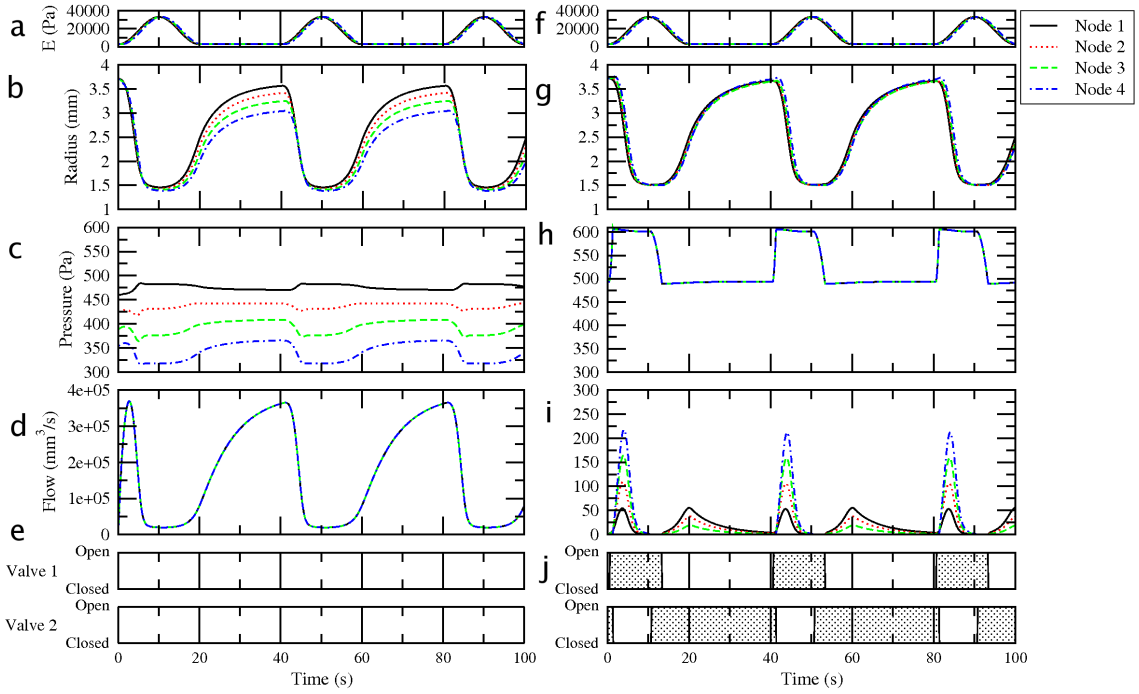

Figure 6.16: Introducing a positive pressure gradient along the vessel, in the direction of flow significantly increases flow. Windows a- e show an outlet pressure of 300 Pa (positive gradient) and f to j show an outlet pressure of 600Pa (negative gradient). For both the inlet pressure is 500Pa, please note the difference in scales for the flow.

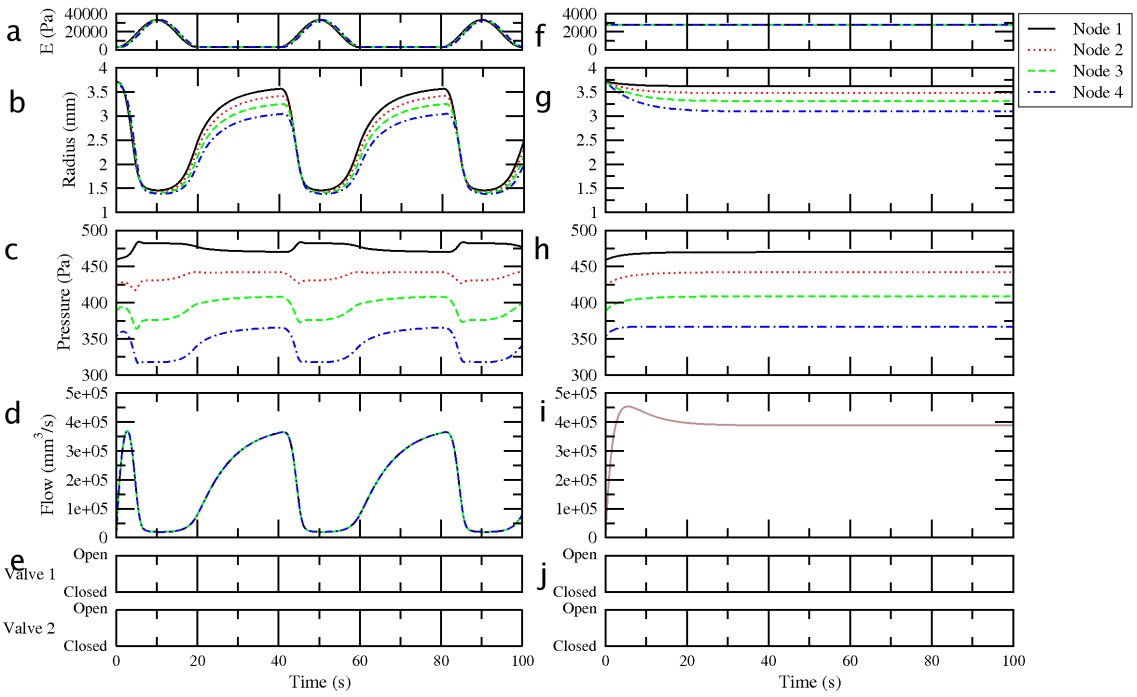

Figure 6.17: Removing contractions when there is a positive pressure gradient of 200 Pa, increases flow. Panels show effect of contractions (a-e) and passive flow (f-j) with a positive pressure gradient. Inlet pressure is 500 Pa and outlet is 300 Pa

consideration in edema may be the pressure gradient at which pumping becomes detrimental to flow. Future studies should discover how much of a positive gradient there is between lymphangions in edema, and the pressure gradient at which contractions become beneficial.

6.4 Conclusions

The present study explored the relationships between the various parameters and the contraction details generated by the wall. The degrees of freedom were reduced as far as possible by using figures from Arkill's results or from the literature and then varying a particular parameter. The lymphangions pump best if all sections of the wall contract in a quickly propagated wave. Almost simultaneous contraction of all sections increases the pressure throughout the lymphangion until the pressure difference is sufficient to open the valve and drain the segment. This is supported by Gnepp [12] who observes that as a general rule increase in frequency of contraction is accompanied by increase in flow speed , except in cases of vessel occlusion. If the modelled wave propagates very slowly, i.e. the contractions in different segments are not simultaneous, the effect is merely to pump the lymph fluid from one part of the vessel to another, without ever building enough pressure difference to open the valve.

Since our initial model used variations in E to generate the contraction behavior, the actual value of E varied; figures 4.4 and 6.2 shows that these variations compared well with the elastic properties of the pumping vessel. Varying all the parameters (except when the boundary conditions caused a pressure gradient in the direction of flow) we were still able to generate qualitatively similar pumping behavior. However some features of the radius-time graph varied such as the radius peak at the start of the contraction and the passive relaxation stage. The affect of such features on the pump and valve mechanics may have important physiological implications.

The table below summarises the effect on average flow of the various parameters.

Parameter Increasing	**Effect on Average Flow**
$\mathbf{E}$	Decreased
$\mathbf{h}$	Decreased
$\mathbf{A}_0$	Increased
γ	Minimal Effect
$\mathbf{T}$	Minimal Effect
ϕ	Decreased
$\mathbf{a}_{amp}$	Increased
$\mathbf{T}_p$	Decreased
$\mathbf{P}_{Out}$	Decreased

Chapter 7

Contraction Dynamics

7.1 Introduction

This chapter describes an analysis of the wall model and modelling strategies investigated to produce an improved model of the activity of the lymphatic vessel walls and further understanding of the mechanisms involved. This chapter concentrates on the details of the function of the contraction and the way to model it rather then the variation of parameters as investigated in the previous chapter. The details of the contraction were examined; including the direction of propagation of the wave, how the muscle contraction works and how to model it, the strength of the contraction itself and the speed of travel of the wave.

7.2 Wave Direction

There is some discussion in the literature as to whether the contraction wave travels with the direction of flow or against it and it is pertinent to find whether this in fact makes a difference to the resulting flow. McHale and Meharg [38] observed contraction waves propagating against the direction of drainage allowed by the valve, this will be referred to as a reverse contraction wave. Indeed McHale and Meharg [38] found it was possible to set up in vitro experiments so that contractions move

in the opposite direction to flow (also see section 2.1.2).

The model was set so the phase difference is counted from the down stream end of the vessel rather than the upstream.

7.2.1 Results/Discussion

Figure 7.1 compares a wave propagating forwards and backwards. The major difference caused by a reversed contraction wave is the negative peak in flow at the start of every contraction, before valve two opens see graph 7.1 d and i. This is due to propulsion against the direction of flow, by the wave. For the forwards wave (7.1 i), this simply adds to the existing peak.

Other differences between the forward and reverse propagating contractile wave are minimal; for the reverse wave, the maximum flow is slightly increased, which is probably due to the later opening of the valve, but the average flow is slightly reduced for the same reason.

We would suggest, though, that the pumping through a branching network is likely be easier with a reverse contraction wave, which would be able to propagate up both branches at a bifurcation. A forward propagating wave arriving at a bifurcation would need to co-ordinate with any wave propagating down the other branch, otherwise lack of coherence between the waves would be likely to lead to reduced efficiency. Reverse contraction waves have been observed in experiment [38].

At first glance a contraction wave propagating against the direction of flow seems counter intuitive but there is a possibility that a reverse wave actually aids the draining process. We submit that the pumping throughout the network would be able to co-ordinate much more effectively with reversed propagation, as the wave can thus pass to the branches off a larger trunk. If the wave is propagated forwards, the impulse to contract would be passed to different points in the trunk, from the smaller branches at different times without co-ordination. With that in mind it now seems intuitive that a co-ordinated system would produce a greater output, therefore a reverse wave would be more effective if an entire network was being considered.

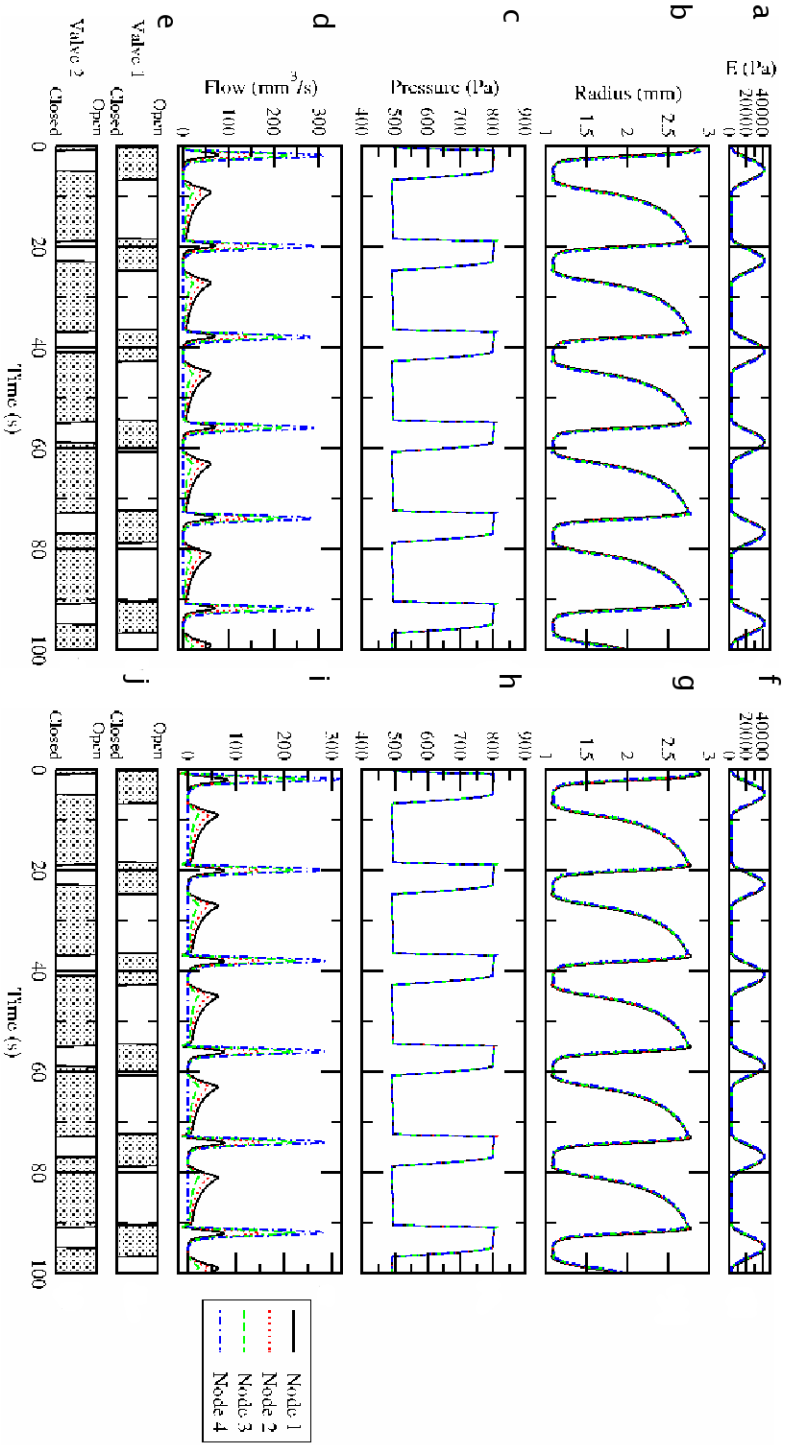

Figure 7.1: Direction of propagation of the contractile wave has minimal effects on flow. Panels a to e show a forwards propagated wave and f to j show a reverse wave in comparison to the direction of flow.

7.3 Representing the muscular activity using a variation of Young's modulus (E) or relaxed radius (A_0)

When muscle contractions occur the interlocking fibres move together and the material becomes stiffer and thicker. It is not immediately clear whether it would be appropriate to drive such a contraction by varying the relaxed radius (i.e. representing the interlocking fibres moving together) or by changing the Youngs' modulus (so the material simply becomes stiffer). Alternatively it may even be most accurate to use both methods, however it was found that both have a similar effect so it does not seem necessary to couple the two methods.

7.3.1 E driven Wave

This is the method for driving the contraction developed in chapter 5 and used throughout sections 5, 6 and 7.2 unless otherwise stated. The input sine pause function changes the Young's modulus so each contraction is modelled by varying the stiffness of the material. In this setup, the relaxed radius A_0 remains the same throughout. Only the stiffness of the material changes as shown in figure 7.2. So the radius A_1 at pressure P_1 is different depending on how contracted the vessel is, varying between A_{1C} (contracted radius) and A_{1R} (relaxed radius).

7.3.2 A Driven Wave

When A is driving the contraction wave, the value for Young's modulus is constant and the unstretched radius varies with the sine pause configuration developed in section 5 to drive the E varying function. This time before introducing an internal pressure, the unstretched radius A_0 varies between A_{0C} (contracted) and A_{0R} (relaxed). The thick walled tube equation [19] determines the pressure radius relationship.

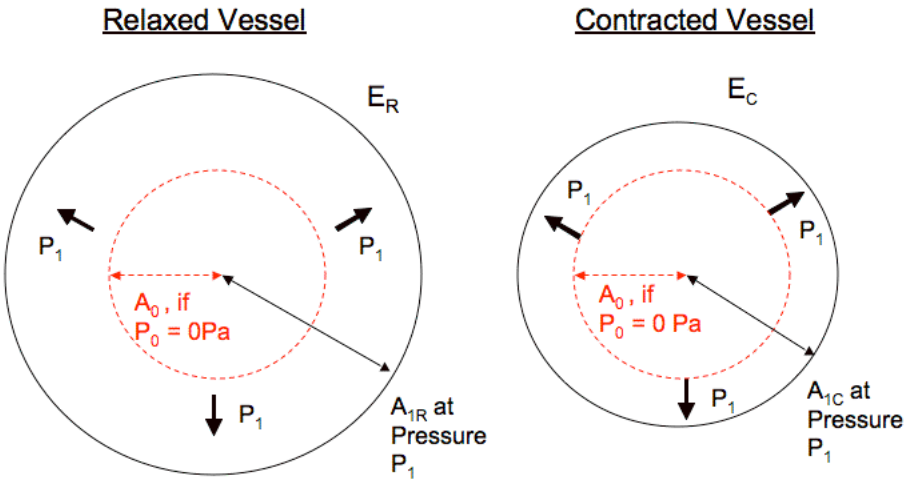

Figure 7.2: The contracted and relaxed vessel using the Young's modulus (E) driven contraction model

Thick Walled Tube Equation:

$$\Delta P = E\Delta a_{out}^2 \frac{(a_{out}^2 - a_{in}^2)}{2(1-\sigma^2)a_{in}^2 a_{out}} \tag{7.1}$$

Equation 7.1 assumes that the elastic tube does not change in length on inflation. The radius at a certain pressure P will change depending on the point in the contraction cycle, if we assume the radius is driving the contraction. If we use the internal pressure P_0 as 0 when the radius is A_0 , then we are always comparing the radius to that at an unstretched state (A_0). If the muscle is relaxed we can then term the radius A_{0R} (so it is unstretched and uncontracted). If it is contracted, it would then become A_{0C}. During the actual cycle the vessel is always slightly stretched so it will be A_0 plus a certain width caused by the increase in pressure. So the radius (A_1) at pressure P_1 will depend on how contracted the vessel is and the difference between P_0 and P_1, varying between A_{1R} and A_{1C} as shown in figure 7.3.

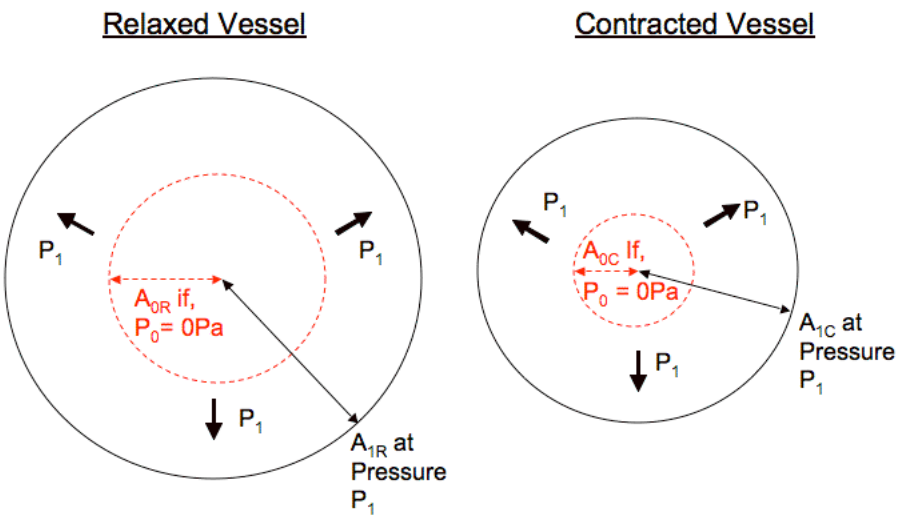

Figure 7.3: The contracted and relaxed vessel using the unstretched radius (A_0) driven contraction model

Kp

Bergel describes the thick walled tube equation in [19], see equation (7.1). For calculation purposes it is useful to rearrange this equation to give the value Kp as below as in equation (7.2).

$$Kp = \frac{(a_{out}^2 - a_{in}^2)}{2(1-\sigma^2)a_{in}^2 a_{out}} \tag{7.2}$$

The table below shows the variables used, otherwise all the variables for a standard run were used as in section 6.2.

Contraction Model	**Amplitude**	**A_0 Passive (mm)**	**E_0 (Pa)**
E	5.5 E_0	1.25	5000
A_0 Corrected	0.425 A_{p0}	1.25	5000

Looking at Arkill's results in chapter 4 we would like the total change in E during a contraction to be approximately 11E_0 , which gives an amplitude of 5.5 E_0. The calculations were a bit more complicated for the radius driven model, as they need to be based on A_0 Passive. We would like the radius to vary between approximately

Contraction Model	Average Flow (mm^3/s)
E	3.7613
A	7.4×10^{-10}
Corrected A	3.631

Table 7.1: The average flow using 3 different models, E, A and corrected A

2.55 and 1.5 mm. This gives a total change of 1.05 mm. If the maximum unstretched radius A_0 is 1.25mm then 1.05mm gives a change of 84%. This was rounded to 85%, giving an amplitude of 0.425 A_0.

7.3.3 Results/ Discussion

As shown in figure 7.4 the initial results for an A_0 driven contraction wave came out negligible in comparison to the E driven wave results, without enough pressure to open the valve. It was found that the assumption that the parameter Kp (shown in equation 7.2) was the same throughout the cycle, did not hold true if the unstretched radius changed during the cycle. This Kp was calculated to combine various terms that appeared not to vary with time (in order to save on processing time in calculating the thick walled tube equation 7.1). This value does however require the radius at a pressure of zero (the unstretched radius) which in this A_0 driven model changes throughout the cycle. This value of Kp does not change for the E driven model as the value for A_0 does not change.

With the correct amplitude of variation, the A_0 driven wave model now gave results very similar to the E driven model for a similar change in radius as shown in figure 7.3.3. The average flow is very similar, see table 7.1 and either model could be used. As the model using E gave an opportunity to save processing time, (by calculating Kp just once at the beginning of the simulation) this was used in most cases.

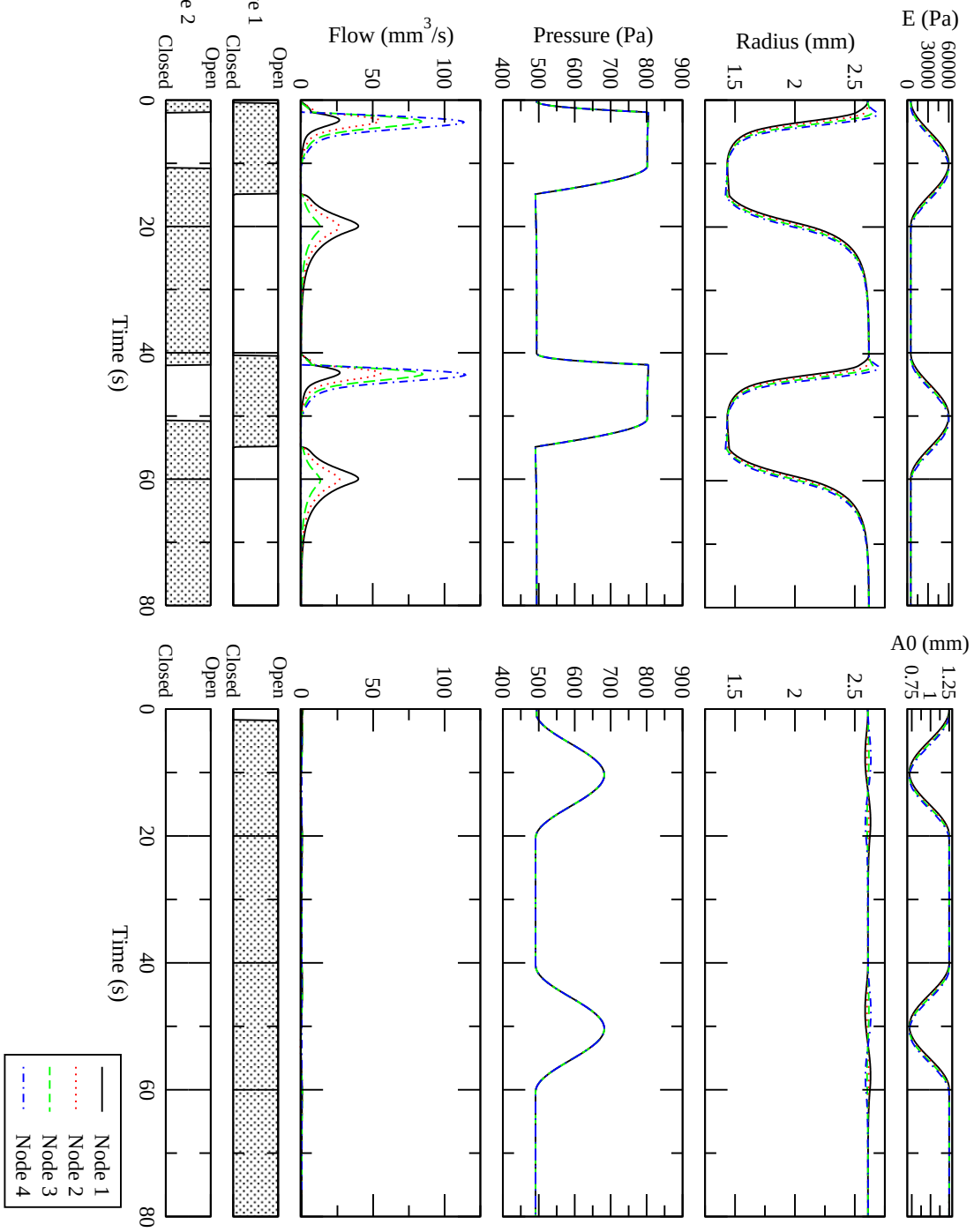

Figure 7.4: A comparison of the input function A, P, Q and valve timings for the E driven model (a - e) against the initial A driven model (f-j). Using the A driven model gives a very low contraction when k_p is calculated at the start of the run.

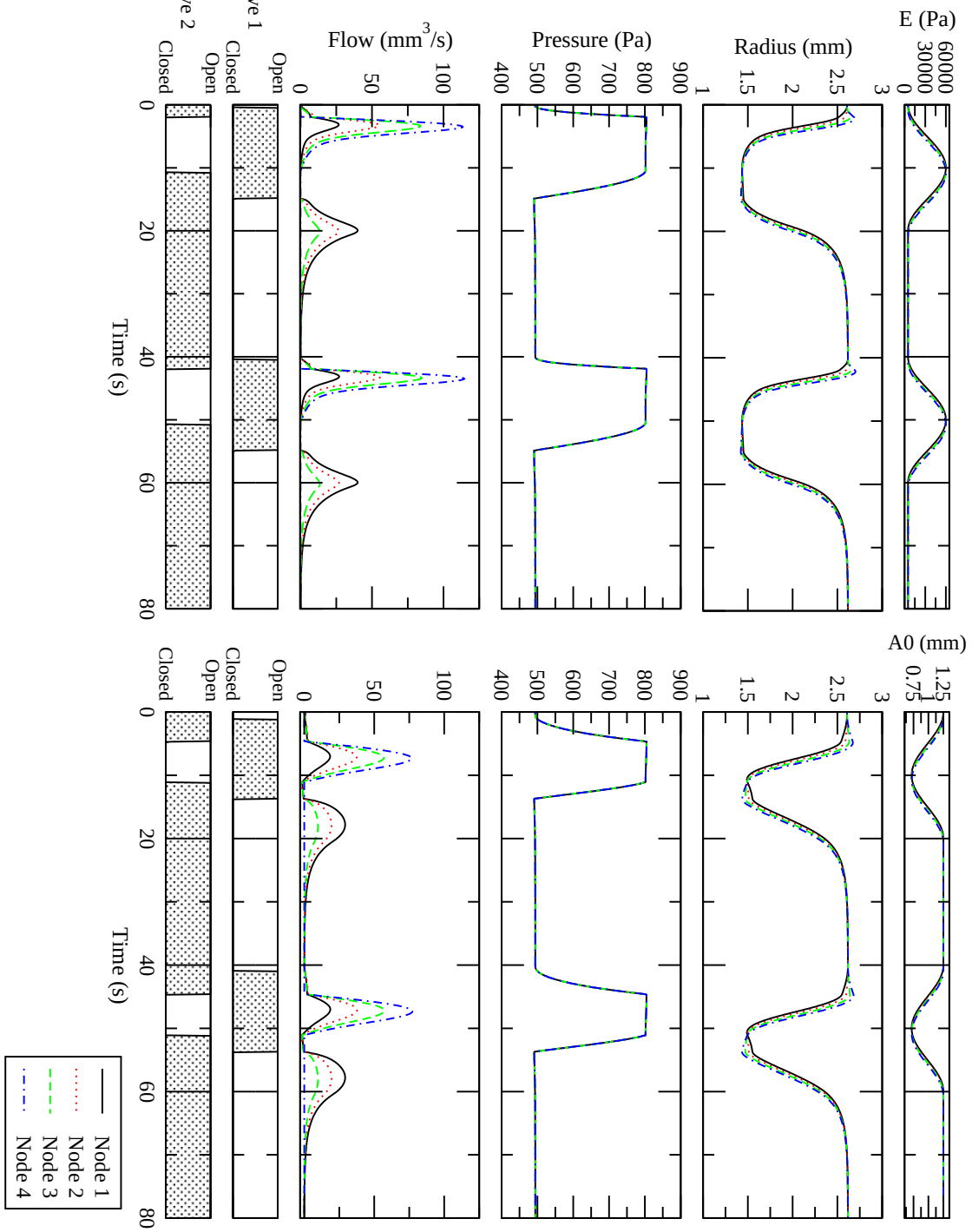

Figure 7.5: A comparison of the Input function A , P, Q and valve timings for the E driven model (a - e) against the corrected A driven model (f-j), which include a time varying Kp giving results very similar to the E driven model.

7.4 Matching Model to Experimental Results

This section explores characteristics of the radius time and pressure radius relationships and their variation with various parameters. This enabled the matching of characteristics on both graphs to experiment while keeping within experimental error margins.

7.4.1 Introduction

Within physiology, parameters have a much wider distribution about the mean than traditional engineering. This variation occurs even within one species, depending on the part of the body and the age and size of the animal. This can cause complications in accurately modelling a sensitive system, where 5 % is not considered a large error. There are some values which are extremely difficult to measure accurately in experiment (e.g. the value for the radius at a pressure of 0 Pascals). Unfortunately this particular value is one of several that are critical to the model and are prone to error. Data trends can be a far more useful basis for representing a system rather than individual points, as trends are more robust to causes of inaccuracies.

Rather than trying to match all the characteristics of a particular vessel, we investigated the more useful data trends, which should give a much more accurate model. This was undertaken by matching the gradients on the pressure radius graph (e.g. graph 7.7) while maintaining the radius time profile. Ideally for our model we would like both the behaviour relating the pressure to the radius and the radius to the time (including the shark fin shape due to passive relaxation) to match. Until now if the radius time model output matched experiment well, the pressure radius did not and vice versa.

7.4.2 Method

We compared the pressure versus radius and radius versus time graphs from experiment to those on the model, using the same parameters. Lines were set up on the

pressure versus radius graph to represent the model's input for minimum, maximum and midway points in the contraction cycle.

Ideally the maximum and minimum lines from the model would lie along the edges of the rhombus from experimental results, following the maximum and minimum behaviour we had identified in vitro. As can be seen from graph 7.7 the radius pressure relationship does not match experimental results in terms of gradient and origin on the graph.

In order to match the initial gradient and postioning on the radius pressure graph with the model, the parameters could be changed within the bounds of error (if the parameters are sensitive enough).

Initially we used the radius time and pressure-radius data from different experiments. These did not match and had very different maximum and minimum radii. This made it difficult to set the origin of the input lines. It was found however, that by changing the results to the percentage contraction, the graphs matched very well.

7.4.3 Results/Discussion

Various parameters were varied within the experimental error limits and the effect on the pressure-radius and radius-time graphs observed. It was often found that when one parameter was varied another would also need to be changed in order to match the experimental results as shown in figure 7.8. The parameters that had the greatest effect on the pressure- radius relationship were found to be the boundary pressures P_{B1} and P_{B2}, the relaxed unstretched radius A_0, the wall thickness h and Young's modulus of the wall E and the change in E (E_{amp}).

The boundary pressures allowed the results to be shifted vertically. Both pressures could be lowered in order to lower the position of the results on the graph, while keeping the pressure difference the same. This measure affected the output but not the input lines of the model, with the results coming out lower down on the graph with a lower pressure. This was useful as the relationship between the lines was more similar to the *in vitro* results in the lower portion of the graph, keeping well

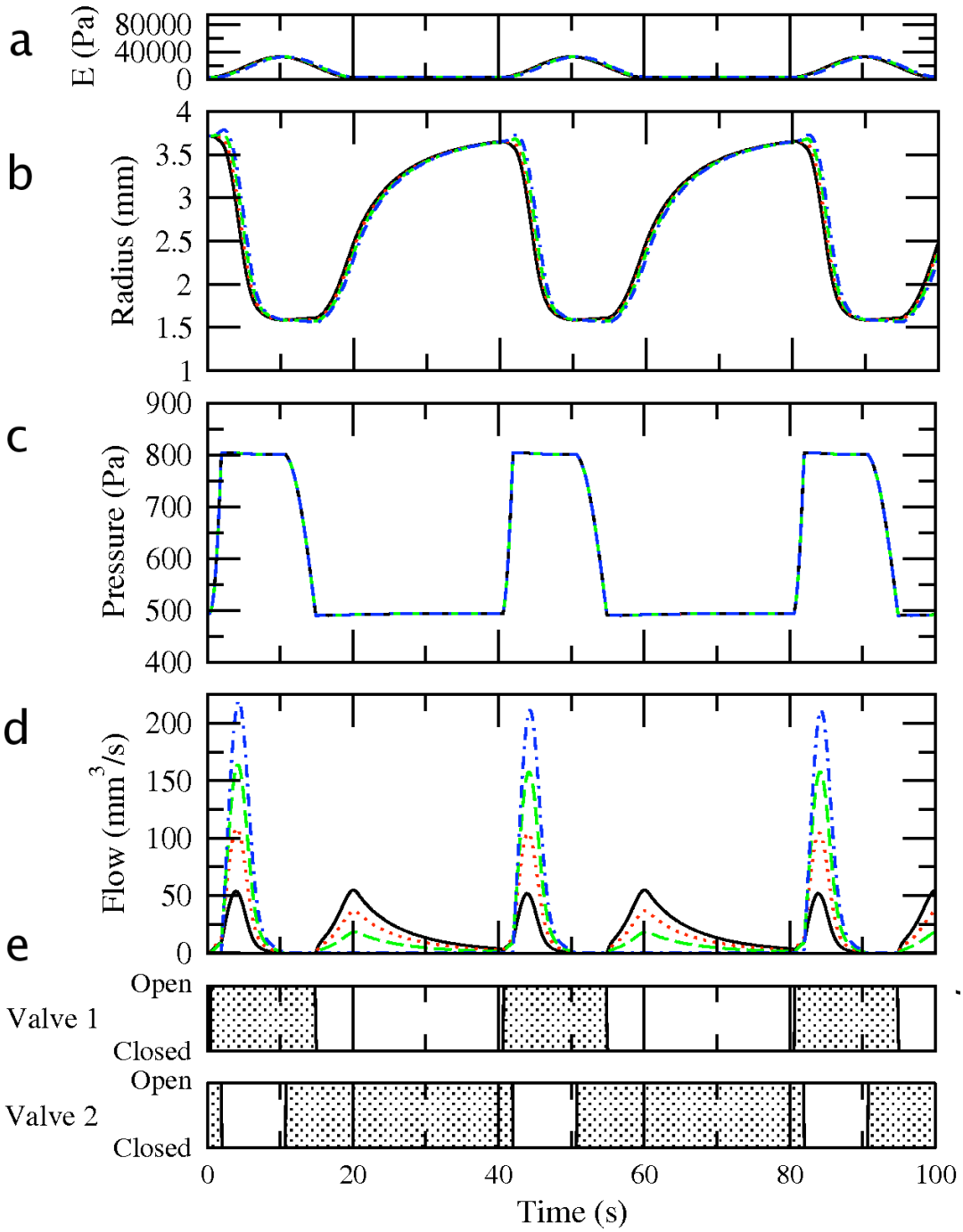

Figure 7.6: The model output before matching the radius vs time and pressure vs radius profiles to those found in experiment, showing the variation with time of radius, pressure and flow, where $E_0 = 2750$

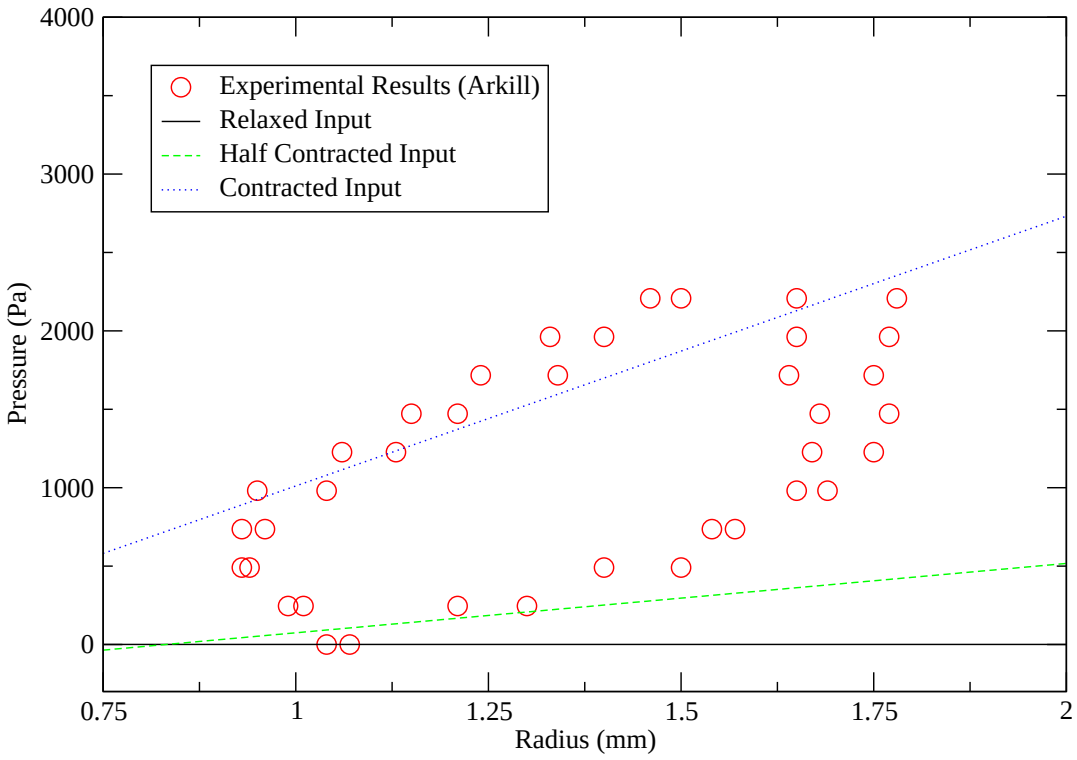

Figure 7.7: The radius pressure relationship before matching the radius vs time and pressure vs radius profiles to those found in experiment, where $E_0 = 2750$

below the point at which the gradients change on the pressure radius graph.

Increasing the relaxed unstretched radius A_0 shifted the model input lines to the right, but this often meant that the Young's modulus or wall thickness would need to be increased in order to adjust the fit of the gradient now the line had moved. This type of change is shown in figure 7.8. Increasing the Young's modulus or wall thickness increased the gradients of the lines on the pressure-radius graph, making the vessels stiffer.

Increasing the contraction amplitude E_{amp} (change in the Young's modulus) generated a larger contraction and a larger angle between the lines. This made the maximum gradient steeper but kept the minimum input the same (i.e. the maximum contraction was stronger but the minimum stayed the same). Increasing this E driven contraction amplitude helped to encourage the shark fin shape with a longer passive relaxation stage. As discovered in section 7.3.2 with the radius driven contraction wave, this is due to the increased change in volume the vessel undergoes during a contraction.

As can be seen in figure 7.9 and 7.10 the relationship was fitted satisfactorily using the inputs shown in the table above. Any measure which increased the change in radius or the change in contraction strength also encouraged the saw tooth shape to emerge, by giving a longer passive relaxation stage. The graph 7.9 fits well for the values of pressure used 500 - 800 Pa.

It is also possible that the original discrepancy in the direct implementation of the experimental parameters to the pressure radius graph is because some other factor has not been represented properly by the model so far. The resistance seems a likely candidate. It would seem likely that the resistance increases in a curve as the valve closes and the volume that can pass decreases non-linearly (also see chapter 8).

A further consideration is that the in vitro experimental radius-pressure relationship changed gradient after a certain point. This is due to the material's ability to change properties with strain mentioned in chapter 1. This is not represented by the current modelling method, but the first gradient covers results within the physiolog-

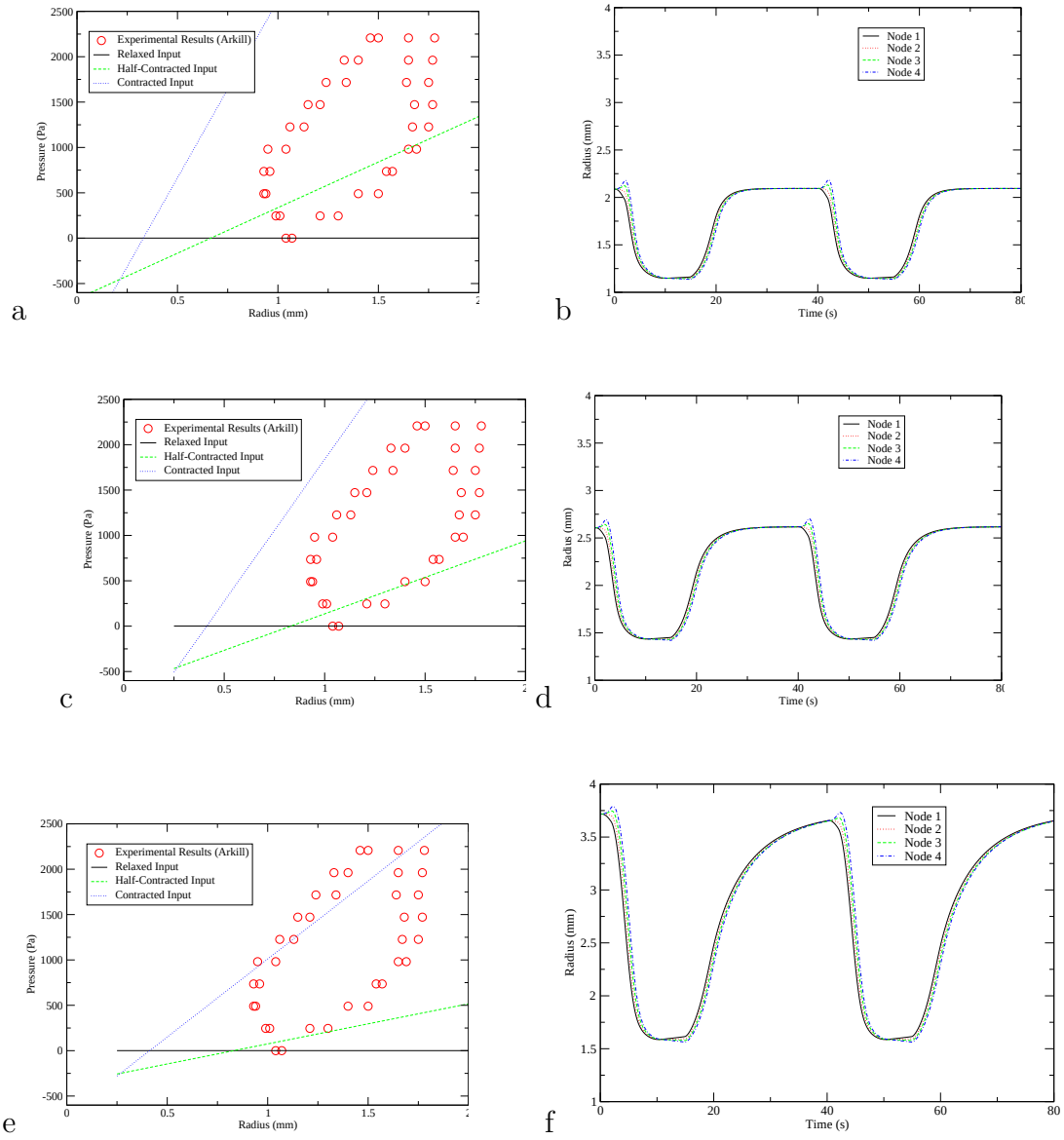

Figure 7.8: The effect of varying A_0 and decreasing E. For panels a+ b A_0=0.001 m, E= 5000 N/m^2. For c + d E=5000 N/m^2, A_0 = 0.00125 m. For e + f E=2750, A_0 = 0.00125.

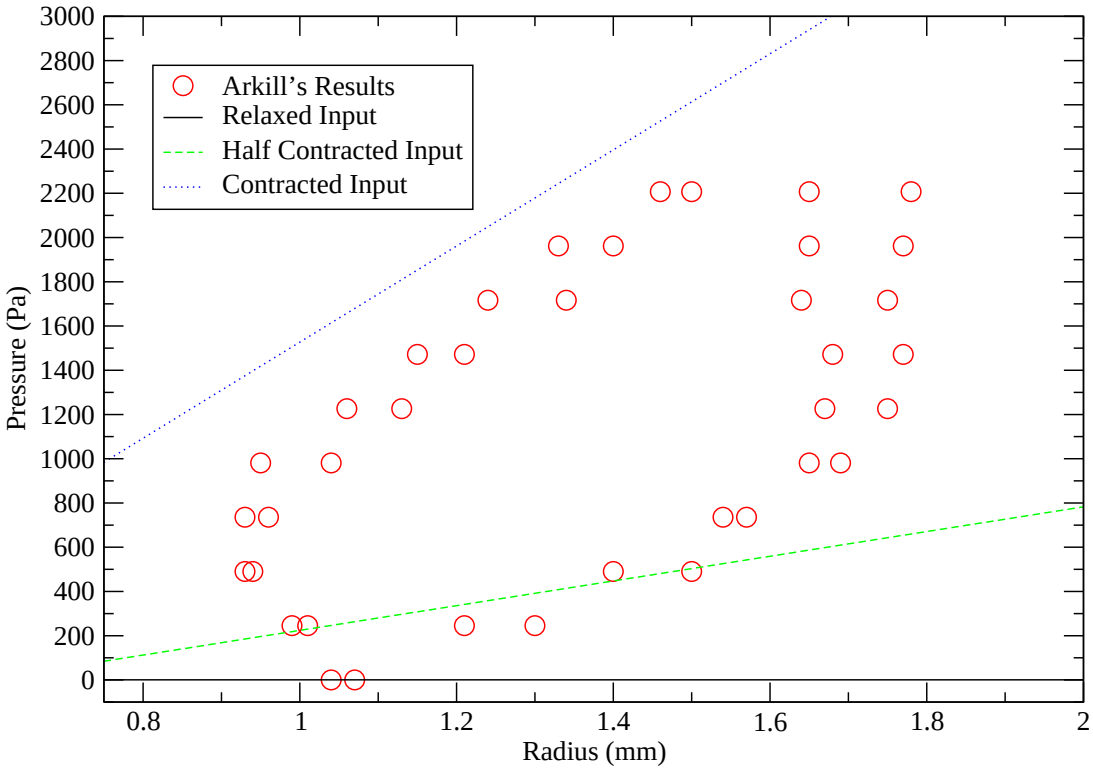

Figure 7.9: The radius pressure relationship after matching the model to the experimental profiles for radius vs time and pressure vs radius.

Parameter	**Before**	**After**
E_0 (N/m^2)	2750	2500
Eamp	$5.5E_0$	$8E_0$
h	$7\%A_0$	$7\%A_0$
A_0(mm)	1.25	0.9
T_p	40	18
T_c	$T_p/2$	$T_p/2$
P_{B1}	500	500
P_{B2}	800	800

Table 7.2: Table to show the inputs used before and after matching

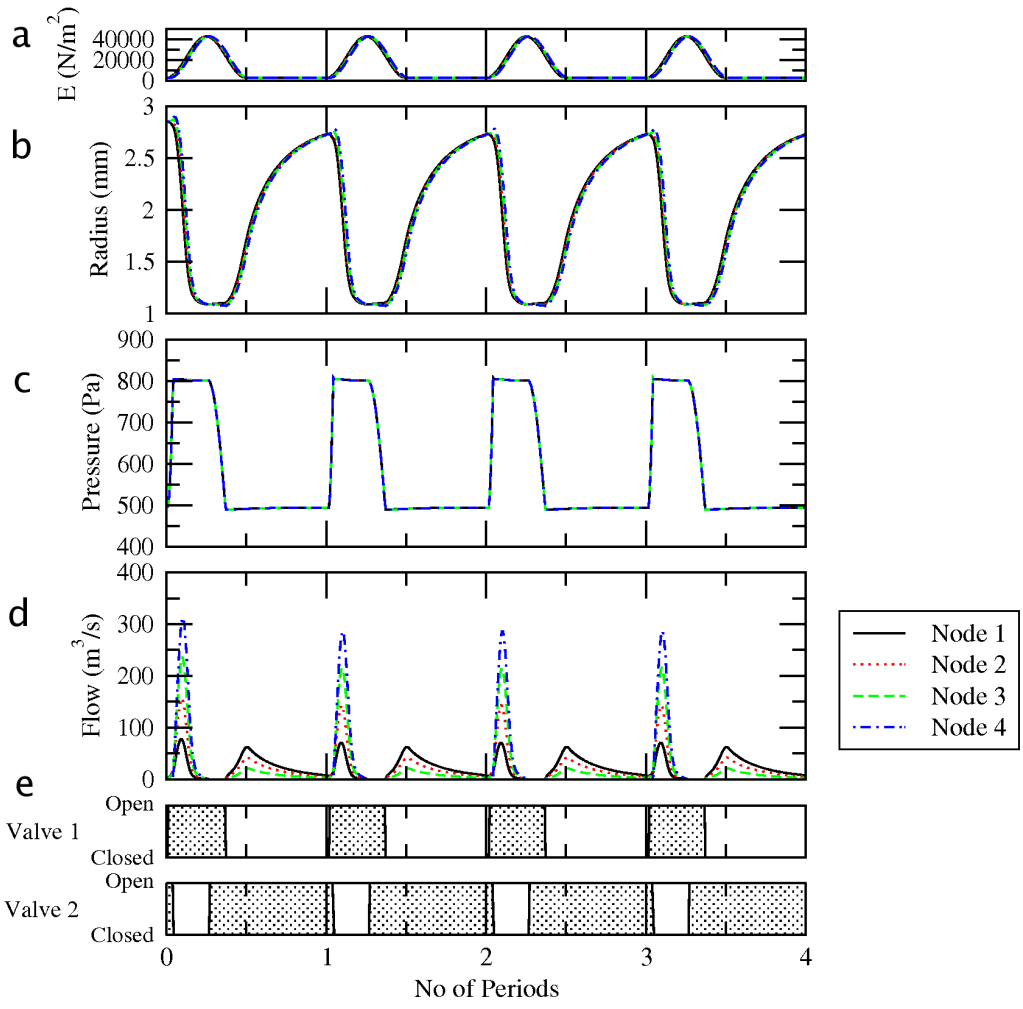

Figure 7.10: The model outputs for radius, pressure and flow with time after matching to the experimental profiles for radius vs time and pressure vs radius

ical range. One method for modelling the two different gradients is examined further in section 7.5 using a direct relationship between pressure and radius. This allows the gradient to change, as occurs in the experimental results. Another variation in modelling set up was also explored in section 7.3.2 where the unstretched radius is used to drive a contraction wave. This also changes the shape of the pressure versus radius graph but does not give 2 gradients.

7.5 Modelling the dynamic behaviour using a direct relationship between pressure and radius

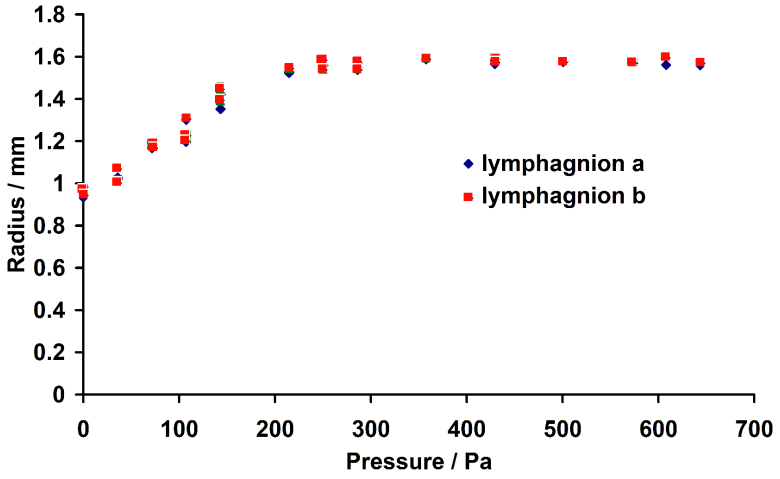

Figure 7.11: Static compliance of a lymphatic vessel from experiments performed by Arkill and described in chapter 4

Experimental results derived by Arkill in chapter 4 produced the graphs 7.11 and 7.12, showing the relationship between pressure and radius for a relaxed or pumping vessel. These experimental results agreed with the findings by [5]; in that the material appeared to become less extensible and compliant above a certain strain. This

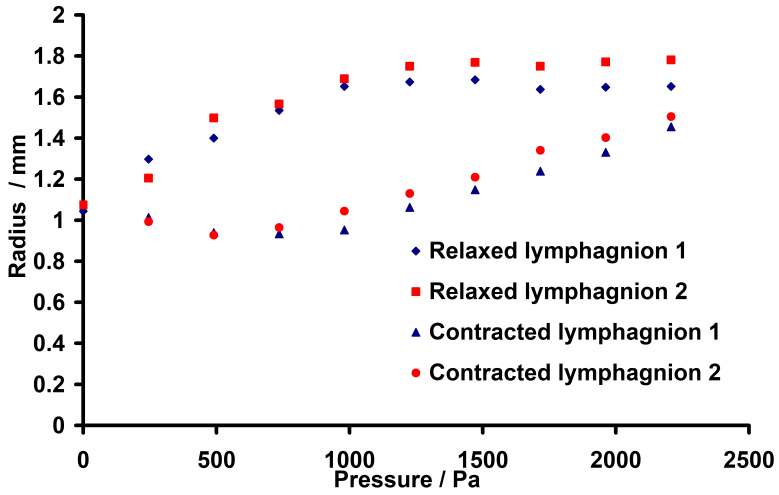

Figure 7.12: Compliance of a pumping lymphatic vessel from experiments performed by Arkill and described in chapter 4

is not accounted for in the models used up to this point, with the contraction driven by radius or elasticity. A second model was designed, using a direct relationship between the experimental results for radius and pressure. This negated the requirement for values for the Young's modulus and the radius at zero pressure, which are extremely difficult to measure accurately due to difficulties finding the wall thickness and point at which zero pressure is reached. These values were only needed to relate the pressure and radius and we now have a direct relationship between the two values.

7.5.1 Passive wall model

The direct relationship setup for a relaxed vessel is shown in figure 7.13. The lines were adjusted to fit Arkill's results shown in 7.11. The two gradients show that the material becomes stiffer after a threshold strain of a_2. The general equation could be used as below, where the gradient m and the intercept c changed above

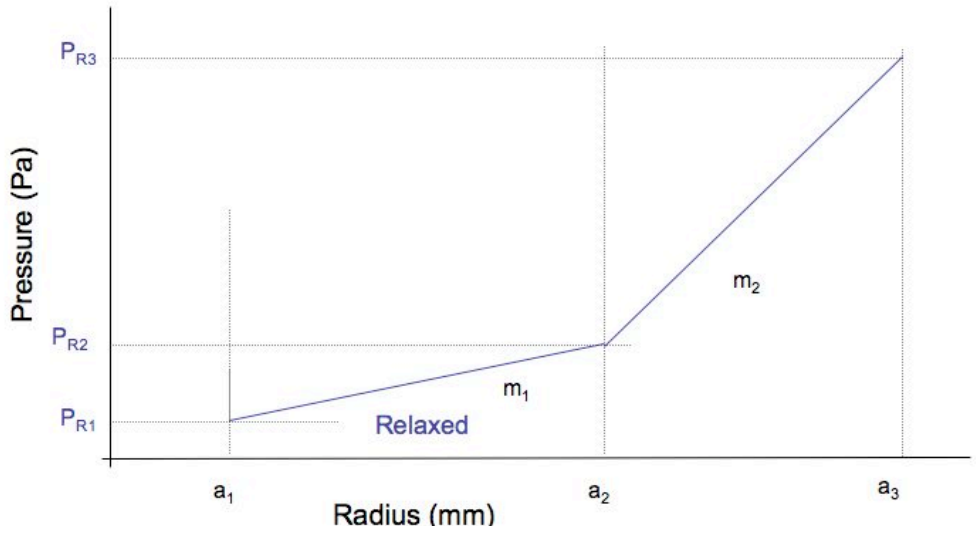

Figure 7.13: The direct relationship model setup for a relaxed vessel

the threshold strain.

$$P = m.a + c$$

7.5.2 Contracting - 1 Gradient

For the first representation of the contracting vessel with the direct relationship method it was assumed the material only had one phase and the gradient of the pressure radius graph remained the same throughout. The contraction was included in the form of a sine wave with a pause, this time using a contraction index I_c rather than a varying Young's modulus E or relaxed radius A_0. This index causes the line to move between P_R (the line describing a relaxed vessel) and P_c (the line describing a fully contracted vessel) depending on the degree of contraction as shown in figure 7.14.

The general equation became:-

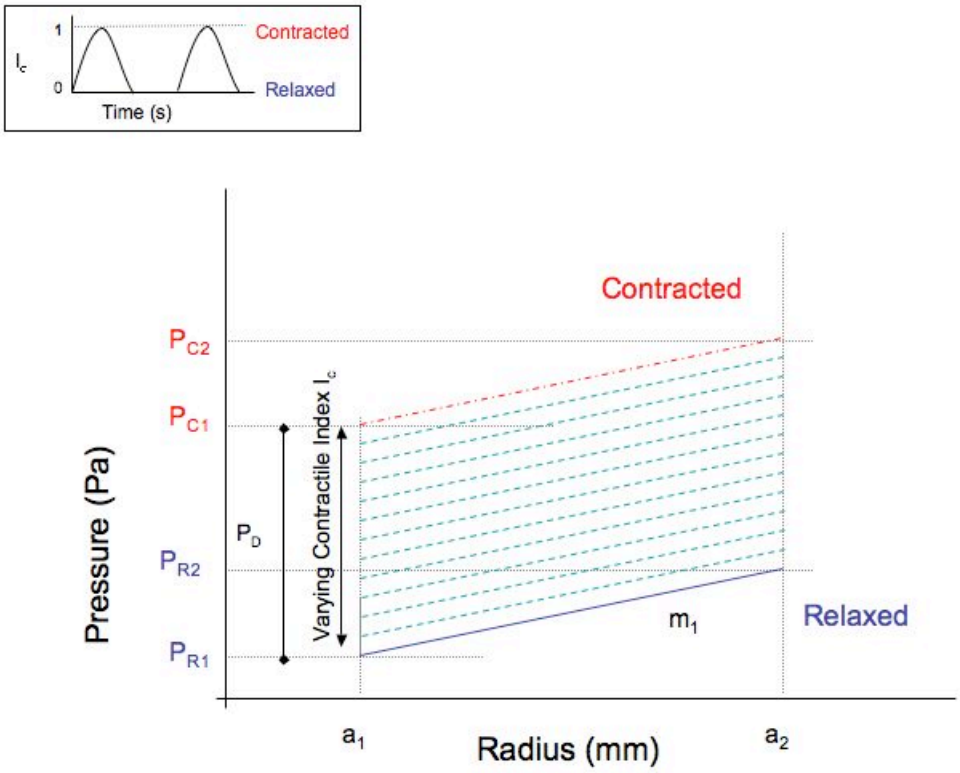

Figure 7.14: Direct Relationship setup for contracting vessel using 1 gradient

$$P = \frac{a - c}{m} + (P_D \times I_c) \tag{7.3}$$

7.5.3 Contracting- 2 Gradients

A second region was added in the same way, to include the variation in material properties with strain, this described a stiffer tube above the threshold a_2 as shown in figure 7.15 . The pressure range P_D at this new position was kept the same, inorder to ensure a smooth transition between the two phases. The contraction index I_c was used in the same way.

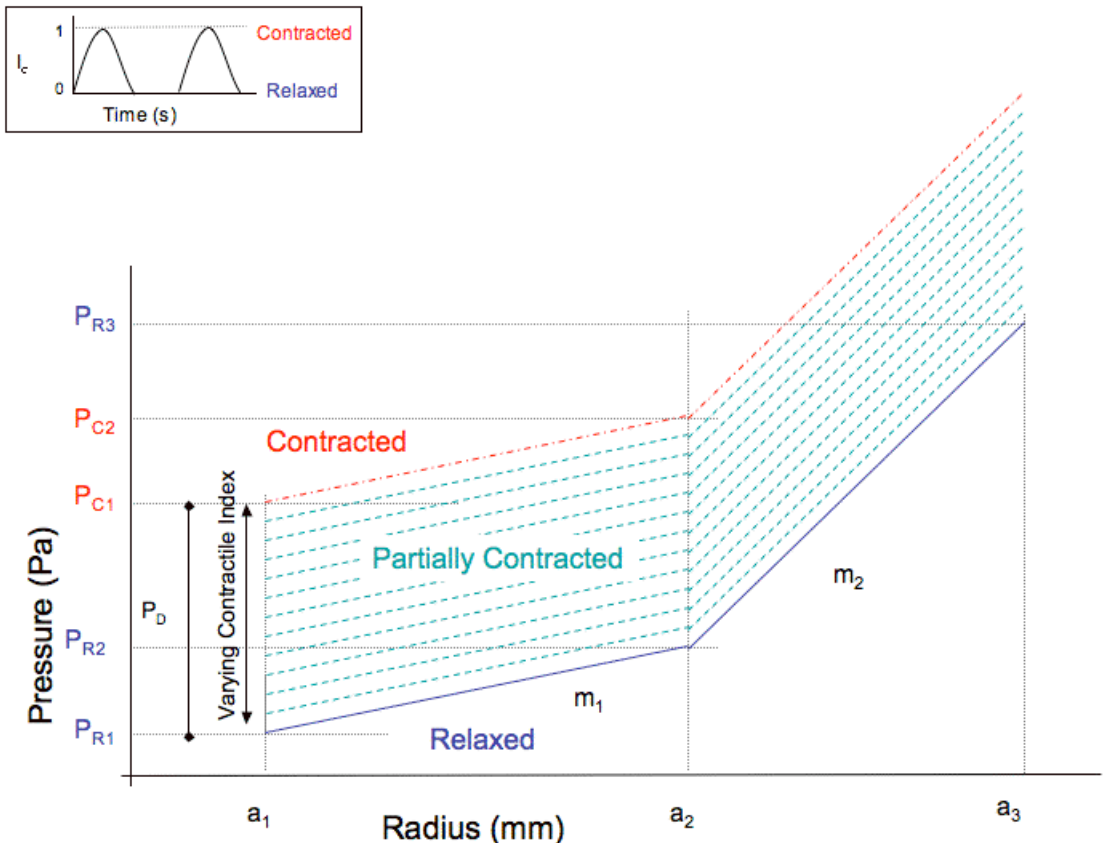

Figure 7.15: Direct Relationship setup using 2 gradients to show the change in the stiffness after a threshold strain is reached. The dashed lines show the midway points for the semi-contracted vessel at different contractile indices.

Parameter	Value
P_{R1} (Pa)	0
P_{C1} (Pa)	1325
P_{R2} (Pa)	1156
P_{C2} (Pa)	2479
P_D (Pa)	1325
a_1 (mm)	1.05
a_2 (mm)	1.65
m_1	5.84 x 10^{-7}
m_2	5.84 x 10^{-8}

Table 7.3: The values used for the direct relationship model set up

The equation remains as :-

$$P = \frac{a - c}{m} + (P_D \times I_c) \tag{7.4}$$

The gradient m and the intercept c depend on whether the point is before or after the threshold radius a_2. The contraction index I_c depends on the amount of contraction the vessel is undergoing. The table 7.3 gives the values relating to diagram 7.15, where a is radius, P, pressure and m gradient. The table 7.4 denotes (where possible) the parameters used in comparison to the parameters from the model developed in the previous chapters.

7.5.4 Results

Graph 7.17 shows the pressure radius relationship for the input for this Direct Relationship model. This is able to follow Kenton's results much more closely.

As shown in 7.16 f-j the passive relaxation did not occur in this direct relationship model as found in the other model 7.16 a-e. This seems likely to be due to the way the model was set up. Once the contraction has finished the pressure radius relationship is set to a particular line on the graph (the bottom line on figure 7.15) which does not

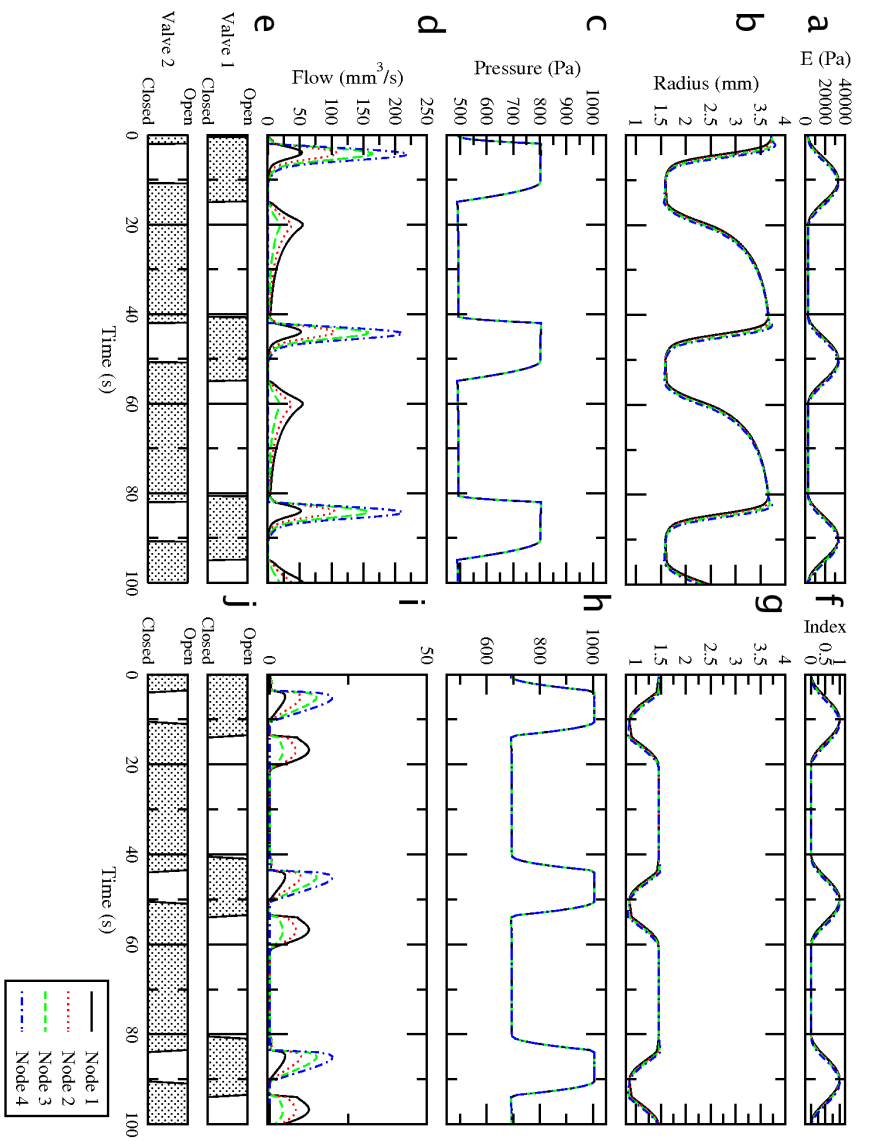

Figure 7.16: The Direct Relationship model (f-j) in comparison to the stabilised Reddy Implementation (a-e), E=2750. The shark tooth shape is not present and the radius and flows are much smaller.

Parameter	Previous Model	Direct Relationship
E_0 (N/m^2)	2750	N/A
Eamp	$5.5E_0$	N/A
h	$7\%A_0$	N/A
A_0(mm)	1.25	1.05
T_p	40	18
T_c	$T_p/2$	$T_p/2$
P_{B1}	500	500
P_{B2}	800	800

Table 7.4: The values used for the direct relationship model set up in comparison to the previous model

account for the passive relaxation of the vessel. Furthermore the magnitude of the contraction was much smaller. To try to improve this by increasing the amplitude of contraction alone takes the relationship away from the experimental pressure radius relationship and the radius time shape becomes even more unrealistic. Matching both graphs in a similar way to section 7.4 may be possible but would be very time consuming. As the passive relaxation behaviour may be important this does not seem worth pursuing at this point.

7.6 Conclusions

The contraction pulse was found to be as effective backwards or forwards in one lymphangion in the 1-d computational model and we submit that a reversed wave would be able to propagate throughout the network allowing more efficient transport.

The model was developed to use a varying Young's modulus E and relaxed radius A_0 to drive the contraction wave inorder to differentiate between two features of a contraction; the muscles stiffening and shortening. It was found that this did not significantly effect results and the E model was chosen as the standard as this had

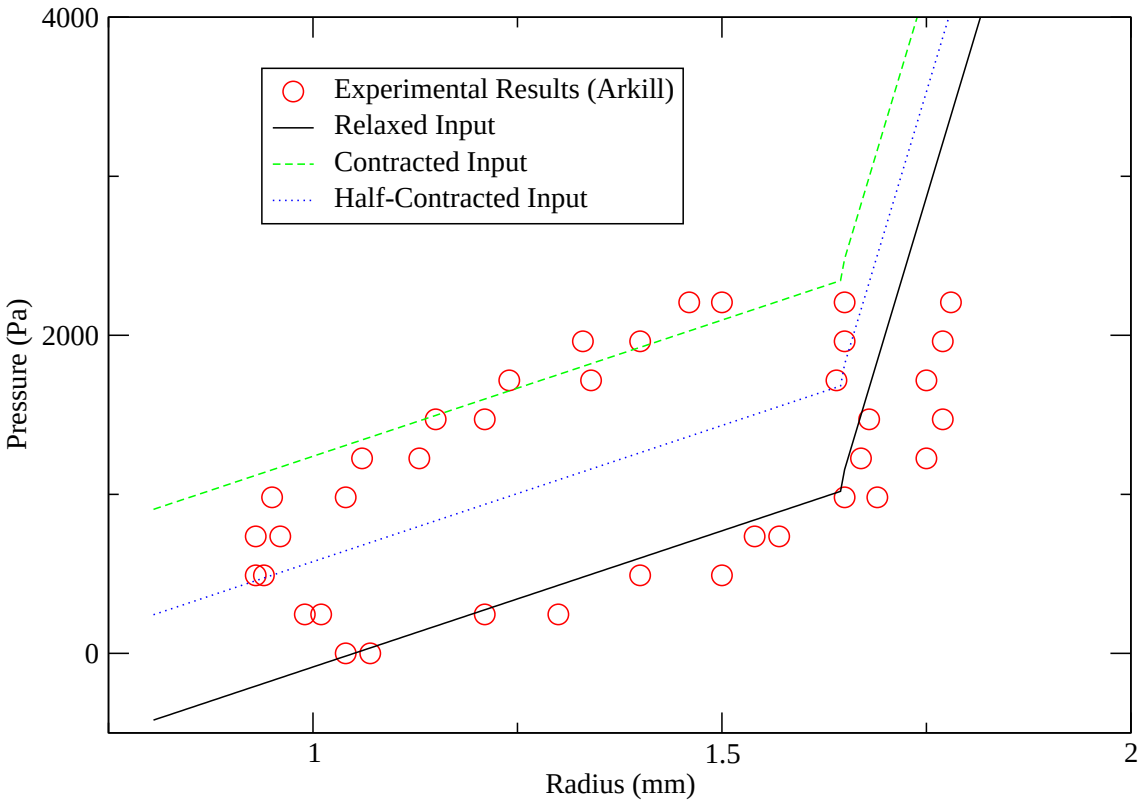

Figure 7.17: The pressure radius relationship for the Direct Relationship model inputs in comparison to Arkill's results described in chapter 4

fewer calculations per time step and therefore a shorter processing time. This A_0 driven wave also begins to explore the effect of the twisting (during contraction) on the vessel. It shows that the decrease in cross sectional area due to twisting has a similar effect to if the material was just stiffening.

The data trend of the relationship between pressure and radius was seen to be more important than the exact value for the radius at zero pressure. Therefore these pressure-radius properties and the relationship to the radius time characteristics were investigated by varying parameters within experimental limits and the effect of those parameters noted. It was found that the experimental pressure-radius and the radius-time characteristics could be reproduced within experimental error limits.

A direct relationship model was also explored, this did not produce a contraction of sufficient amplitude. Furthermore, the radius peak at the beginning of the

contraction and the slow passive relaxation phase were missing and so it did not give the shark fin radius time profile as found in experiment and previous models. This type of profile may be an important indicator of the pump efficacy such as the efficiency of the valve as discussed in the next chapter.

Chapter 8

Valve Investigation

8.1 Introduction

A preliminary investigation of the valve was undertaken using the computational modelling package Fluent (commercial code). Both a static and dynamic model (using prescribed motion) were constructed in order to improve the 1-d resistance model. This study illuminated several areas for future investigation but no qualitative understanding was possible. Small changes in the motion or parameters made a large difference to the results. Improved knowledge of the parameters and motion is required for progress in this direction although ideally an fully Fluid Structure Interaction model of the valve is required.

In the previous chapters it was found that the valve modelling details are very important to the 1-d model, although there is very little experimental information available on the mechanics of these valves. Computer modelling of the valve motion has a distinct advantage, as the in vitro parameters are very hard to measure without causing damage or affecting the results. Instrumentation needs to measure values inside the vessel itself without affecting the flow in order to quantify parameters: such as the opening and closing pressures of the valve, and the valve timings and opening configurations. These values can then lead to calculation of the resistance of the valve and stresses on the valve leaflets.

8.2 Valve Characteristics

This section reviews what is known of the parameters and mechanics involved in lymphatic valve function and compares them to those of the heart and venous valves due to the more thorough knowledge in these regions and the likelihood of similar function.

8.2.1 Heart Valves

The two major heart valves are the aortic (tricuspid) and mitral (bicuspid) valves, the valves exposed to the highest flow velocities. As heart valve complications are often due to the flow characteristics involved, these valves (which undergo the greatest stress) have been examined in the most detail. The position of these two valves within the heart is shown in figure 8.1.

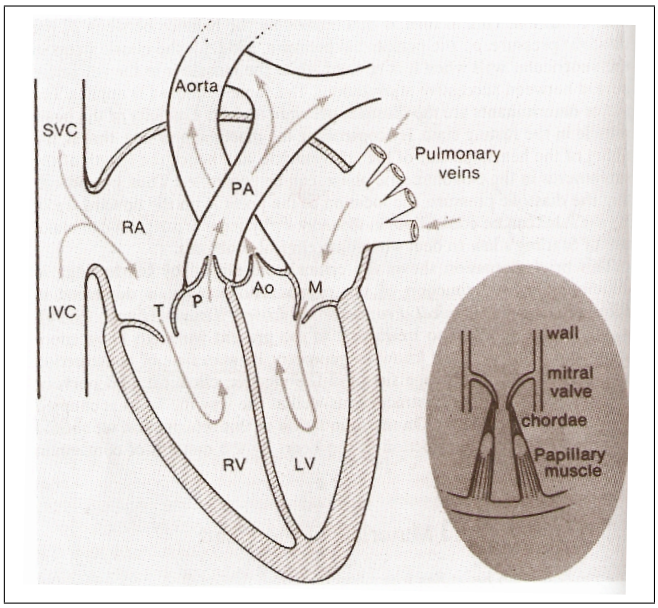

Figure 8.1: Schematic of the Heart from [104]. Ao = aortic valve (tricuspid), M = Mitrial valve (bicuspid) , LV= Left Ventricle

Although there are major structural differences (such as number of cusps) between the mitral and aortic valves, the mechanical function and parameters (such as the pressures, radii and velocity) are of similar order. Furthermore, the venous

valves seem to posses the same basic mechanics. The efficiency of all these valves appears to depend on the development of recirculation in the area behind the leaflet shown in figures 8.2 and 8.3. This recirculation is encouraged by the sinuses or the ventricular chamber itself. The heart valve leaflets are non-muscular flaps [24] made of connective tissue 0.1 mm thick [1]. Collagen fibers distributed along these flaps have been found to both reduce stresses during flow through the heart and reduce fluttering [91]. Due to the similar parameters such as the Reynold's number Re, magnitude of flow and the nature of the mechanics involved in the function of the mitral and aortic valves the two are not always differentiated in the following section. It is more concerned with discovering if these same fluid mechanics are involved with the lymphatic valve function, and which parameters are of a similar order of magnitude.

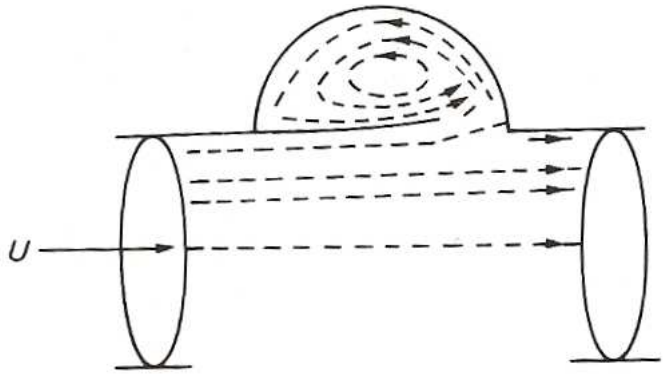

Figure 8.2: Streamlines around the fully open aortic valve [1]

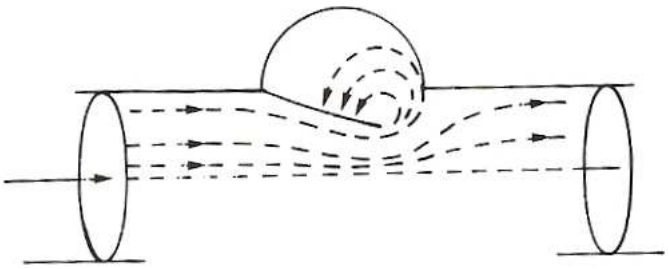

Figure 8.3: Streamlines around the partially open aortic valve [1]

Buxton and Clarke [26] found similar recirculation in a 3-d Fluid Structure

Interaction model of the venous valve, in the area behind the valve leaflets. Bellhouse [107], developed a model of the mitral valve and showed that the size and shape of the area behind the valve leaflets was critical to the development of this recirculation: regurgitation occurred when it was not present.

In a heart model by Timm (1942) it was found that the flow still presented the same circular motion behind the valve leaflets in laminar flow [17] and Dinnar states that steady flow can be assumed [23] in the aortic valve. The Reynolds number (for flow) was varied in a model of the heart between 20 and 200, and there was still no qualitative difference in the nature of the flow [103]. Therefore it seems the recirculation is due to the shape and does not require turbulence: the same mechanism should work in the lymphatic system at lower flow rates. Such a shape means that the pressure drops between the valve leaflets, mid flow; while the pressure behind the valve leaflets remains the same (due to the recirculation). This gives a relatively stable half-closed position during most of ejection. In fact the mitral valve has been found to be so efficient that it begins to close while there is still forwards flow [1]; thereby minimising regurgitation.

In the aortic valve, 5% of the fluid is regurgitated at each valve closure [103]. Not all of the regurgitation is necessarily leakage: some may be part of the volume contained within the valve itself [17].

There is a difference between the pressure that will trigger opening or closing in the heart valves. This is important because, during closing, the pressure rises from its initial zero pressure gradient across the valve up to 0.55 mmHg (73 Pa) (as can be seen in figure 8.5). This is still lower than the few mm (400Pa) required to trigger opening. Without this difference, the very mechanism of closing would open the valve again. The 1-d model of the lymphatic system described in chapter 5 suffered from fluttering if the opening and closing pressures were both zero (see section 5).

For the aortic valve, literature documents the opening stage as taking from around 20-30ms [103] to 160 ms [23] or even longer. This discrepancy may firstly be due to a lack of differentiation between the opening or closing time. Secondly it may be due to whether the stage before the actual opening is included (where the valve gives,

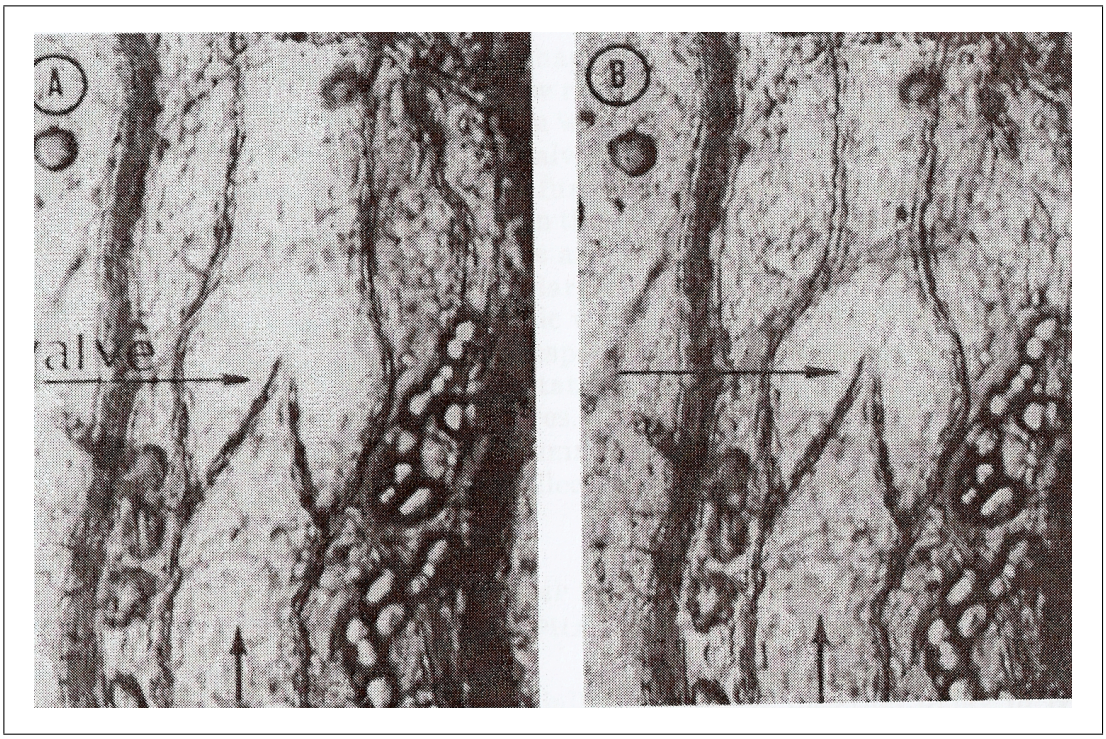

Figure 8.4: Cat mesenteric lymphatic valve taken from [27] relaxed (A), pumping (B); scale × 183

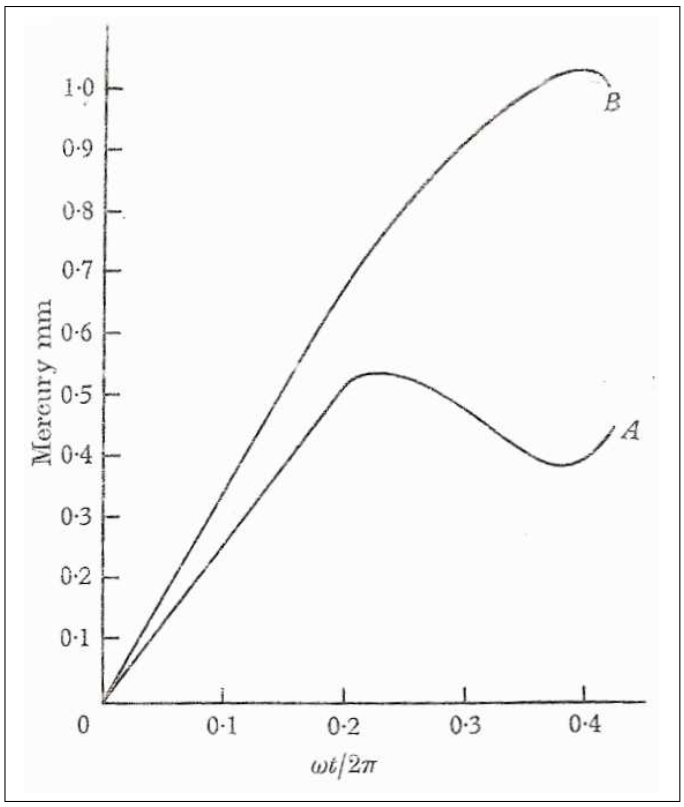

Figure 8.5: The pressure across the cusps during mitral valve closure taken from [24]

but does not open). When the opening and closing stages are measured seperately, results indicate that the opening phase is faster than the closing phase. The results of Bellhouse and Talbot [24] show a ratio of approximately 3:5 opening to closing.

8.2.2 Lymphatic Valves

Chapter 2 includes a detailled description of what is known of the valves, and this section is intended as a summary to indicate information that is helpful in producing a 2-d model. There have been very few morphological studies of the lymphatic valves, but these include [27, 59, 53, 50]. In the lymphatic system Zweifach and Prather in [108] and [27] found that a pressure from between 1.0 and 2.7 cm H_20 was enough to open a valve (between 100 and 270 Pascals). The lymphatic valves seem likely to have timings of a similar order to heart valves, which take longer to close than open. It must take a number of time steps to open or close the valve if the model is to remain stable. Sinuses have been described by Leak and Jamuar [50] giving the vessels the well known beaded appearance. These could allow recirculation as in the heart valves. If the lymphatic valves have similar mechanics to heart valves, there may be a similar partial closing stage (see section 2.2) and faster opening than closing times. A partial closing time such as this would increase resistance to flow in the second portion of the contraction cycle and may be connected to the shape of the radius with time relationship. In the 1-d valve model the closing and opening sequences were set to take 20 ms. A shorter time than this produced instabilities and from 20 - 200 ms had little effect on the results. This range is also comparable to the heart valve timings [23, 103].

$$Re = \frac{\rho U d}{\mu} \tag{8.1}$$

The Reynold's number (Re) can be used to determine the nature of flow e.g. laminar or turbulent, and is related to the velocity of the flow and radius of the valve. The heart valves can have a Reynold's number as high as 8000, which is transitional flow

and means that the flow could be turbulent or laminar. The Re for the lymphatic system will depend on the diameter of the vessel and flow velocity and therefore on the position in the network and species of animal.

Figure 8.6: Sequence of pictures of lymphatic valve opening and closing taken using boroscope by Arkill

8.3 Computational Modelling

The 1-d model uses a linearly varying resistance with time, during the closing or opening phase. When the valve is fully open the resistance is related to the radius of the tube by the relationship in the equation shown below.

$$Rv_i = k_p \left(\pi a^2\right) \tag{8.2}$$

As introduced in chapter 5, there appear to be inconsistencies with the units of this equation from Reddy's work. However it seems likely that this relationship is aiming to describe the valve mechanics arising from the change in momentum of a fluid stream when it impinges on a solid object. It is as if a hose is squirting on a door to keep it open. For the lymphatic valve model used by Reddy, this was constant except for when it was closed, for which the flow was then set to zero. However it would seem more intuitive if the resistance increases as the gap between the valve leaflets decreases. In the 1-d model developed in section 5 a

linearly decreasing resistance (during valve opening) was used. This was however only an approximation mainly used to improve stability of the model by replacing the sudden sharp change involved when the valve was completely opened in one timestep. The resistance time behaviour of the lymphatic valve during opening and closing is not available in the literature; but study of this would allow improvements to the 1-d representation of the valve.

8.3.1 Method

Gambit (commercial code) was used to construct a mesh of a lymphatic valve from a micrograph by Zweifach and Prather [27] of a valve from a rat's mesentery. Gambit (the preprocessor available from Fluent) is a geometry and mesh generator and points were used from measurements taken at intervals of 1 mm from the micrograph (corresponding to 6.25 μm) along the outline of the vessel. The dimensions were scaled up, to bring the radius to 0.96cm, equivalent to the largest of the valves found in a cow's mesentery.

The tip of the leaflet was constructed as a rounded shape as this is more realistic physiologically than a sharp shape which would intrude on flow and increase flow disruption. To generate a symmetrical structure, only half the vessel was drawn, with a line of symmetry set at the centre of the tube. The flow within this mesh could then be studied using Fluent (commercial code; ANSYS INC), at different valve openings. Fluent is a Finite Volume, Computational Fluid Dynamics program, solving the Navier Stokes in 2 or 3 dimensions. The differencing scheme used was the 1st order upwind differencing scheme with the SIMPLE algorithm and steady solver. The mesh contained approximately 2886 cells with a slight variation depending on the valve position. The output pressure was set to 800 Pa and the input to 810 Pa; representing the pressure drop of 10 Pa observed in the 1-d model when the valve was first fully open. Two dimensions were considered accurate enough in these preliminary investigations, approximating the valve as having a uniformly round opening and generating symmetrical flow.

Type of Mesh Tool	Parameter	Value
Smoothing	Spring Constant Factor	0.8
	Boundary Node Relaxation	1
	Convergence Tolerance	0.001
Remeshing	Min Length Scale (m)	0.0001
	Max Length Scale (m)	0.0005
	Max Cell Skewness	0.75
	Size Remesh Interval	1
	Size Function Resolution	3
	Size Function Variation	0.75
	Size Function Rate	0.99

Table 8.1: The smoothing and remeshing parameters used in the dynamic model

A representation of the valve with no sinus region was also constructed for comparison to the flow within a valve containing the sinus region. The original 2-d model was then scaled to different sizes to see the effect on flow of the position of the valve within the network.

A dynamic model was also constructed in Fluent (commercial code) by assigning motion to the valve leaflets from the original static model using the parameters in table 8.1. This showed that motion effected the results significantly. However the results changed too much when parameters were varied, within the known bounds, for any conclusions to be reached. A better experimental quantification of the time varying pressure, velocity and position of leaflets would be required for useful results by this method.

8.4 Results

Recirculation behind the valve leaflet was reduced by removing the sinus.

With a smaller scale vessel the recirculation behind the valve leaflets is reduced

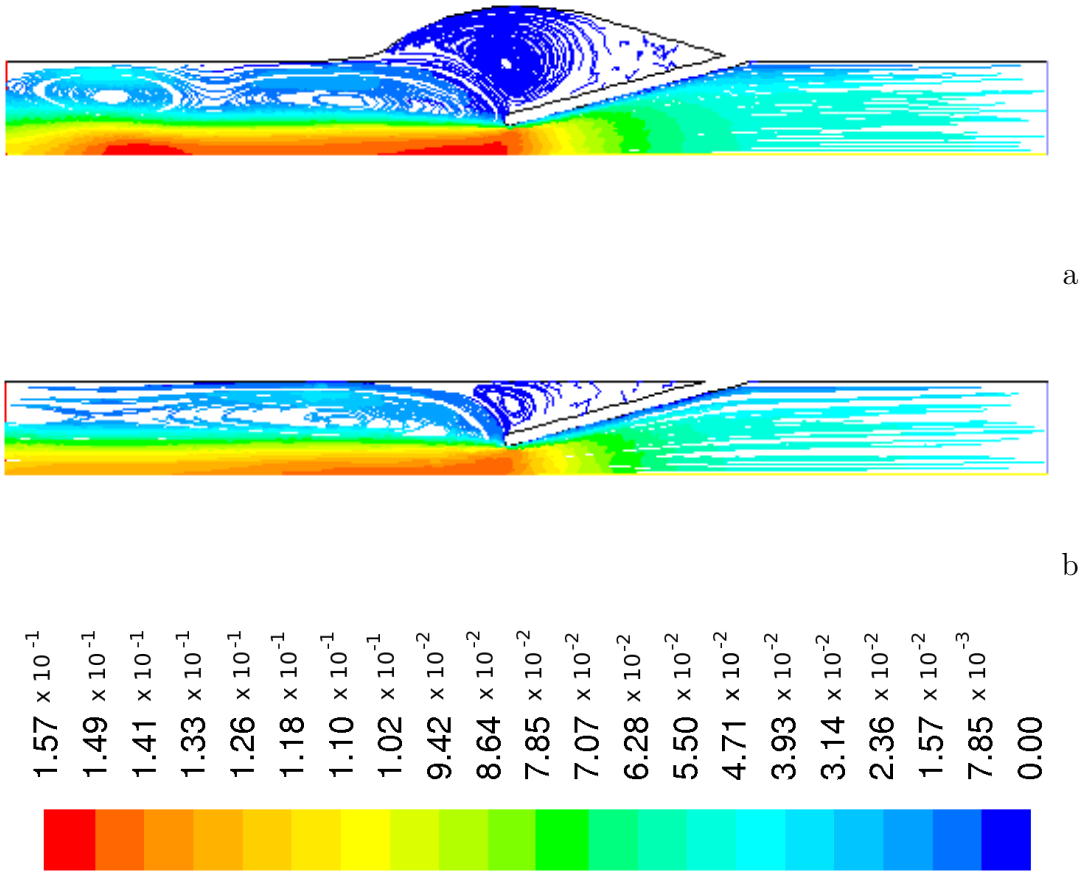

Figure 8.7: The velocity streamlines (m/s) (a) with and (b) without a sinus region, for a 9.6mm radius vessel. Recirculation is much more pronounced when a sinus is present.

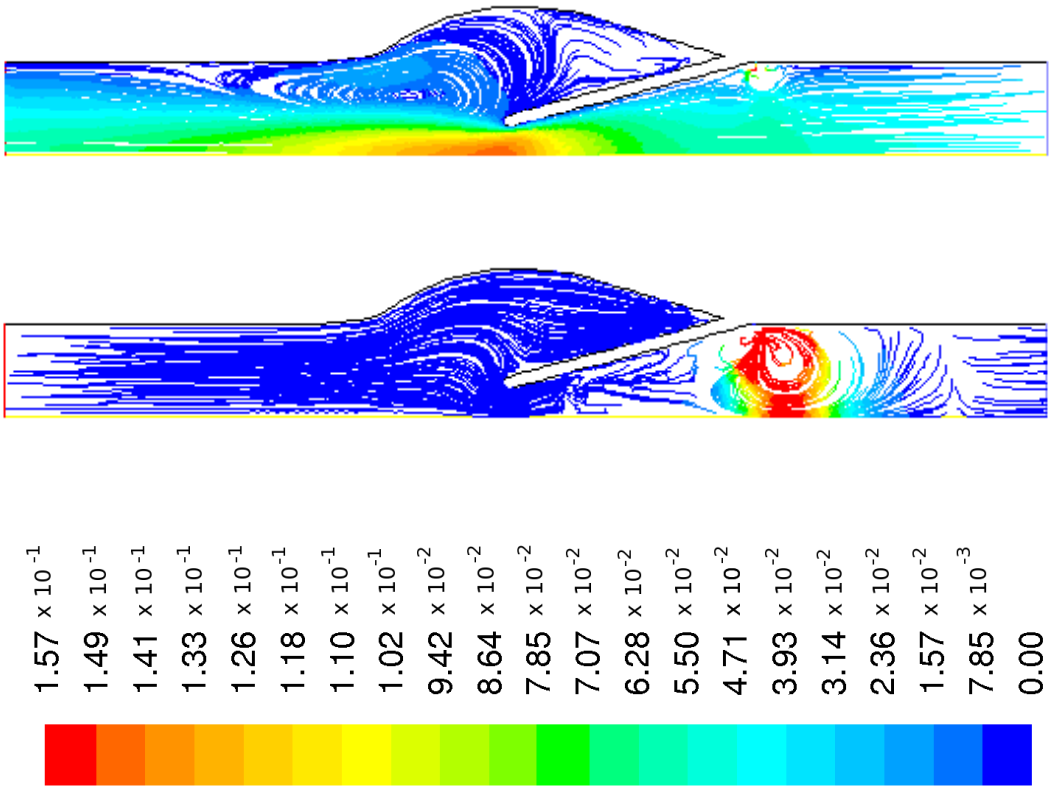

Figure 8.8: Velocity streamlines (m/s) for smaller scales of valves (a) 0.96 mm radius (b) 0.48 mm radius (c) 0.096 mm radius, for which creeping flow occurs through the valve and recirculation is prevented

as shown in figure 8.8. The recirculation in front of the valve is seeded by an angular edge, which should be removed in future investigations.

8.5 Conclusion

Recirculation was seen throughout the modelling study, indicating it is likely to be an important part of the valve closing mechanism. A future study of the endothelial pattern in the sinus area of valves from different positions would confirm whether recirculation is occurring as the cells tend to line up with flow. The static 2-d valve model showed similar behaviour to the backwards facing step. With flow seperation at the tip of the valve lading to recirculation behind the valve leaflet. On examining a very small scale of the model, creeping flow was seen, which prevented recirculation behind the valve leaflet. When the sinus was removed, no recirculation was seen, showing the shape behind the valve leaflet to be an important factor in the dynamics. The addition of motion had a large effect on the resistance. Furthermore the dynamic model showed very different results if the prescribed motion was varied a small amount. In order to use this method to investigate the resistance; a much better quantification of the valve timings, pressures, flow velocities and leaflet shapes is required throughout the cycle. Ideally a full Fluid Structure Interaction model should be used, this would require a good representation of the dimensions and moments, but less dynamic detail from experiment as the motion is decided from first principles.

Some aspects of the experimental studies of the mitral valve by Bellhouse [107] appear to be relevant to the dynamics of the lymphatic valve. Bellhouse compared results for a large and small ventricle and the recirculation did not occur in the large ventricle as the shape behind the leaflet was too large. The valve opening area with time shows a square shape when there is no recirculation. With recirculation, a radius peak was present at the start of flow with an earlier onset of a more gradual curved closure. These two features are similar to features found using the lymphatic 1-d model and experiments; the radius peak and shark tooth shaped radius-time graph involving a curved relaxation period. This type of wall behaviour could be an indicator of conditions for recirculation and therefore more efficient valve function due to the reduced backflow.

(a) Type A developed with McHale for the mesenteric lymphatics, also presented by and Albertine et al [59] and Leak and Jamuar [50] in the pulmonary lymphatics.

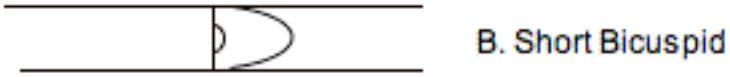

(b) Type B was described in the skeletal muscle by Mazzonni [55].

(c) Type C was described by Lauweryns [56, 57] in the lung lymphatics and by Gruntzig et al [58] in the conjunctiva of bovine eyes).

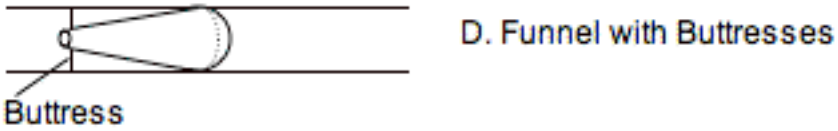

(d) Type D is described by Schmid-Schonbein in his review of the microlymphatics [11].

Figure 8.9: Comparison of different valve descriptions from the literature and the structure found in the mesentery as discussed in section 2

As shown in figure 8.9 various different valve structures have been described in the literature. There are reports of both bicuspid and funnel shaped valves, some with buttresses and different length to width ratios. As discussed in section 2 it seems likely that the different valve characteristics will be required in different parts of the network. This would generate different resistances, and opening and closing thresholds to suit the surrounding conditions such as the flow speed, pressure difference across the lymphangions, softness of the tissues, shape of the vessel and the external forces.

After describing the funnel shape in the microcirculation shown in figure 8.9 (type D) Schmid Schonbein describes the valves as undergoing an Re from 10^{-2} - 10^{-4}, therefore creeping flow. During creeping flow, viscous forces dominate and the inertia of the fluid is negligible, which would prevent recirculation (in fact no sinus region is mentioned at this level). Creeping flow is also present in the flow through the valve aperture of the 2-d static results for the smallest valve (in figure 8.8 c)and recirculation does not occur. The same phenomena is found in experiments such as flow around a sphere when Re is less than or equal to 0.5. Without the recirculation a possibly crucial part of efficient valve closure would be missing if the structure found in larger vessels was still used in the smaller scaled vessels. This seems to indicate that in these smaller vessels, with lower flow, a different valve design is required as the leaflets depend on reversal of flow for closure rather than the reversal of the pressure gradient. A funnel shape would mean that the valve is never more than slightly open, so only the end of the normal closing cycle is required (the final snapping shut as flow reverses) and the valve can still close with a minimum of regurgitation.

The pressure drop (and therefore resistance) caused by the 2-d valve model (type A) varied alinearly with the scale of the valve in figures 8.8. Shorter leaflets caused a lower resistance but a smaller aperture increased the resistance, with the two mechanisms becoming more dominant at different scales. Therefore valve leaflets may need to be longer in a smaller vessel to apply the same resistance. The standard valve found in the mesenteric collecting lymphatics is much longer than the heart

valves, otherwise the resistance would be too low in these smaller vessels. The flow and pressures are much lower in smaller vessels, requiring a sensitive valve, according to Schmid- Schonbein [11] this funnel shape is extremely sensitive, able to operate under extraordinarily low flow rates. So, as long as the material is soft and in a funnel shape (irrelevant to the shape of the vessel) rapid closure occurs on reversed flow. The valve becomes more effective if longer or decreased diameter as there is a larger viscous pressure drop.

Some vessels undergo larger compressive forces such as in skeletal muscle, (figure 8.9 type B) the valves appear to be short but tough, they do not need to be very sensitive with larger changes in pressure. In such a position one of the longer, funnel-shaped valves would be likely to suffer damage. In the conjunctiva of the eye there will be small vessels undergoing minimal compressive forces so the funnel shape is better suited. In such a position the valve may not need to be held in place by buttresses as described by figure 8.9 type C. Schmid-Schonbein [11] attributes the buttresses to prevention of reversal of the leaflets. These may also aid closure as tension would begin to flatten the shape of the aperture. Buttresses could also hold the leaflets steady in areas undergoing larger changes in compressive forces. The valve resistance and structure may also be related to the valve opening threshold but this is left to future work.

Chapter 9

Conclusions and Future Work

This chapter details the conclusions and physiological implications for this project. It concludes with a section suggesting future work with an emphasis on modelling.

9.1 Conclusions

In chapters 5 to 7 a computational model was developed which described the behaviour of a single lymphangion improving on an existing model by Reddy [4]. The parameters used were based on, and validated against, literature and experimental measurements of the elastic properties of lymph vessels measured in the laboratory. This computational model is able to reproduce the pumping behaviour of the real vessel using a simple contraction function. It suggests that lymphatic pumping is governed by simple and fast contraction pulses travelling in the retrograde direction to the flow.

The above model was initially based on Reddy's work [4] but after reducing the time step, various stabilizing methods were found to be necessary to obtain accurate results from this model. These additions represented a more physiologicalically accurate condition. Any short sharp changes imposed on the system were replaced with gradual changes. For example, the abrupt opening and closing of the valve and on/off of the contraction were replaced with modified sine waves. To further

improve the stability and physiological accuracy terms to represent the inertia and longitudinal tension of the lymphatic vessel wall were also added to the conservation of momentum equation and compared to values obtained experimentally. The tension term is not necessary in the setups looked at, but would be necessary if the tube collapsed or the cross sectional area underwent a large change for some other reason.

The Courant number was calculated for the model and compared with a CFL (Courant-Freidrichs-Levy) condition of 1. This criteria is necessary to confirm convergency of results due to the size of the cells and timestep and 1 is the standard value used for modelling blood vessels. In order to further check the model's accuracy, it was configured to be compared with Poiseuille's flow equation. First, a very stiff vessel (with no contractions and a pressure gradient to allow flow) was used in order to try to replicate the behaviour of an inelastic tube to allow Poiseuille flow. The flow was the same for both the direct calculations and the model results, indicating that the model was behaving as expected. This procedure was repeated for two vessels of greater compliance and but this time they were compared to a modified Poiseuille relationship; to account for the elasticity of the tube. This calculated solution compared well to the model results.

The sensitivity of the model to a variation of parameters was investigated in chapter 6. The stiffness of the vessel walls was increased by increasing the Young's modulus E and wall thickness h resulting in decreased flow. Flow was increased by increasing the volume change during contraction, either by increasing the unstretched radius A_0 or the amplitude of contraction A_{amp}. When the contractile wave speed was increased (by decreasing the phase difference) the flow was increasd. Similarly, increasing the frequency of contraction by decreasing the period also increased flow. Once the phase difference and period are decreased to a certain level they will start to decrease flow. In respect of the phase difference; if all the segments contracted simultaneously, the pressure gradient across the valve would not change, therefore negating any pumping effect. The lymphangions pump most effectively if all sections of the wall contract almost simultaneously, irrespective of the direction of propa-

gation of the contraction wave. A quickly propagated contraction wave increases the pressure throughout the lymphangion until the pressure difference is sufficient to open the valve and drain the segment. If the wave propagates more slowly, the effect is merely to pump the lymph fluid from one part of the vessel to another, without ever building enough pressure difference to open the valve.

In respect of the period; if the contractions happened too quickly there would not be enough time for complete relaxation, reducing the total change in volume possible due to a contraction. Decreasing the output pressure so that passive flow was generated, with a gradient of 200 Pa, increased the maximum flow to around 2000 times the value when pumping against a pressure gradient. When the contractions were omitted for this case, a larger flow was possible due to the lack of restriction caused by the reduction in radius. Qualitatively similar behaviour was produced when these parameters were varied (except if the pressure gradient was set to be positive). However, there were changes to features in the radius-time profile such as the radius peak and the passive relaxation time. These features may be physiologically important, possibly indicating efficient valve function or effecting the pumping efficiency due to the walls. It was found in section 7.4 that increasing the total change in volume during contraction increased the passive relaxation time.

Chapter 7 explored the relationships between the contraction pattern of the wall and flow generation. The differences between the forward and reverse propagating contractile wave are minimal. We would suggest, however, that pumping through a branching network would probably be more effective with a reverse wave, which would be able to propagate up both branches at a bifurcation. A forward propagating wave arriving at a bifurcation would need to co-ordinate with any wave propagating down the other branch, otherwise lack of coherence between the waves would most likely lead to reduced efficiency. Reverse contraction waves have been observed in experiment [38].

In chapter 7 it was found there was very little difference in the model if the contraction was driven using a variation in the relaxed radius or the Young's modulus. A further modelling method was additionally explored which related the radius

directly to the pressure but this did not allow the passive relaxation stage of the vessel's contraction cycle to occur. The relationships between pressure and radius, and radius and time were investigated. Matching the model to gradients on the pressure-radius graph obtained from experiments is likely to be more accurate than using individual experimental measurements for critical points; for example the unstretched radius, which was difficult to obtain accurately from experiment but has a large effect on the pressure-radius relationship. We examined the radius-pressure and radius-time graphs and the parameters involved in changing characteristics of the results. This led to a closer match to the experimental results while keeping the parameters within the error limits.

A preliminary investigation into computational modelling of the lymphatic valve was undertaken in chapter 8. Further experimental parameters for the current model or a full Fluid Structure Interaction model would be required in order to produce results which would allow development to the 1-d valve model. The valve was modelled in 2-d using Fluent, firstly using a static model and then a dynamic model. Recirculation behind the valve leaflets was a feature throughout, indicating this may aid valve closure as occurs in heart valves. The initial dynamic model presented assymetry in the opening to closing stages. This is because the pressure gradient was at the largest magnitude at the end of the contraction cycle, with the pressure gradient against the direction of flow. For the 2-d dynamic model this was also partly because the speed was higher on closing. Removal of the sinus, in the static 2-d model, reduced the amount of recirculation and pressure behind the leaflet apparently reducing the closing efficiency. Reducing the scale of the static model produced less recirculation in the sinus region until there was none during creeping flows. This appears to indicate that another closing mechanism is required for very low Re number flows. A second, dynamic 2-d model introduced a negative pressure gradient during closing and showed positive flow could continue against the pressure gradient until the valve was nearly closed.

9.2 Physiological Implications

9.2.1 Wall configuration

An increase in stiffness of the vessel walls (as investigated in chapter 6) leads to a smaller radius throughout the cycle, therefore a smaller change in volume, lower flow and faster return to the vessels original relaxed shape. In situ, the Young's modulus of the walls is likely to increase (therefore increasing stiffness) with age and disease as has been found in blood vessels. In blood vessels the material has been found to act as if it is stiffening with age. This has been attributed to; the vessels getting larger [104], the signal processing breaking down [109] glycation of the elastin (bonding with sugar) [110] and the change in amounts of collagen and elastin [111]. These changes in composition of collagen and elastin show an increase in volume fraction but reduction in dry weight, so other components are also reducing. An increase in wall thickness also increases stiffness. This may also occur due to damage or inflammation. Dresden and Evert [112] and Wilson et al [113] found increased amounts of collagen in areas effected by lymphoedema, causing a thickening of the vessel. In situ increased stiffness may be accompanied by a larger relaxed radius caused by permanent damage due to over-stretching with further detrimental effect to the pumping efficacy.

The investigation of the relaxed radius described in chapter 6 has implications for lymphatic network re-growth [64] after an operation. These re-grown vessels are usually smaller than the original vessels and will give a lower flow. This makes the vessels more susceptable to over-stretching. Permanent damage from over-stretching during lymphedema would effectively cut out the beginning of the stress strain curve. This means a large stress would be required for a small deformation.

Increased damping of the vessel walls causes a lower maximum flow as shown in chapter 6 and this flow reduction potentially causes less damage. The addition of damping begins to account for the viscoelasticity of the walls. The tension of the walls did not have any effect in the cases which were investigated. It is likely to

be more relevant if a mechanism occurs which causes a large change in area with longitudinal position, such during collapse of the vessel.

Increasing the amplitude and therefore the magnitude of contraction increased the average flow as described in chapter 6. As the minimum radius decreases (creating a greater magnitude of contraction) any further decrease in minimum radius contributes less and less to the total change in volume due to contraction. Contraction magnitude and average flow do not have a linear relationship. Therefore there is likely to be an optimum magnitude of contraction and after this it is more effective to increase the frequency of contraction (providing the vessel still has enough time to fully relax before the next contraction starts). It is generally more effective to increase the radius at the start of the contraction to give a larger volume for the same change in radius. This might be done by increasing the relaxed radius or allowing the vessel to relax for longer at the end of the cycle (if it would not have otherwise relaxed completely). In terms of representing the effect of the muscle contractions, varying the contraction by the Young's modulus E or the unstretched radius A_0 gave very similar results and both may occur in reality. The decreasing of A_0 represents the muscular fibers knitting together, making the tube narrower and increasing E represents a stiffening of the vessel walls. The model using a varying A_0 may also begin to represent the twisting of the vessel that has been observed in vitro by McHale (private correspondence).

A faster contraction wave speed (i.e. smaller phase difference) generates a higher flow and makes the most efficient use of the contraction coordination as investigated in chapter 6. The speed of reaction of the following segment is therefore important whether triggered by nerves or the internal pacemaking of each lymphangion. This reaction time is likely to increase with age and damage. As discussed in chapter 3 one of the causes of a type of hereditary lymphoedema is the unusual distribution of smooth muscle which would give a less coordinated contraction.

Increasing the frequency does not always improve the pumping, for example, where the vessel has not had time to relax to a sufficiently large radius before the next contraction. The pause between each contraction appears to be important as

the passive relaxation is a major feature of the radius time cycle. This returns the vessel to the starting radius, allowing the next contraction to cause a greater change in volume, than if it had started immediately after the previous contraction, with the same amount of effort. If the period is too small (i.e. the frequency of contraction is too high) the vessel will not be able to relax completely before the next contraction.

A positive pressure gradient in the direction of flow, allowing passive flow is more likely in cases of edema. In section 6.3.8 a gradient of 200 Pa was introduced in the direction of flow causing a greater flow if contractions were stopped due to the increased resistance caused by the narrowing of the tubes. Medication could induce relaxation of the lymphatic vessels to improve passive flow if the pressure gradient is appropriate. Before advising relaxation of the vessels in edema, the pressure gradient at which the contractions cease to be effective should be found and compared to a typical gradient between lymphangions in cases of edema (information which is not currently available to the author's knowledge).

The direction of the contraction wave did not effect the muscular effort for the same flow on a small segment of lymphatic vessel. On a larger branching network, a backwards wave could give greater coordination, travelling from one to many rather than many to one, and our results indicated that a fast coordination was beneficial.

In [114], the Quick-Stewart team conclude that during edemous flow, contractions restrict flow due to the increased resistance caused by the narrowing of the tube (see section 2.4 for the background on Edema). Our findings in chapter 5 confirmed that with a sufficiently large pressure gradient in the direction of flow, the addition of contractions reduced flow. Further investigation is necessary to find the pressure gradient at which pumping limits flow. This should be compared with the variation of pressure gradients across individual lymphangions in edema to determine the likelihood of these pressures occurring. Our findings in chapter 6 also confirmed their observation that a contraction wave propagating in either direction is just as effective.

Further important observations from the Quick-Stewart team include the conclusion that the co-ordination of the contraction wave minimally effects lymph flow

[72] and the supposition that different areas of the same vessel or branches could act as a conduit while others pump [114]. Such a lack of coordination cannot always be advantageous and seems unlikely to be the physiological norm; our findings in chapter 6 indicated that a fast propagation of the contraction wave was beneficial. Contractions in an in vitro pumping lymphatic vessel can be observed to pass along the vessel as a 'mexican wave'. The lack of continuity of smooth muscle and therefore contraction is regarded as one of the causes of primary edema. In the ground breaking work by Petrova et al [115] it was found that a major cause of a type of hereditary lymphoedema (FOXC2 gene mutation) involved an unusual distribution of smooth muscle. The smooth muscle lacked coordination and the areas with no smooth muscle would be forced to become conduits. This indicates that, at least in some cases, it is detrimental to have a lack of co-ordination along the lymphatic vessels and for lengths of vessels to act as conduits. McHale and Hollywood [35] describe a large amount of electrical and muscular continuity along normal lymphatic vessels, broken only at particular sites. It could be inferred that at the positions of these breaks in connectivity the vessel could change from a pump to a conduit, but seems unlikely in areas of good conductivity. Note that the smooth muscle contractions are caused by both the slow myogenic response and the faster electrical triggering.

If a contracting segment leads to a section of conduit, the pressure gradient between the two sections (and therefore flow) would be restricted by the outlet pressure of the conduit section. The pressure gradient (and therefore flow) between two pumping sections can however be much larger, for example, when the contraction has just finished in one section and is just starting in the upstream section

It is also important to consider the electrical pulses travelling in the nerves of the lymphatic system which trigger the sequential contractions along the vessels. This allows a faster propagation of the contraction wave than if each lymphangion was triggered by the stretch sensors alone. If an area of vessel is then to act as a conduit the electrical signal for contractions at one end would be isolated from the vessels at the other end, leading to a lack of coordination in pumping.

There are further modes of mal-coordination/coordination that the Quick/Stewart team could investigate, some of which might even cause damage to the vessel walls, for example where two joined areas of network contained a wave travelling in opposite directions. Furthermore, their contractions cannot propagate within the space of a lymphangion as an entire lymphangion contracts at once. This may affect the pumping efficacy, our results (which include this greater detail) indicate a fast coordinated wave is desirable to generate a large pressure to overcome the resistance of the valve (see chapter 6).

Future work in this area should include mapping out the sites of breaks in continuity and their effect on the pump/conduit behaviour of a model if there are indeed areas that act as a conduit. The details of the contraction waves should also be investigated and any connection with the conduit behaviour or breaks in continuity.

9.2.2 Valves

The efficiency of the valve mechanisms is also very important. The lack of valves in hereditary edema is critical to the development of the disorder as discussed in section 2.4 . Valve incompetency and damage due to over-stretching are also major factors in the build up of edema [63, 10]. Having a good valvular seal on closure with an ability to withstand a high retrograde flow is very important and is likely to be compromised by over-stretching of the valve materials. The material of the lymphatic valves is important, varying with age, and disease. Furthermore the dynamic shape and flow patterns are likely to be very significant to the efficiency. Lymphatic valves are often compared with heart valves (which have been more thoroughly investigated and seem to undergo similar mechanisms). Often heart valve problems are caused by damage to the material or the nature of the flow in that region. Copying these specialist mechanics for heart valve prosthetics has proved very difficult, but once the material has been damaged, there is little that can be done except to replace it with a prosthetic. Bellhouse [107] found that the size and shape of the structure around the mitrial valve outlet affected the recirculation and the valve closure efficiency. This

also affected the opening time relationship so that, when recirculation occurred, an earlier start to closing was seen with a gradual curved return to shape and a radius peak at the start of contraction. These are possibly indicators of a good flow profile for recirculation and seem similar to features found in the radius-time relationship of the lymphatic 1-d model and experiments. It may therefore be beneficial to encourage this type of profile.

The exploration of the valves in chapters 2 and 8 appears to indicate that different valve structures are beneficial in different areas of the body.

9.2.3 The Treatment of Edema

Probably the most realistic treatments for edema could involve preventing the damage to valves and walls in the buildup to lymphoedema by advising certain procedures or drugs to those at risk e.g. after surgery. A balance could be found between removing enough lymphatic vessels to ensure the cancer is removed and leaving in enough vessels to cope with the volume of lymph.

Certain drugs could be used to reduce or strengthen contractions depending on the case or even encourage a certain wave form, which might for instance improve valve efficiency. As previously discussed, the passive relaxation and radius peak may be features to investigate further for this type of effect.

Further into the future it may be possible to consider transplanting a healthy lymphatic vessel from a different limb to the affected area. The fitting of prosthetic lymphatic valves may even be considered, once more is known about their properties.

9.3 Future Work

The models of the lymphatic system could be improved in two ways. Firstly a multi-scale model could be made, for example of the entire network, or a particular limb in a patient specific model. Secondly further investigation could be undertaken of the details of the system such as the valve and wall dynamics. For example

an idealized 2 or 3-d Fluid Structure Interaction of the walls and valves, which in turn could be used to further inform the larger scale model. The existing model could however be used to examine the larger flow and pressure gradients in edema further and the implications for damage through the stresses on the materials and strategies for avoiding damage. It is generally agreed that an increase in flow in the lymphatic system would aid the body's natural healing processes and is of paramount importance to the recovery from lymphoedema. However the factors involved in increasing flow need to be balanced with the other effects which may cause damage.

To improve on existing models of the lymphatic network (e.g. the model by Reddy [6] and others discussed in chapter 3) the single unit of a lymphangion designed here could be developed into a chain to represent a longer lymphatic vessel. The vessels could be scaled to represent different vessels thoughout the network including the effect of bifurcations. Each lymphangion should be represented as simply as possible without losing accuracy (retaining features such as the passive relaxation and the radius peak). It is likely to prove beneficial (due to computational cost) to represent the lymphatic capillaries using lumped parameter modelling. It may also prove possible to reduce the number of cells in our 1-d model of the lymphangion, while retaining an accurate solution (taking the number of cells below 4). Furthermore it may be possible to represent the contracting walls accurately enough using a lumped parameter model (a more simple model using an electrical analogue or other direct relationship between pressure and radius. To date such models have not shown certain features which may have physiological implications such as the passive relaxation stage. The properties of the lymphatic nodes (e.g. their resistance) could also be represented. The position of the vessel in the network will have implications on the resistance and flow velocities involved partly due to the lymphatic valves.

It appears that the dimensions of the valves are altered in different positions within the body to cope with different surrounding tissue conditions, vessel size and differing pressure gradients. In the smallest vessels creeping flow is likely to occur, where the fluid inertia is negligible and viscous forces dominate. This will remove

any re-circulation and therefore the valve will need to function differently. A funnel shaped valve has been described by Schmid-Schonbein [11] and Lauweryns [56, 57] in lymphatic microvessels, which could enable efficient closure without re-circualtion in the sinus region as the valve tip is closer to the closed position throughout the cycle. An examination of the flow velocity, and dimensions, efficiency and retrograde pressure stamina of the valves from different positions of the body would develop this area further.

According to Picard [52] when lymphatic valve damage occurs it is usually widespread throughout the system rather that just in the peripheral circulation (where damage to the venous valves tends to occur). A further relevant study in the lymphatic system would be to discover if this tendency to widespread valve damage can be isolated to an oedematous limb and if valve damage is a major factor in different stages of lymphoedema. It would be extremely interesting to follow up on the initial findings for the experimental studies regarding the valve gap with pressure, which could inform any further valve modelling.

Using the 1-d model in chapter 7 it was found that with a large enough pressure gradient in the direction of flow (as can occur during edema) there was greater flow if the pumping activity of the vessel was prevented. This confirmed work by Quick et al which suggests that the induction of relaxation in edema could be beneficial. The gradient at which this becomes true would be a critical point to discover and compare with the gradients across lymphangions in edema. Various other effects should also be more thoroughly investigated before the prevention of contractions in the vessels during and edema. These include the effects of gravity and the wider network and the possibility of transient waves in the vessel walls when they are relaxed.

In order to improve representation of the wall and valve dynamics in the 1-d model further, it would be beneficial to undertake additional in vivo and in vitro experiments and probe the dimensions and valve activities further experimentally. Image based meshing could be used to generate a more accurate 2-d or 3-d model. This could be derived from MRI, CT or Micro CT scans. There is then image-based

meshing software available such as Simpleware (commercial code) which can be used to construct a mesh from the MRI e.t.c. data. Techniques such as these would also allow in vivo data to be taken in order to study the effects of the surrounding structure including the effects of the anchoring filaments and if these prevent change in the vessels cross-sectional shape. Furthermore the vessels have been seen to twist during in vitro contractions and it is not known if this occurs in situ. Image based meshing would give an extremely accurate representation of the dimensions of the vessel and position of the valve at different pressures. Dynamic data would need extremely high resolution which is not possible through typical MRI machines. It would also be possible to explore whether collapse does occur in vivo in the larger vessels and the effect of the nodes and branches on flow. If collapse is found to be a significant occurrence in vivo in the collecting lymphatics it may be useful to perform a 3-d Fluid Structure Interaction model of the walls as well as the valves. MRI could be used as a non-intrusive technique to examine patient suffering from different types of lymphoedema to investigate the mechanics involved insitu. For pre-op cancer patients MRI could inform a patient specific model which could then be used to determine the areas of the network most at risk from the cancer (eg sentinel nodes), helping the surgeon develop a strategy to remove these areas and leave a functioning network. Alternatively MRI could inform a basic generic model to suggest general treatments to post-op patients or operative strategies.

Although an ideal valve model would be informed by further experimental data valve modelling could also be improved simply by using the information currently available and improving the modelling techniques in 1-d and 2-d as discussed in the sections below.

9.3.1 1-d Modelling Improvements

Inorder to improve the 1-d computational modelling of the valve dynamics, the valve timings found in the heart (or even the lymphatics valves if known) could be used. The valve could be treated as the closing or opening as a closing or opening of an

area of tube. This should be a more accurate representation of the valve than the initial setup which used a linearly increasing resistance as the valve closed. This new model would use a linearly varying radius with time, during the closing or opening phase, while the resistance is related to the radius of the tube throughout the cycle by adding an extra viscous term which would only relate to the valves as shown in the equation below.

$$Rv_i = -4\mu \left(\frac{1}{a_i^2} + \frac{1}{a_{i+1}^2} \right) Q_i \tag{9.1}$$

This should enable an alinear relationship between opening and resistance, as indicated by the initial findings of the 2-d model.

In addition to the basic setup (varying the radius linearly or using part of a sine wave) some stability factors will need to be considered. First, if the radius is allowed to go to zero this would introduce a divide by zero into the radius calculation for the adjacent cell. It would be better to jump from a very small radius, to an imposed flow of zero or to a big enough resistance to limit flow and retain a non-zero radius.

Secondly, the 1-d representation of the valve may need finer resolution, using a greater number of cells in order to produce a stable and accurate solution. This would prevent a sharp change from a small to a large radius between the narrowest point of the valve during closure and the neighbouring cells representing the vessel walls.

The effect of such changes to the representation of the resistance in the 1-d model on the shape of the radius time profile would be extremely interesting. The slow curve on relaxation and radius peak may be connected with the valve mechanism as well as the passive relaxation time.

The experimental work used 2-4 lymphangions so that the mechanical details such as the propagation of the contractile wave were not affected. In the 1-d model this contractile behaviour would not be effected by using a single lymphangion so it was possible to examine this smaller region in the interests of computational costs. This

did however involve static boundary conditions, which would be varying in vivo as neighbouring lymphangions also pump. Therefore a future model would use several lymphangions in a row, pumping in sequence in order to examine the interplay of the wall and valvular activity and its effect on the dynamic pressures, radii and flow. The vessels have also been shown to taper (McHale private correspondence) going from a narrower vessel upstream to a wider vessel as adjoining vessels contribute more fluid. This effect could be included by varying the unstretched, relaxed radius (A_0 Passive) of the vessel with distance and may be important in a model of the network.

9.3.2 2-d/3-d valve representation

The representation of the valves in 2 or 3 dimensions could also be improved. The main drawbacks of the current dynamic modelling of the valve is the dominance of the valve movement on the fluid, without the fluid effecting the motion of the leaflets. Furthermore the leaflets are stiff for the model but extremely floppy in reality. The stiffness could be partially rectified by adding hinges to the leaflets to allow some flexibility in the movement. This may not be worthwhile if the movement of the leaflets continued to dominate the resulting fluid in this way. The optimum solution would be a fully coupled Fluid Structure Interaction (FSI) model as detailled below but if this is not possible the time varying boundary pressures and valve movements would improve the accuracy of the prescribed motion. The variation in pressure at the inlet and outlet could be derived from the 1-d model, see figure 5.8. The speed of the valve leaflets is likely to vary during the opening or closing sequence as in the heart valves although these details have not been examined for the lymphatic valves and it is difficult to obtain this type of information

The 6 degrees of freedom (6 DOF) capabilities within fluent could prove a useful tool if the mechanics involved can be represented satisfactorily. This 6 DOF, allows the representation of simple solid mechanics in order to produce simple Fluid Structure Interaction (FSI) models. The current drawback is that the representa-

tion of certain movements are not possible. It is not recommended in the manual to try to represent hinges as shown in figure 9.1, although we have been informed by Fluent staff that it should be possible and may become easier in future editions. Alternatively a method using a sliding deformed right-angle shape as in figure 9.2 could be used. It may be possible to use this type of mechanism to represent the valve movement just as accurately without the need for hinges. Once an in vitro or in vivo visualisation of the valve motion has been undertaken it will be clearer as to how accurate either of these strategies are.

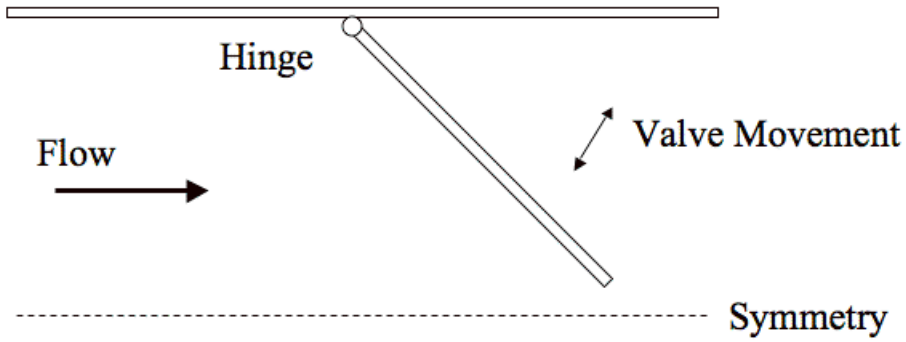

Figure 9.1: A simplified schematic of the lymphatic valve using a hinge to allow the valve motion.

A fully coupled FSI solution would allow the most accurate representation of the valve mechanics including the floppy material of the leaflets. For FSI analysis, a combination of programs such as Abacus, Fluent and MPCCI can be used or simply one program such as OpenFOAM (open source code). OpenFOAM is an open field operation and manipulation CFD tool box produced by OpenCFD Ltd under GNU public licence. The use of FSI is described in section 3.4. Examples of valve representation with FSI include a simulation of a venous valve [26] and an aortic valve model [86, 90, 91], also see section 3.5.1.

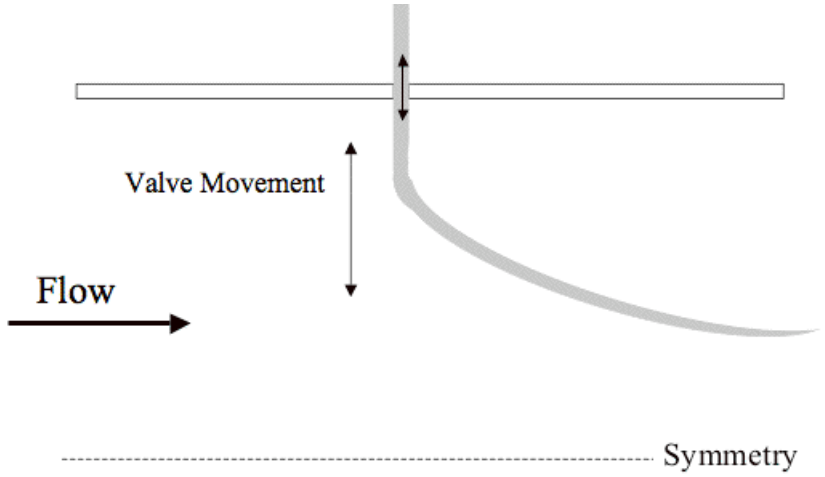

Figure 9.2: A possible schematic for the representation of a valve in Fluent's 6 degrees of freedom fluid structure interaction capabilities without the need for problematic hinges.

Further 2/3-d modeling of the valves could examine the forces on the valves in different conditions in order to determine conditions likely to cause damage.

Nether the less, the simple approach taken in this thesis has allowed various physiological insights regarding the function of the lymphatic vessel wall and valvular function.

Bibliography

[1] C. G. Caro, T. J. Pedley, R. C. Schroter, and W. A. Seed. *The Mechanics of the Circulation*. Oxford University Press, 1978.

[2] American Medical Association AMA. The lymphatic system [online], Undated, Accessed 7 March 2008. http://www.medem.com.

[3] L. V. Leak and J. F. Burke. Ultrastructural studies on the lymphatic anchoring filaments. *The Journal of Cell Biology*, 36:129–149, 1968.

[4] N. P. Reddy, T. A. Krouskop, and P. H. Newell. Biomechanics of a lymphatic vessel. *Blood Vessels*, 12:261 – 278, 1975.

[5] Deng XY, Marinov G, Marois Y, and Guidoin R. Mechanical characteristics of the canine thoracic duct: what are the driving forces of the lymph flow? *Biorheology*, 36:391–399, 1999.

[6] N. P. Reddy, T. A. Krouskop, and P. H. Newell. A computer model of the lymphatic system. *Comp.Biol.Med.*, 7:181 – 197, 1977.

[7] N. P. Reddy. A note on the lymphatic vessel network design. *J.Biomechanics*, 13:529 – 531, 1980.

[8] C.M. Quick et al. Lymphangion pumping can decrease lymph flow in edema: preliminary model predictions. *FASEB Journal*, 17(4):A129, 2003 (suppl).

[9] C.M. Quick et al. Modeling strategies for optimizing lymph flow. *FASEB Journal*, 18(4):A658, 2004 (Suppl).

[10] W.L. Olszewski. Lymphatic continuum: Contractility patterns of normal and pathologically changed human lymphatics. *Annals- New York Academy of Science*, 979:52–63, 2002.

[11] G. W. Schmid-Schonbein. Microlymphatics and lymph flow. *Physiological Reviews*, 70(4), October 1990.

[12] NC Staub and AE Taylor, editors. *Edema*. Raven Press, New York, 1984.

[13] Sir James Lighthill. *Mathematical Biofluiddynamics*. Regional Conference series in Applied Mathematics. SIAM, 1975.

[14] J. B. Grotberg and O. E. Jensen. Biofluid mechanics in flexible tubes. *Annual Review of Fluid Mechanics*, 36:121–147, January 2004.

[15] Meisner JK, Stewart RH, Laine GA, and Quick CM. Lymphatic vessels transition to a state of summation above a critical contraction frequency. *Am. J. Physiol. Regul. Integr. Comp. Physiol.*, 293:R200–R208, 2007.

[16] D. N. Ku. Blood flow in arteries. *Annu. Rev. Fluid Mech.*, 29:399–434, August 1997.

[17] D. A. McDonald. *Blood Flow in Arteries*. Edward Arnold, 1974.

[18] D. J. Patel and R. N. Vaishnav. *Cardiovascular Fluid Dynamics 2*. Academic Press London and New York, 1972.

[19] D. H. Bergel. The static elastic properties of the arterial wall. *J. Physiol.*, 156:445–457, 1961.

[20] Y. Nishimaru. Lymphatics and lymph flow. *Hiroshima Journal of Medical Sciences*, 17(2):53–76, June 1968.

[21] M. Swartz. The physiology of the lymphatic system. *Advanced Drug Delivery Reviews*, 50(1-2):3–20, August 2001.

[22] C.K. Drinker. Extravascular protein and the lymphatic system. *Ann. N. Y. Acad. Sci.*, 46:807, 1946.

[23] U. Dinnar. *Cardiovascular Fluid Dynamics*. CRC Press, Florida, 1981.

[24] B. J. Bellhouse and L. Talbot. The fluid dynamics of the aortic valve. *J. Fluid Mech.*, 35(4):721–735, 1969.

[25] B. J. Bellhouse. Fluid mechanics of a model mitral-valve and left ventricle. *Cardiovascular Research*, 6(2), 1972.

[26] G.A. Buxton and N. Clarke. Computational phlebology:the simulation of a vein valve. *J. Biol. Phys.*, 32:507–521, 2006.

[27] B. W. Zweifach and J. W. Prather. Micromanipulation of pressure in terminal lymphatics in the mesentery. *American Journal of Physiology*, 228(5):1326–1335, May 1975.

[28] Anonymous. Lymphedema [online]. Wikipedia, the free encyclopedia, undated. Accessed 7 March 2008.

[29] L.X. Zhuang J. Chen, X.Y. Lu and W. Wang. Numerical analysis of the non-newtonian blood flow in the non-planar artery with bifurcation. *Journal of hydrodynamics B*, 16(3):248–253, 2004

[30] L.X. Zhuang Y.L. Lu, X.Y. Lu and W. Wang. Breaking symmetry in non-planar bifurcations: distribution of flow and wall shear stress. *Biorehology*, 39:431–436, 2002.

[31] D. Zawieja. Lymphatic biology and the microcirculation: Past, present, and future. *Microcirculation*, 12:141–150, 2005.

[32] J. R. Casley-Smith. Are the initial lymphatics normally pulled open by anchoring filaments? *Lymphology*, pages 120–129, 1980.

[33] N. P. Reddy and K. Patel. A mathematical model of flow through the terminal lymphatics. *Med. Eng. Phys.*, 17(2):134–140, 1995.

[34] Bank AJ, Wang HY, Holte JE, Mullen K, Shammas R, and Kubo SH. Contribution of colllagen, elastin, and smooth muscle to in vivo human brachial artery wall stress and elastic modulus. *Circulation*, 94:3263–3270, 1996.

[35] N. G. McHale and M. A. Hollywood. Influence of nerves on lymphatic contractility. *Lymphology*, 27:15–24, 1994.

[36] H. Mislin and R. Schipp. *Progress in Lymphology*, chapter Structural and functional relations of the mesenteric lymph vessels. Georg Tieme- Verlag, Stuttgart, 1966.

[37] Ohhashi T, Mizuno R, Ikomi F, and Kawai Y. Current topics of physiology and pharmacology in the lymphatic system. *Pharmacology and Therapeutics*, 105:165–188, 2005.

[38] N. G. McHale and M. K. Meharg. Coordination of pumping in isolated bovine lymphatic vessels. *Journal of Physiology- London*, 450:503–512, 1992.

[39] AA Gashev, MJ Davis, and DC Zawieja. Inhibition of the lymph pump by flow in rat mesenteric lymphatics and thoracic duct. *J. Physiol*, 540:1023–1037, 2002.

[40] N. G. McHale, J. M. Allen, and H. L. A. Iggulden. Mechanism of alpha-adrenergic excitation in bovine lymphatic smooth muscle. *American Journal of Physiology - Heart*, 252(5):H873–8, May 1987.

[41] N. G. McHale and M. A. Hollywood. Influence of nerves on lymphatic contractility. *Lymphology*, 27:15–24, 1994.

[42] A. R. Hargens and B.W. Zweifach. Contractile stimuli in collecting lymph vessels. *American Journal of Physiology*, 233(1):H57–H65, 1977.

[43] Zhang et al. The role of the microlymphatic valve in the propagation of spontaneous rhythmical lymphatic motion in rat. *Clinical Hemorheology and microcirculation*, 23(2-4):349–353, 2000.

[44] Gashev AA, Davis MJ, Delp MD, and Zawieja DC. Regional variations of contractile activity in isolated rat lymphatics. *Microcirculation*, 11:477–492, 2004.

[45] A.A. Gashev. Physiologic aspects of lymphatic contractile function - current perspectives. *Lymphatic Continuum: LymphaticBiology and Disease*, 979:178–187, 2002.

[46] C.Pippard and I. C. Roddie. Resistance in the sheep's lymphatic system. *Lymphology*, 20:230–234, 1987.

[47] Auckland and Reed. Interstitial -lymphatic mechanisms in the control of extracellular fluid volume. *Physiological Review*, 73(1), Jan 1993.

[48] J. S. Lee. Lymph pressure in rat interstinal lymph duct with lymphatic obstruction. *Am. J. Physiol.*, 251(Gastrointet. Liver Physiol. 14):G321–G325, 1986.

[49] M. Papp, G.B. Makara, and B. Hajitman. The resistance of in situ perfused lymph trunks and lymph nodes to flow. *Experimentia Basel*, 27:391–392, 1971.

[50] L. V. Leak and M. P. Jamuar. Ultrastructure of pulmonary lymphatic vessels. *American Review of Respiratory Disease*, 128(2):S59–S65, 1983.

[51] V. Navas, P. J. OMorcho, and C. C. C. Morchoe. Lymphatic valves of the rat pancreas. *Lymphology*, 24:146–154, 1991.

[52] J.D. Picard. L'imagerie des valvules veineuses et lymphatiques. *Journal des Maladies Vasculaires (Paris)*, 22(2):105–111, 1997.

[53] D. R. Gnepp and F.H.Y.Green. Scanning electron-microscopic study of canine lymphatic vessels. *Lymphology*, 13(2):91–99, 1980.

[54] M. Takada. Ultrastructure of lymphatic valves in rabbits and mice. *American Journal of Anatomy*, 132(2):207–217, 1971.

[55] M.C. Mazzonni. Structure of lymphatic valves in the spinotrapezius muscle of the rat. *Blood Vessels*, 24:304–312, 1987.

[56] J. M. Lauweryns. Stereomicroscopic funnel-like architecture of pulmonary lymphatic valves. *Lymphology*, 4:125–132, 1971.

[57] JM Lauweryn, A Baert, and L Boussauw. The pulmonary lymphatics: Macroscopic and microscopic studies. *Annual Review of Respiratory Disease*, 101:448–450, 1970.

[58] J. Gruntzig, A. Djajadisastra, D. Uthoff, and H. Mehlhorn. Fine-structure of conjunctival lymphatic valves. *Klinsche Monatsblatter fur Augenheilkunde*, 205(3):147–155, september 1994.

[59] K. H. Albertine, L. M. Fox, and C. C. C. OMorchoe. The morphology of canine lymphatic valves. *Anatomical Record*, 202(4):453–461, 1982.

[60] Trzewik J, Mallipattu SK, Artmann GM, Delano FA, and Schmid-Schonbein GW. Evidence for a second valve system in lymphatics: Endothelial microvalves. *FASEB Journal*, 15(10):1711–1717, 2001.

[61] F.E. Curry et al. The revised starling principle and steady state reabsorption from interstitium to blood. *Proceedings of the 5th World Congress of Biomechanics*, 2006.

[62] B. Zangg-Vesti, J. Dorfflermelly, M. Spiegel, SH. Wen, U. K. Franzeck, and A. Bollinger. Lymphatic capillary pressure in patients with primary lymphoedema. *Microvas. Res.*, 46:128–134, 1993.

[63] W.L. Olszewski. On the pathomechanism of development of post-surgical lymphedema. *Lymphology*, 6(1):35–51, March 1973.

[64] G. Oliver and M. Detmar. The rediscovery of the lymphatic system: old and new insights into the development and biological function of the lymphatic vasculature. *Genes and Development*, 16:773–783, 2002.

[65] E. O. Carew and T.J. Pedley. An active membrane model for peristaltic pumping: Part 1- periodic activation waves in a infinite tube. *J. Biomech. Eng*, 119:66–76, February 1997.

[66] C. D. Bertram. Flow phenomena in floppy tubes. *Contemporary Physics.*, 45:45–60, 2004.

[67] M. Heil and T. J. Pedley. *Flow Past Highly Compliant Boundaries and in Collapsible Tubes*, chapter Flows in deformable tubes and channels: Theoretical models and biological applications. Kluwer Academic, 2003.

[68] C. Cancelli and T. J. Pedley. A seperated flow model for collapsible tube oscillations. *J. Fluid Mech.*, 157:375–404, 1985.

[69] Muthuchamy M, Gashev A, Boswell N, Dawson N, and Zawieja D. Molecular and functional analysis of the contractile apparatus in lymphatic muscle. *FASEB journal*, express article 10.1096/fj.02-0626fje, March 28 2003.

[70] C. M. Quick, A. M. Venugopal, A. A. Gashev, D. C. Zawieja, and R. H. Stewart. Intrinsic pump-conduit behaviour of lymphangions. *Am. J. Physiol. Regul. Inter. Comp.*, 292:R1510–R1518, 2006.

[71] M.W. Lambert and J. N. Benoit. Mathematical model of intestinal lymph flow and lymphatic pumping. *FASEB Journal*, 5(A2078), 1992.

[72] A. M. Venugopal et al. Lymphangion coordination minimally affects mean flow in lymphatic vessels. *Am. J. Physiol. Heart Circ. Physiol.*, 293:H1183–H1189, 2007.

[73] G. N. Jager, N. Westerhof, and A. Noordergraaf. Oscillatory flow impedance in electrical analogue of arterial system representation of sleeve effect and non-newtonian properties of blood. *Circ. Res.*, 16:121–133, 1965.

[74] N. Westerhof and A. Noodergraaf. Arterial viscoelasticity; a generalized model. effect on input impedance and wave travel in the systematic tree. *J. Biomech*, 3:357–379, 1970.

[75] V. Stembera and F. Marsik. One-dimensional mathematical model of the flow through a collapsible tube with applications to blood flow through human vessels. *Theoretical and Computational Fluid Dynamics*, not yet published.

[76] F. Marsik, S. Prevorovska, Z. Broz, and V. Stembera. Numerical model of the human cardiovascular system-korotkoff sound simulation. *Cardiovascular Engineering: An International Journal*, 4(2):193–199(7), June 2004.

[77] Carmody CJ, Burriesci G, Howard IC, and Patterson EA. An approach to the simulation of fluid-structure interaction in the aortic valve. *Journal of Biomechanics*, 39(1):158–169, 2006.

[78] C. M. Scotti and E. A. Finol. Compliant biomechanics of abdominal aortic aneurysms: A fluid-structure interaction study. *Computers and Structures*, 85(11-14):1097–1113, Jun 2007.

[79] V. Diaz-Zucanni, D. Rafirou, D. R. Hose, P.V.Lawford, and A.J. Narracott. Multi-physics and multi-scale modelling in cardiovascular physiology:advanced user methods for simulation of biological systems with ansys/cfx. *Computational Science-ICCS 007, PT 1 Proceedings*, 4487:794–801, 2007.

[80] T. K. Hung and G. B. Schuessler. Computational analysis as an aid to the design of heart valves. *Chem. Eng. Prog. Symp. Ser.*, 67:8–17, 1971.

[81] A. D. Au and H.S. Greenfield. Computer graphics analysis of stresses in blood flow through a prosthetic heart valve. *Comput. Biol. Med.*, 4:279–91, 1975.

[82] Hose DR, Narracott AJ, Penrose JMT, Baguley D, Jones IP, and Lawford PV. Fundamental mechanics of aortic heart valve closure. *Journal of Biomechanics*, 39(5):958–967, 2006.

[83] C. S. Peskin. Flow patterns around heart valves in a numerical method. *J. Comput. Phys.*, 10:252–271, 1972.

[84] C. S. Peskin. Numerical analysis of blood flow in the heart. *J. Comput. Phys.*, 25:220–252, 1977.

[85] C. S. Peskin and D. M. McQueen. Flow patterns around heart valves for numerical analysis of blood flow through the heart. *J. Comput. Phys.*, 37:113–32, 1980.

[86] J. De Hart, G. W. M. Peters, P. J. G. Schreurs, and F. P. T. Baaijens. A 2-dimensional fluid structure interaction model of the aortic valve. *J. Biomech.*, 33:1079–1088, 2000.

[87] C. S. Peskin and D. M. McQueen. A 3d computational method for blood flow in the heart i: Immersed elastic fibers in viscous incompressible fluid. *J. Comput. Phys.*, 81:372–405, 1989.

[88] C. S. Peskin and D. M. McQueen. A 3d computational method for blood flow in the heart ii: Contractile fibres. *J. Comput. Phys.*, 82:289–97, 1989.

[89] C.S. Peskin and D.M. McQueen. *Case studies in mathematical modelling-ecology, physiology and cell biology*, chapter Fluid dynamics of the heart and its valves, page 410. Upper Saddle River NJ: Prentice Hall, 1997.

[90] De Hart J, Baaijens FPT, Peters GWM, and Schreurs PJG. A computational fluid structure interaction analysis of a fiber-reinforced stentless aortic valve. *J. Biomech.*, 36:699–712, 2003.

[91] De Hart J, Peters GWM, Schreurs PJG, and Baaijens FPT. A computational fluid structure interaction analysis in the aortic valve. *J. Biomech.*, 36:103–112, 2003.

[92] T. Ohhashi. Active and passive mechanical characteristics of bovine mesenteric lymphatics. *Am. J. Physiol.*, 239(Heart Circ. Physiol. 8):H88–H95, 1980.

[93] S. Armenio, S. Cetta, and G. Tanzini. Spontaneous contractility in the human lymph vessels. *Lymphology*, 33:325–327, 1981.

[94] S. Armenio, S. Cetta, and G. Tanzini. Spontaneous contractility of the lymphatic vessels in man (spanish). *Angilogia*, 33:325–327, 1981.

[95] J. Eisenhoffer, A. Kagal, T. Klein, and M.G. Johnston. Importance of valves and lymphangion contractions in determining pressure gradients in isolated lymphatics exposed to elevations in outflow pressure. *Microvascular research*, 49:97–110, 1995.

[96] A. A. Gashev and D. C. Zawieja. Physiology of human lymphatic contractility. *Lymphology*, 34(3):124–134, 2001.

[97] W.L. Olszewski and A. Engeset. Intrinsic contractility of prenodal lymph vessels and lymph flow in human leg. *Am. J. Physiol.*, 239:H775–783, 1980.

[98] O. Sorensen, A. Engeset, W. I. Olszewski, and T. Lindmo. High sensitivity optical lymph flow-meter. *Lymphology*, 15:29–31, Oct 1982.

[99] K.D. Thornbury, H.R. Harty, and J. G. McGeown. Mesenteric lymph-flow responses to splanching nerve-stimulation in sheep. *American Journal of Physiology*, 264(2):H604–H610, Feb 1993.

[100] J. L. R. Fox and P. Y. van der Weid. Effects of histamine on the contractile and electrical activity in isolated lymphatic vessels of the guinea-pig mesentery. *British Journal of Pharmcology*, 2002.

[101] B. W. Zweifach. Micropressure measurements in the terminal lymphatics. *Bibl. Anat.*, 12:361–365, 1973.

[102] Anonymous. Deborah number [online]. Wikipedia, the free encyclopedia, undated. Accessed 7 March 2008.

[103] A. P. Yoganathan, H. Z. Me, and S. C. l. Jones. Fluid mechanics of heart valves. *Annu. Rev. Biomed. Eng.*, 6:331–362, 2004.

[104] Y.C. Fung. *Biomechanics: Circulation.* Springer, 1984.

[105] N. Fowler, E.Y.K. Ng, and W. L. Siauw. Unsteady viscous flow model on moving the domain through a stenotic artery. *Proc. Instn. Mech. Engrs.*, 215(H)(2), March 2001.

[106] T. J. Pedley and X. Y Luo. Modelling flow and oscillations in collapsible tubes. *Theoretical and Computational Fluid Dynamics*, 10:277–294, 1998.

[107] Bergel, editor. *Cardiovascular Fluid Dynamics 1.* Academic Press London and New York, 1972.

[108] B. W. Zweifach. Physiology of terminal lymphatics in the mesentery. *Pfluegers Arch.*, 336(suppl):S65–S69,S79, 1972.

[109] A. R. Smith, F. Visioli, B. Frei, and T. Hagen. Age-related changes in endothelial nitric oxide synthase phosphorylation and nitric oxide dependent vasodilation: evidence for a novel mechanism involving sphingomyelinase and ceramide-activated phophatase 2a. *Aging Cell*, 5:391–400, 2006.

[110] Emiliana Konova, Stephan Baydanoff, Milena Atanasova, and Angelika Velkova. Age-related changes in the glycation of human aortic elastin. *Experimental Gerontology*, 39(2):249 – 254, 2004.

[111] M. Anne Cattell, John C. Anderson, and Philip S. Hasleton. Age-related changes in amounts and concentrations of collagen and elastin in normotensive human thoracic aorta. *Clinica Chimica Acta*, 245(1):73 – 84, 1996.

[112] M. H. Dresden and A. Evert. Collagen metabolism in experimental filariasis. *J. Parasit.*, 70(2):208–212, 1984.

[113] S. F. Wilson, J. Guarner, A. L. Valme, J. Louis-Charles, T.L. Jones, and D.G. Addis. Histopathologic improvement with lymphedema management. *Emerging Infectious Diseases, Leogane, Haiti*, 2004.

[114] C. M. Quick, A. M. Venugopal, A. A. Gashev, D. C. Zawieja, and R. H. Stewart. Intrinsic pump-conduit behaviour of lymphangions. *Am. J. Physiol. Regul. Inter. Comp.*, 292(4):R1510–R1518, 2007.

[115] T.V. Petrova, T. Karpana, C. Norrmen, and R. Mellor et al. Defective valves and abnormal mural cell recruitment underlie lymphatic vascular failure in lymphoedema distichiasis. *Nature Medicine*, 10:974–981, September 2004.

Glossary of Terms

Adventitia The outermost connective tissue covering of any organ, vessel, or other structure not covered by a serosa; instead, the covering is properly derived from without (i.e., from the surrounding connective tissue) and does not form an integral part of such organ or structure.

Bicuspid Having two points or cusps.

Cusp As leaflet.

Diastole The normal rhythmical dilatation of the heart during which the chambers are filling with blood.

Fibroadipose Relating to or containing both fibrous and fatty structures.

In vitro Within a glass, observable in a test tube, in an artificial environment.

In vivo Within the living body.

Intima Inner layer of blood vessel, comprising an endothelial monolayer on the luminal face with a subcellular elastic extracellular matrix containing a few smooth muscle cells.

Lamina Flat sheet, as in basal lamina.

Laminar In or consisting of thin plates or layers; having the form of a thin plate or lamina.

Leaflet A leaf like organ or part especially any of the flaps of the bicuspid or the tricuspid valve.

Lymphangion Length of lymphatic vessel between two valves

Media Avascular middle layer of the artery wall, composed of alternating layers of elastic fibres and smooth muscle cells.

Micrograph A photograph taken through a microscope.

Reynold's number A measure of the ratio of inertial forces to viscous forces quantifying the relative importance of these two types of forces for given flow conditions.

Sinus Cavity such as found behind a valve leaflet.

Systole The normal rhythmical contraction of the heart, during which the blood in the chambers is forced onward.

Tricuspid Having three points or cusps.